Publication No. 02-173-236

EFFECT OF PARTICLE CHARACTERISTICS ON FATTY ACID FLOTATION OF FLORIDA PHOSPHATE ROCK

Volume III – Phosphate Encapsulation/Liberation Studies

Prepared by

UNIVERSITY OF FLORIDA
and UNIVERSITY OF UTAH

under a grant sponsored by

April 2010

The Florida Institute of Phosphate Research was created in 1978 by the Florida Legislature (Chapter 378.101, Florida Statutes) and empowered to conduct research supportive to the responsible development of the state's phosphate resources. The Institute has targeted areas of research responsibility. These are: reclamation alternatives in mining and processing, including wetlands reclamation, phosphogypsum storage areas and phosphatic clay containment areas; methods for more efficient, economical and environmentally balanced phosphate recovery and processing; disposal and utilization of phosphatic clay; and environmental effects involving the health and welfare of the people, including those effects related to radiation and water consumption.

FIPR is located in Polk County, in the heart of the Central Florida phosphate district. The Institute seeks to serve as an information center on phosphate-related topics and welcomes information requests made in person, or by mail, email, or telephone.

Florida Institute of Phosphate Research
1855 West Main Street
Bartow, Florida 33830
(863) 534-7160
Fax: (863) 534-7165
http://www.fipr.state.fl.us

EFFECT OF PARTICLE CHARACTERISTICS ON FATTY ACID FLOTATION OF FLORIDA PHOSPHATE ROCK

FINAL REPORT

VOLUME III
PHOSPHATE ENCAPSULATION/LIBERATION STUDIES

Hassan El-Shall
Principal Investigator

Department of Materials Science and Engineering
UNIVERSITY OF FLORIDA
Gainesville, FL 32611

with

Jan D. Miller
Co-Principal Investigator

and
Team Members

C.L. Lin, M. I. Al-Wakeel, J. Nalaskowski, L. Hupka, and O. Ozdemir
Metallurgical Engineering Department
College of Mines and Earth Sciences
UNIVERSITY OF UTAH
Salt Lake City, UT 84112

Prepared for

FLORIDA INSTITUTE OF PHOSPHATE RESEARCH
1855 West Main Street
Bartow, FL 33830 USA

Project Manager: Patrick Zhang
FIPR Project Number: 05-02-173R

April 2010

DISCLAIMER

The contents of this report are reproduced herein as received from the contractor. The report may have been edited as to format in conformance with the FIPR *Style Manual*.

The opinions, findings and conclusions expressed herein are not necessarily those of the Florida Institute of Phosphate Research, nor does mention of company names or products constitute endorsement by the Florida Institute of Phosphate Research.

PERSPECTIVE

Patrick Zhang, Research Director - Beneficiation & Mining

Fatty acid flotation is the key step in phosphate beneficiation, and has significant impacts on both the operational cost and product grade. The Bone Valley phosphate deposit has been very amenable to fatty acid flotation, and is indeed one of the easiest-to-float phosphates in the world. That is changing as phosphate mining moves further south. The industry now frequently encounters difficult-to-float phosphates, with flotation recoveries 20% lower than normal. The extent of this problem and the reasons for the poor flotation performance are not understood. There has been some speculation on the cause of this problem, such as organic coating on the phosphate surfaces, higher pyrite content, and bacterial action. However, no study has been undertaken to fully investigate it.

Over the years, processing engineers within the Florida phosphate industry have urged FIPR to conduct a study of flotation feed variations to answer the question why some feeds are difficult to float, so that effective methods may be developed to improve flotation efficiency. This topic was also the only immediate research priority supported by most participants at a FIPR-sponsored flotation workshop held in 2004. In response to that top research need recommended by industry representatives, a consortium of three top universities in mineral processing/surface chemistry proposed this comprehensive study of physical, chemical, mineralogical, and surface properties of various flotation feeds to identify important parameters affecting phosphate flotation and develop methods for reducing any detrimental effects.

This characterization study used many of the routine and modern analytical techniques currently available, such as XMT, CT, XPS, CMT, FTIR, EDS and SEM. Poor flotation was found to be caused by one or more of the following characteristics:

1. Encapsulation of phosphate particles in a thin or thick silica shell

2. Heavy contamination of phosphate particles with contaminants like clay, gypsum, aluminosilicates, and dolomite

3. The presence of phosphate as coarse and/or porous particles

4. The presence of adsorption-hindering species such as silanol groups on the phosphate surface.

Although this project has not achieved the ultimate goal of instantaneous diagnostics of “bad” flotation feeds and “quick fixes” when problems are identified, this final report provides a wealth of useful information to both process engineers and researchers.

ABSTRACT

Phosphate flotation has been used by industry for more than a half century but still faces many technical challenges. Such challenges include not only the selection of the chemical reagents but the characteristics of the feed itself. This report deals with the investigation of feed characteristics and how these characteristics affect the flotation separation efficiency of feed material from a particular phosphate operation, specifically why some feed, from the same mine, is efficiently separated with high recovery (good feed) while other feed is more difficult to separate (bad feed). The study was conducted using both traditional analytical techniques and more advanced techniques such as X-ray microtomography. The results reveal that bad feed is highly porous, coarser in size, and, most significantly, exhibits a lower degree of liberation. Such bad feed was inefficiently separated by fatty acid flotation and improved recovery would require controlled grinding in order to improve the extent of liberation.

TABLE OF CONTENTS

TABLE OF CONTENTS (CONT.)

APPENDICES

LIST OF FIGURES

Figure **Page**

LIST OF FIGURES (CONT.)

Figure **Page**

LIST OF FIGURES (CONT.)

Figure **Page**

LIST OF FIGURES (CONT.)

Figure **Page**

LIST OF FIGURES (CONT.)

Figure **Page**

LIST OF FIGURES (CONT.)

Figure **Page**

LIST OF TABLES

Table **Page**

LIST OF TABLES (CONT.)

Table **Page**

EXECUTIVE SUMMARY

MICRO CT ANALYSIS, LIBERATION-LIMITED GRADE RECOVERY CURVES

Summary for 2007 Samples

Micro CT analyses of Four Corners (FCO) Bad, Four Corners Good, CF Industries Bad and CF Industries Good samples received in 2007 are reported together with other physical characteristics such as particle size distribution and surface area. Grade/recovery curves limited only by the liberation characteristics have been constructed from micro CT scans of feed samples in each case.

It is evident from this detailed CT analysis that improved separation cannot be achieved for the Four Corners Good and CF Industries Good samples unless improved liberation of the feed is achieved by size reduction. On the other hand, in the case of the CF Industries Bad sample, some slight improvement in efficiency might be achieved by improved flotation conditions. For example, in the best case for improved recovery, the recovery could be increased from 80% to ~95% at the same grade. In the case of the Four Corners Bad sample considerable improvement in recovery and grade should be possible by improved flotation conditions. In this case it is clear that efficiency is limited by factors other than liberation, such as slime coatings, surface structure, surface composition, etc. The summary with respect to recovery limitation for each of the 2007 samples is presented in Table 20.

Summary for 2008 Samples

Research on the 2008 samples focused on liberation issues and grade/recovery curves for 2008 samples: Hole 1862 Split 2 (1862-S2), Hole 3057 Split 2 (3057-S2), CF Combined, CF West, CF East, FCO, FCO Bad, Hole 464 Split 1 (464-S1), Hole 464 Split 2 (464-S2) and SFM**.** Detailed 3D Micro CT analyses for all 2008 samples are reported. Regarding these ten 2008 samples, CT analysis suggests that in the case of CF West, CF East, CF Combined and 464-S2 the recovery is mostly limited by liberation. In the case of 3057-S2, SFM, FCO, FCO Bad (tailings 2) recovery is to some extent limited by factors other than liberation. Finally, in the case of 464-S1, 1862-S2 and FCO Bad (tailings 1) the recovery is significantly limited by factors other than liberation (see Table 20).

MINERALOGY AND SURFACE CHEMISTRY

Research work was concentrated on two good samples (CF West and CF Combined samples) and two bad samples (1862-S2, 464-S1). However, the

mineralogical studies also included the 464-S2 and CF East Pit samples. Samples considered are as follows:

Sample	Feed BPL (%)	Grade BPL(%)	Recovery (%)
	Bad Samples		
Hole 1862 Split 2	26.72	48.72	25.6
Hole 464 Split 1	27.65	36.79	76.5
Hole 464 Split 2	31.93	57.69	61.0
	Good Samples		
CF Combined	16.94	52.42	96.3
CF West Pit	9.88	43.62	96.6
CF East Pit	12.15	46.16	96.7

The present studies indicate that the feed phosphate samples are composed essentially of quartz and apatite in variable percentages. In addition subordinate amounts of clay minerals (kaolinite, illite, and montmorillonite), gypsum and carbonate minerals (mainly dolomite) were found except for the 464-S1 and 464-S2 feed samples, which are free of carbonate minerals. On flotation separation, almost all phosphate minerals are transferred into the concentrates for the good feeds and the phosphate mineral percentage in the good tails does not exceed 1.5%. In contrast, for the bad feeds there is no great difference between the grade of the concentrates and tailings, except for 464-S2 where the concentrate grade was found to be about 58% phosphate and the tailings grade about 7% phosphate.

Also the present study revealed that the particle size distribution (PSD) has a narrow size range for the good feeds (CF West and CF Combined), while in the bad feeds PSDs have a wide size range and there is a good percent of phosphate in the coarse to very coarse size fraction, significantly coarser than the associated quartz particles. The effect of PSD on the efficiency of separation is obvious where most of the coarse phosphate particles in the bad feeds are lost to the tailings, leaving the concentrates to be of uniform particle size.

In the 1862-S2 sample, gypsum is found in the feed in crystals of cylindrical shape surrounding phosphate particles and sometimes aggregated as coarse particles. Gypsum is a source of calcium that may interfere in the flotation process. The phosphate particles in the tailings are more porous than those in the concentrate, and the phosphate particles in the tailings are one of the following types: coarse, highly porous, kaolinite-coated, or unliberated.

In the feed for 464-S1, some phosphate particles show high porosity and kaolinite is present in the shape of worms, rods or ropes attached or stained on the surface of both phosphate and quartz particles. Sometimes the kaolinite forms a shell around the different particles. In the tailings, kaolinite is acting as binding material for some phosphate and quartz particles, and the phosphate particles are very coarse, unliberated or attached to quartz particles by the kaolinite mineral. As in the other phosphate samples, the phosphate particles are elongated (rods or oval) and spherical or irregular. In this

case, the elongated phosphate particles are more common in the concentrate than in the tailings. CF Combined and CF West Pit good feeds have no such features found in the bad feed material but there is a limited liberation.

The XPS results of phosphate particles in the flotation products of bad samples 464-S1 and 1862-S2 revealed that calcium, phosphorus, fluorine, iron and sulfur exhibit the same behavior and are rich on the surface of phosphate particles in the concentrates. Silica exhibits similar behavior and is abundant on the surface of phosphate particles in the tailings. On the other hand, magnesium and alumina exhibit opposite behavior and increase in the concentrate of 1862-S2 and decrease in the tailings of 464-S1.

The mass concentration difference for phosphorus, calcium, and fluorine in the concentrate and tailings is higher in the case of 464-S1 than in the case of 1862-S2. This difference is expected to explain separation efficiency, and if this difference increases the separation efficiency will increase. Therefore, the separation efficiency of 464-S1 is better than that of 1862-S2, according to the flotation and mineralogical results.

Finally, the factors affecting separation efficiency of the bad feeds (1862-S2 and 464-S1) include the following:

- Particle size distribution
- Presence of a remarkable amount of associated clay, gypsum and dolomite minerals
- High porosity of phosphate particles in some feeds
- Liberation

Particle shape has some effect on separation, as the elongated particles have the ability to float more than the spherical particles.

INTRODUCTION

At times the Florida phosphate industry encounters phosphate rock that gives lower than expected BPL recovery from the rougher flotation circuit in plant operations. The drop in recovery is typically 10% and as much as 30% or more. For example, Figure 1 shows the weekly recovery vs. time for a Florida phosphate beneficiation plant. During this time of operation there were relatively few minor fluctuations in the feed grade BPL with the trend being slightly upward during the period. The recovery dropped about 15% toward the end of this period.

While this is somewhat of an extreme example (prolonged time at low recovery), sporadic low recoveries occur for extended periods like this every few years. If the typical drop in recovery is 10%, and it occurs 10% of the time, at a rock cost of $30/ton, the cost to the industry is at least $6,000,000 per year. In addition, the lost phosphate is a waste of a limited natural resource. It also increases the area of land disturbed per ton of rock recovered.

During the flotation workshop held by FIPR (August, 2004), it became apparent that variation in feed quality from day to day, shift to shift, even from dragline to drag line, represents a challenge to beneficiation plant operators and reagent suppliers. Therefore, a research project was initiated to conduct a characterization study of phosphate feed samples in order to explain limitation to fatty acid flotation recovery.
This report of the FIPR research program deals the following:

- Liberation issues
- Mineralogy
- Surface Chemistry

According to tasks identified in the proposal, important ore characteristics were investigated using X-ray microtomography to address liberation issues, including liberation-limited grade/recovery curves obtained for each sample. SEM analysis, BET measurements, EDS and XPS spectroscopy, and optical microscopy were used to address mineralogy and chemical composition of particle surfaces.

The reported studies were used to explain the flotation results in bench-scale Denver flotation cell experiments. In fact, these analytical results were compared with the flotation results and important factors controlling the flotation response were identified.

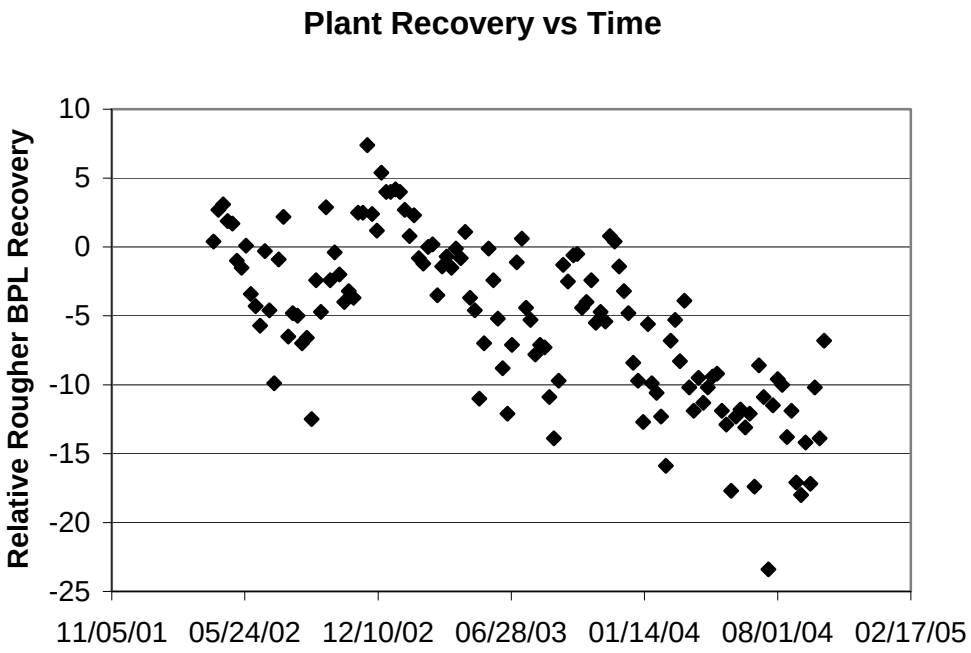

Figure 1. Relative Rougher BPL Recovery During a 3-Year Period of Plant Operation.

METHODOLOGY

MATERIALS

2007 Samples

A total of four feed samples of Florida phosphate were delivered during 2007: two (good and bad) feed samples from the CF Industries plant and two (good and bad) samples from the Four Corners plant. The BPL and insoluble residues of these bad and good feed samples are given in Table 1. Also eight flotation products (four concentrates and four tails) from those feed samples were delivered from the same plants.

Table 1. BPL and Insoluble Residue of the 2007 Good and Bad Feed Samples.

Feed	BPL %	Insoluble Residue %
CF Industries Good	15.76	77.92
CF Industries Bad	19.86	72.05
Four Corners Good	13.30	82.03
Four Corners Bad	8.21	87.47

Both the feed samples and their flotation products were investigated for the same reason, to elucidate the effect of the different parameters, particularly liberation, on the separation efficiency of the different feeds. The flotation data of the good and bad feeds are given in Table 2.

Table 2. Flotation Data of the 2007 Concentrate Samples.

Concentrate	BPL %	Recovery %
CF Good concentrate	38.5	97.3
CF Bad concentrate	58.7	89.1
Four Corners Good concentrate	32.1	92.3
Four Corners Bad concentrate	27.6-32.7	23.0-85.0

According to the flotation results of these samples, both the good and bad CF Industries samples float better than either of the Four Corners samples. The results from this study show that in the case of the CF good sample, a phosphate concentrate product of 38.5% BPL with a recovery of 97.3 % can be achieved at a dosage of 1.0 lb./t and 180 seconds of conditioning time. The best case for the CF bad sample was a product of 58.7% BPL with a recovery of 89.1%.

In the case of the Four Corners good sample, a product of 32.1% BPL with a recovery of 92.3% can be obtained in the best case. On the other hand, the best case for the Four Corners bad sample floats only with a recovery of 23.0% BPL. The scrubbing

process then improved the recovery from 23% to 85%. This indicates that the scrubbing process removed fine particles, mostly of clay, from the surface, and created new surfaces that enabled fatty acid adsorption at the phosphate surfaces.

2008 Samples

Ten new samples received during 2008 include: Hole 1862 Split 2 (1862-S2), Hole 3057 Split 2 (3057-S2), CF Combined, CF West, CF East, FCO, FCO Bad, Hole 464 Split 1 (464-S1), Hole 464 Split 2 (464-S2) and SFM**.**

EXPERIMENTAL PROCEDURES

There are many tools available for liberation analysis. These can be classified into one-dimensional and two-dimensional techniques, such as optical microscopy, scanning electron microscopy, and its modifications, the QEM/SCAN system and the JKTech Mineral Liberation Analyzer (Miller and others 1982, Miller and Lin 1988, Gu and Napier-Munn 1997, Al-Wakeel 1997, Lin and Miller 2001). More recently, three-dimensional (3D) techniques such as X-ray microtomography have been developed (Miller and Lin 2004, Fandrich and others 2007, Videla and others 2007). The spatial interpretation of one- and two-dimensional information extracted from polished or thin sections can be accomplished by a variety of stereological procedures (Schneider and others 1991, Barbery 1991, King and Schneider 1993, King 1994, Lin and Miller 2001).

The topic of stereological correction in mineral liberation analysis has been examined extensively and various models for estimating 3D liberation characteristics from 2D polished section measurements have been proposed, as first demonstrated in 1985 (Lin and others) and more recently reviewed (Latti and Adair 2001). In contrast, direct 3D liberation measurements using X-ray computed tomography (CT) techniques are being used for exposure/liberation analysis at the University of Utah (Miller and Lin 2004).

In this study, a Micromeritics ASAP 2010 Surface Area Analyzer was used for BET surface area measurements. Mineralogical analyses for the phosphate flotation samples were conducted by X-ray diffraction analysis, which was carried out using a Philips X-ray diffractometer and an optical polarizing microscope. Also, some characterization was accomplished using X-ray photoelectron spectroscopy (XPS).

Micro CT Analysis, Liberation-Limited Grade Recovery Curves

Three-dimensional liberation analyses of the phosphate feed and flotation products were obtained using the same XMT system. In this regard, the three-dimensional XMT image data of multiphase mineral particles was post-processed in

order to determine the characteristic relationship between mineral phases and liberation for individual particles from a packed particle bed. First, a 3D watershed algorithm was used to separate individual particles in the packed particle bed, and then compositional information for each individual particle was analyzed using a finite mixture distribution model (Videla and others 2007).

Each sample was analyzed and from the X-ray attenuation coefficient histogram (3D liberation spectrum), the particles were classified into twelve classes based on phosphate volume grade. The grade classes are as follows: 0%, 5%, 15%, 25%, 35%, 45%, 55%, 65%, 75%, 85%, 95% and 100% phosphate. A 3D liberation spectrum of phosphate was obtained for feed and flotation products from each sample.

Correlation of CT Data with Chemical Analysis

The CT data defines the volume fraction of each mineral phase that can be distinguished by XMT and these volume fractions correlate with the corresponding mass fractions from chemical analysis. In fact, the relationship between mass fraction and volume fraction for a given mineral phase A in a binary system consisting of mineral phases A and B is defined by:

$$m_A = \frac{V_A}{V_A + \frac{\rho_A}{\rho_B}\left(1 - V_A\right)} \tag{1}$$

where:

m_A – mass fraction A
V_A – volume fraction A
ρ_A - density of phase A
ρ_B - density of phase B

In this way, the relationship for a given system can be established if the densities of mineral phases are known and are constant from one particle to another. Usually such is not the case and verification of experimental data is difficult.

RESULTS AND DISCUSSION

CHARACTERIZATION OF 2007 SAMPLES

Particle Size Distribution

The particle size distribution for each sample is presented in Figure 2. The results indicate that the d_{50} size of the CF Industries feed (CF good feed: d_{50}=0.263 mm; CF bad feed: d_{50}=0.338 mm) is coarser than the d_{50} size of the Four Corners feed (Four Corners Good feed: d_{50}=0.178 mm; Four Corners Bad feed: d_{50}=0.195 mm).

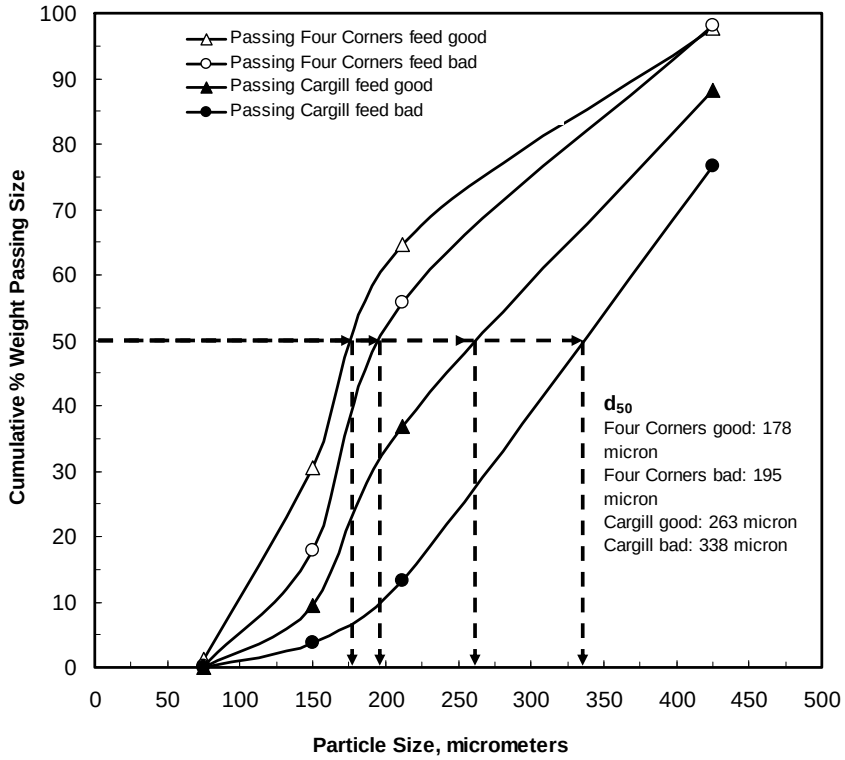

Figure 2. Particle Size Distributions of the Flotation Feeds of 2007 Samples.

It can be clearly seen that, in the case of the CF Industries good sample, there is a significant increase in recovery as the conditioning time increases. But as the collector dosage increases, this effect becomes insignificant. These results show that the conditioning time is significant. In the case of flotation results with the Four Corners good sample, both conditioning time and dosage play an important role in recoveries. This means that the Four Corners sample needs more conditioning time and a higher reagent dosage. This might be due to different types of locked particles in the feed.

Surface Area Analysis

Surface area, average pore diameter and average pore volume were determined for the four feed samples by BET, as given in Table 3. Surface area is an important characteristic with respect to the adsorption of flotation chemicals, including collectors and depressants, at mineral surfaces. When material has a much higher surface area, it is necessary to adjust the dosage of the chemicals accordingly. The results indicate that of the four samples, the Four Corners Good feed has the lowest surface area and the highest pore diameter and pore volume, while both good feeds have less area and larger pore diameters than the bad feeds from the same mine.

Table 3. Surface Area, Pore Diameter and Pore Volume of the Feed Samples.

Sample	BET Surface Area (m^2/g)	Average Pore Diameter ( )	Total Pore Volume (Cm^3/g)
CF Industries Good feed	3.274	7.164 E+01	1.173 E-02
CF Industries Bad feed	3.519	6.900 E+01	1.214 E-02
Four Corners Good feed	1.04	9.80 E+01	5.104 E-02
Four Corners Bad feed	3.479	7.481 E+01	1.300 E-02

Surface area was measured also for the flotation products of the bad feeds, and the results are presented in Table 4. These results indicate that the CF Bad concentrate sample shows a much higher surface area compared to the other samples.

Table 4. BET Surface Area of "Bad" Samples.

Sample	Surface Area (m^2/g)
Four Corners Bad Conc.	3.12 ± 0.01
Four Corners Bad Tail	3.23 ± 0.02
CF Industries Bad Conc.	10.12 ± 0.04
CF Industries Bad Tail	1.75 ± 0.01

Further analysis is necessary to confirm these results and to study the effect of surface area/porosity in more detail.

Mineralogical Analysis by X-Ray Diffraction (XRD)

The mineralogical analyses of the 2007 samples by XRD are shown in Figures 3-8. Results indicate that both CF Industries and Four Corners feed samples have the same mineral composition, which includes essentially quartz and fluorapatite, in addition to a remarkably high percentage of feldspars.

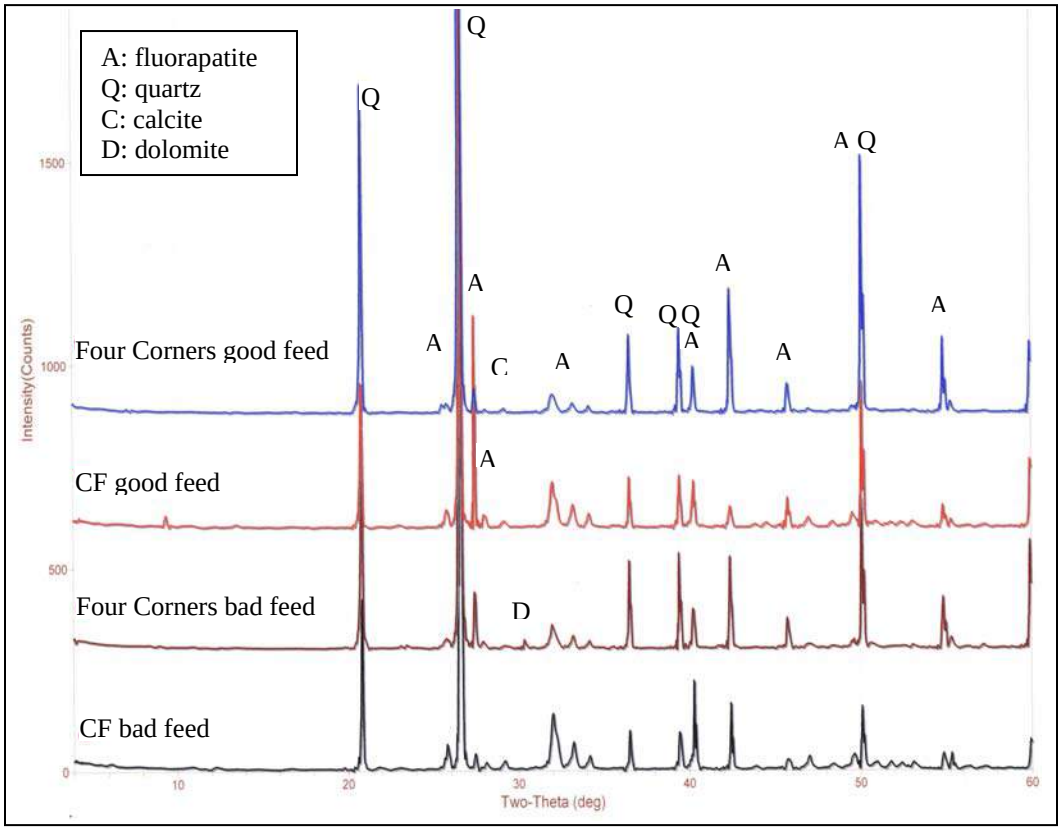

Figure 3. XRD Patterns of the CF Industries and Four Corners Good and Bad Feeds.

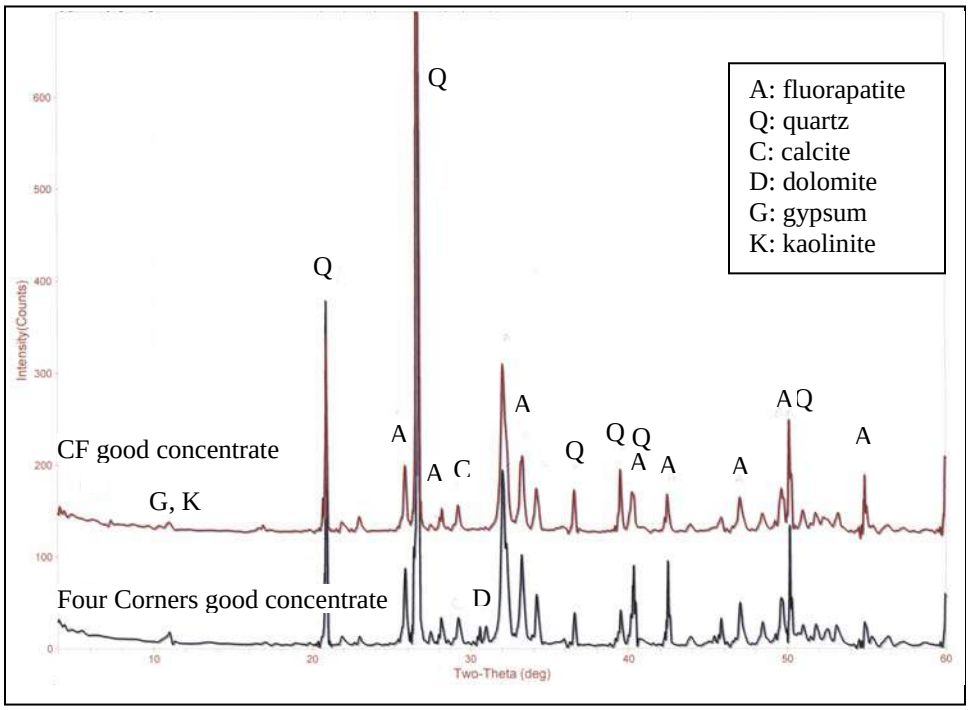

Figure 4. XRD Patterns of the Concentrates of the CF Industries and Four Corners Good Feeds.

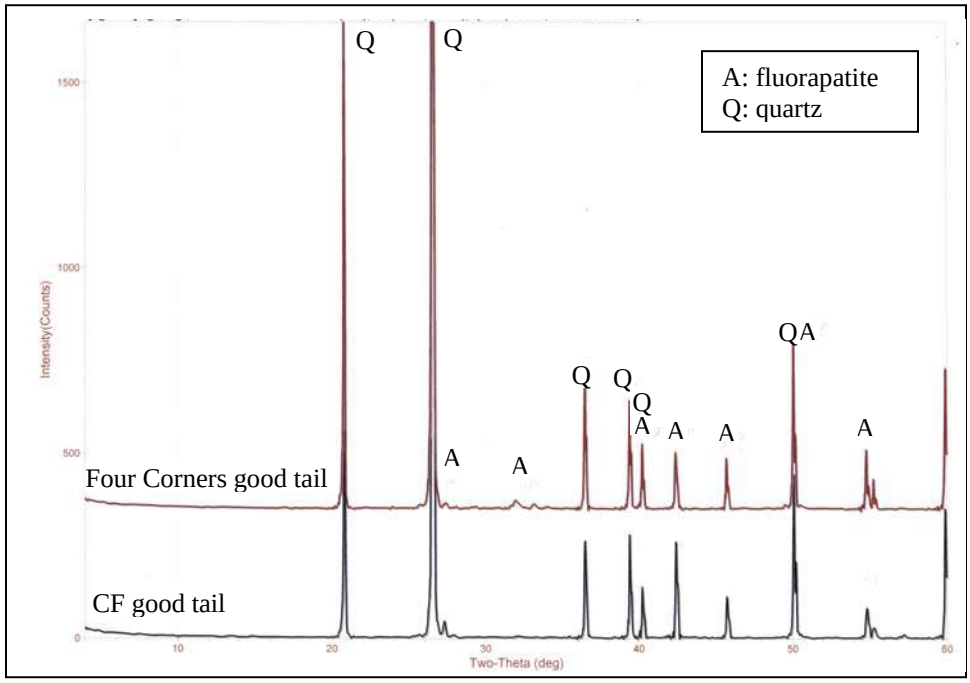

Figure 5. XRD Patterns of the Tails of the CF Industries and Four Corners Good Feeds.

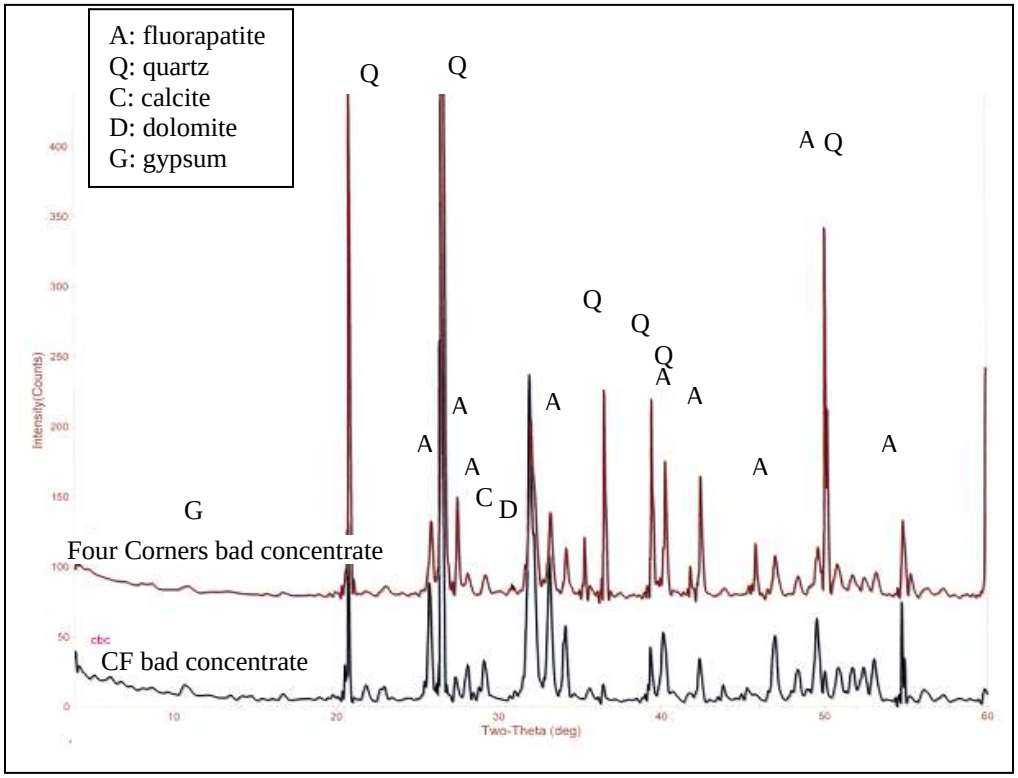

Figure 6. XRD Patterns of the Concentrates of the CF Industries and Four Corners Bad Feeds.

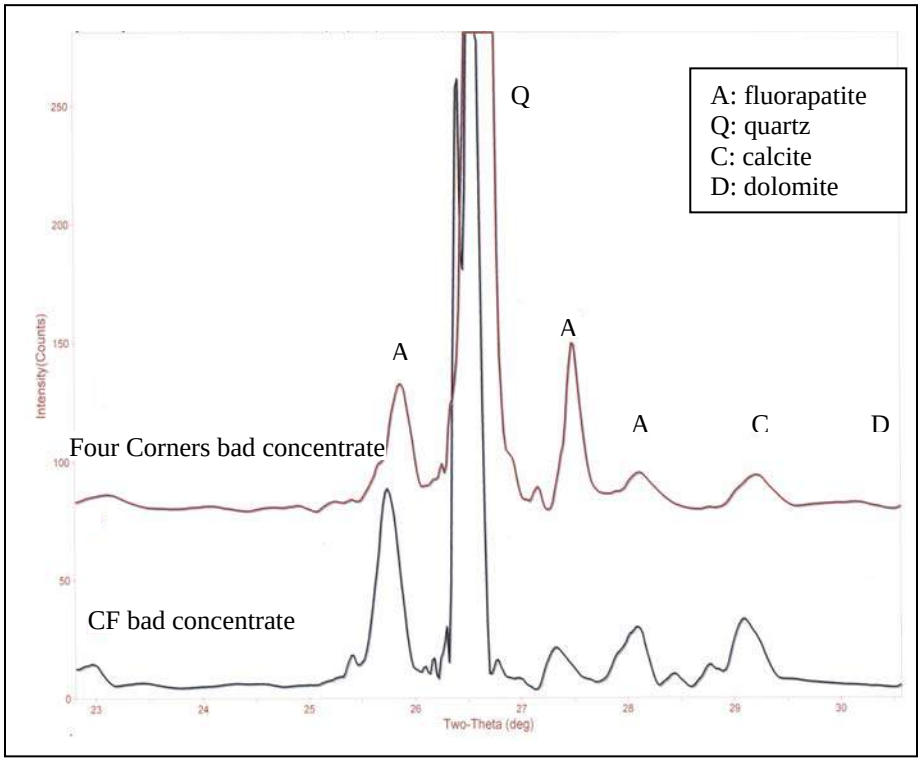

Figure 7. XRD Patterns of the Concentrates of CF Industries and Four Corners Bad Feed Samples.

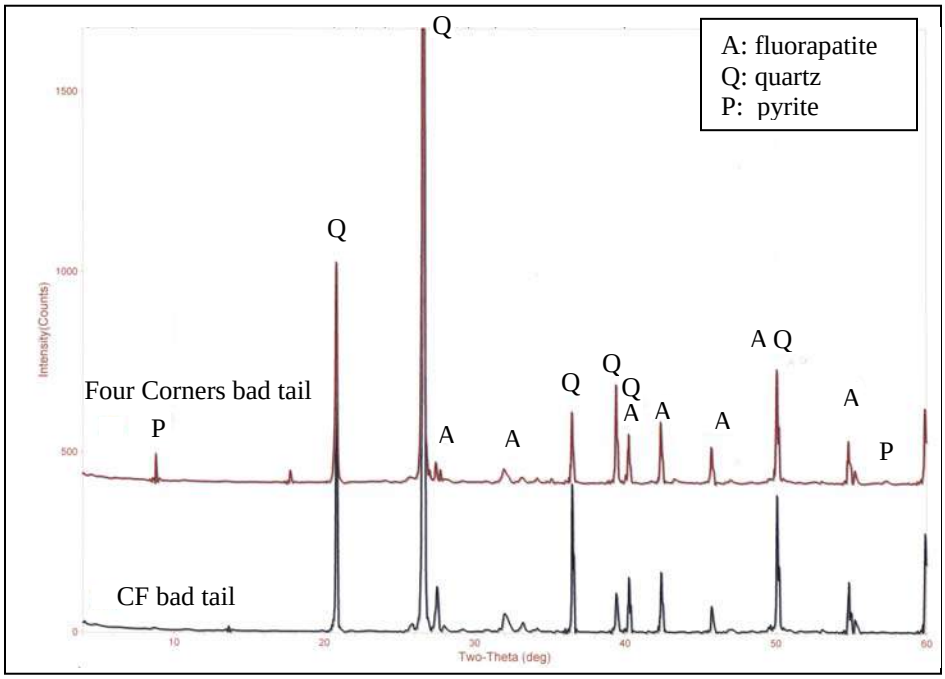

Figure 8. XRD Patterns of the Tails of the CF Industries and Four Corners Bad Feed Samples.

The CF Industries Bad feed samples, contains a very small percent of carbonate (dolomite) which is concentrated in the concentrate after flotation, as indicated by a very short peak.

Along with the CF Industries samples, Four Corners Good and Bad feed samples have the same mineral composition which includes essentially quartz and carbonate fluorapatite. In addition, the Four Corners Bad feed has a remarkably high percentage of dolomite and a very small percentage of pyrite.

Mineralogical Analysis by Optical Microscopy

The microscopic investigation shows that the CF Industries Good phosphate feed is of coarse to fine sand size (d_{50}=0.263 mm, lower medium sand size), moderately sorted (Figure 9). Quartz particles are angular to subrounded, while phosphate particles are well rounded to subrounded particles in addition to phosphate bone fragments, generally found in elongated and spherical shapes. Phosphorite mineral particles exhibit different colors—pale yellow, yellow, dark yellow, brown, dark brown, bluish grey or dark grey; the dark phosphate particles are the most abundant.

CF Industries Bad feed is very coarse to very fine grained (d_{50}=0.338 mm, upper medium sand size) and ill-sorted. Quartz particles are angular to subrounded, and frequently are partially covered with thin layers of phosphate or interlocked with other phosphate particles (Figure 9). Phosphate particles are well rounded to subrounded and are bone fragments of different colors that are elongated in shape. The phosphate particles are yellow, white, brown, dark gray and black, with the lighter-colored grains abundant. Fine quartz inclusions are abundant in the phosphate particles. Sometimes the phosphate particles are siliceous, especially the coarse grains. Carbonate minerals are found as microcrystalline to rhombic crystalline particles and shell fragments.

After flotation most of the apatite is separated into the concentrates while quartz is found in the tailing products. Nevertheless, some apatite is found in the tailings, especially in the CF Industries Bad tailings. In the concentrates a small percent of gypsum or kaolinite, which was not found in the XRD patterns of the feeds, is floated with the apatite mineral, in addition to the carbonate mineral (dolomite) in the CF Industries Bad concentrate.

Along with the CF Industries samples, Four Corners Good and Bad feed samples have the same mineral composition which includes essentially quartz and carbonate fluorapatite. In addition, the Four Corners Bad feed has a remarkable percent of dolomite and a very small percent of pyrite. Both microcrystalline and rhombic crystalline carbonates were found in the Four Corners Bad feed.

The microscopic investigation shows that the Four Corners Good feed is of very fine to medium particle size (d50=0.178 mm, fine sand size), occasionally coarse, and moderately sorted. Phosphate particles are well rounded to subangular and vary in shape

from spherical to elongated, but the latter shape is more common. They have different colors ranging from pale yellow to brown to dark brown and bluish grey or dark grey and black, but the latter two types are abundant. Sometimes very fine sulfide particles, represented mainly by pyrite, were observed by reflected light and disseminated in phosphorite particles. Quartz particles are angular to subangular and frequently of irregular shape (Figure 10).

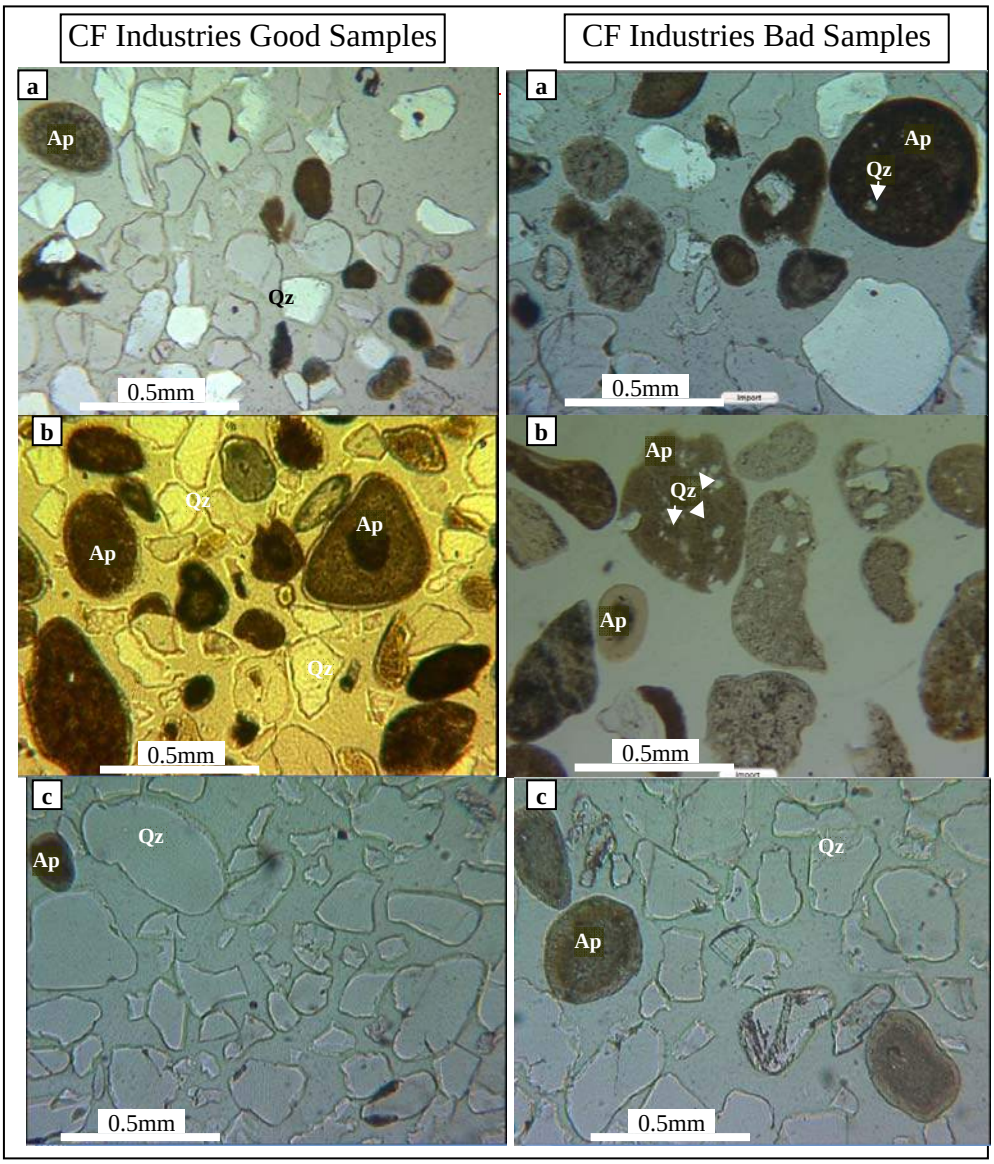

Figure 9. Micrographs Showing the Mineralogy of the CF Industries Feeds and Flotation Products: a: Feed, b: Concentrate, c: Tailings, Plane Polarized Light.

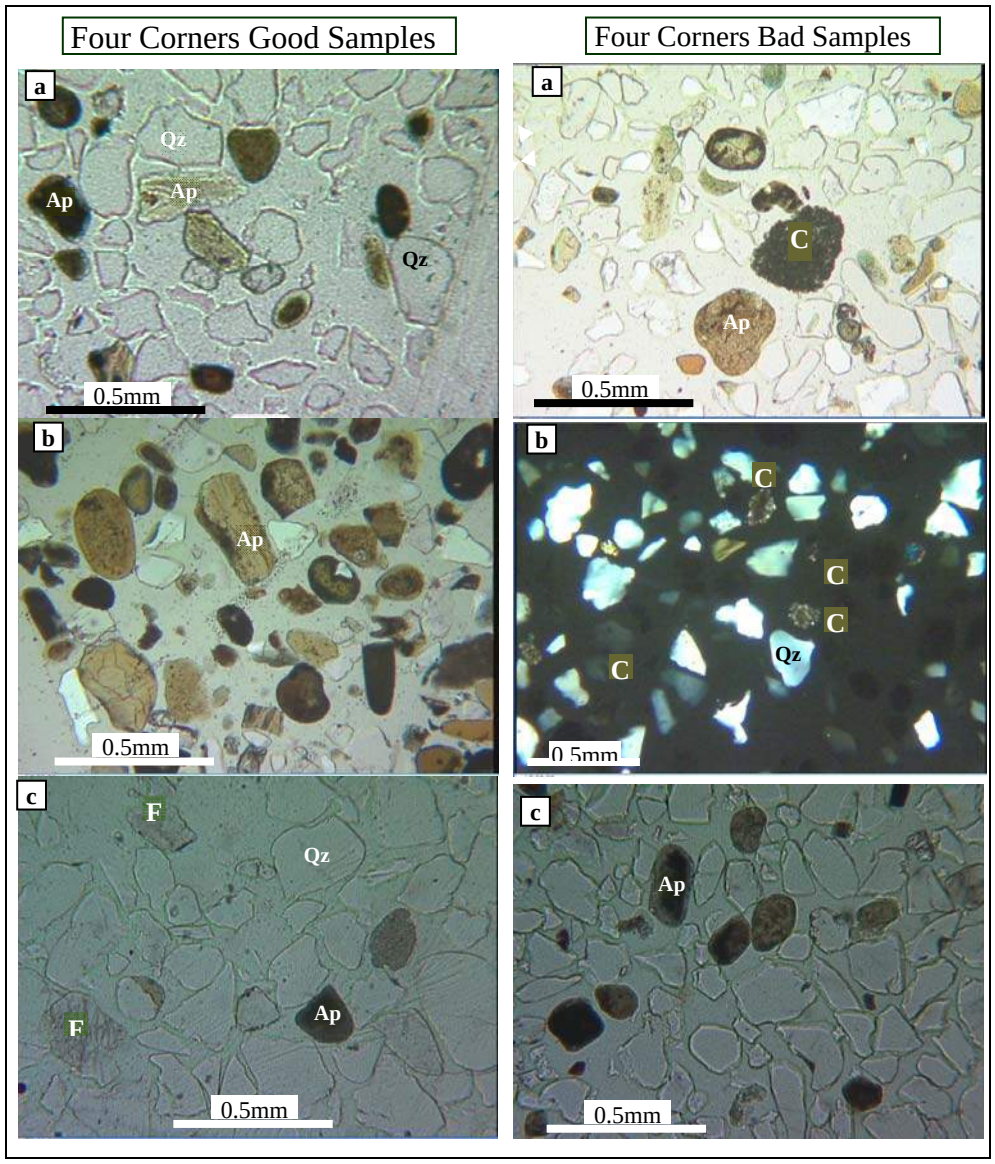

Figure 10. **Micrographs Showing the Mineralogy of the Four Corners Feeds and Flotation Products: a: Feed, b: Concentrate, c: Tailing; C: Carbonate, F: Feldspar, Ap: Apatite, Qz: Quartz.**

Surface Chemistry—SEM and EDS Analysis

SEM, in conjunction with energy dispersion spectroscopy (EDS), gives a unique opportunity to analyze the shape of particles as well as their surface and subsurface elemental composition. The EDS signal is collected from a depth of several micrometers, thus giving an idea about the bulk composition rather than that of the surface. As shown in this initial report, it is possible to obtain information about the elemental composition of a large population of particles, and subsequently to focus on the individual particles.

XMT analysis of particle shape was complemented by scanning electron microscopy analysis of the sample shape. Additionally, analysis of the sample elemental composition was performed using energy dispersion spectroscopy. Bad and good feed samples from the two different plants were analyzed using a Hitachi SEM and an EDAX EDS analyzer at a working distance of 25 kV and 26 mm. Overall, a low-magnification image was taken for each sample with the corresponding large area EDS scan showing the overall elemental composition of the observed image. Subsequently, images and EDS spectra of selected particles were taken.

Figure 11 shows an image of the CF Industries Bad feed sample, while Figure 12 presents a spectrum of a large area of the sample. Peaks corresponding to aluminum, silicon, phosphorus and oxygen can be distinguished, silicon being the most prominent.

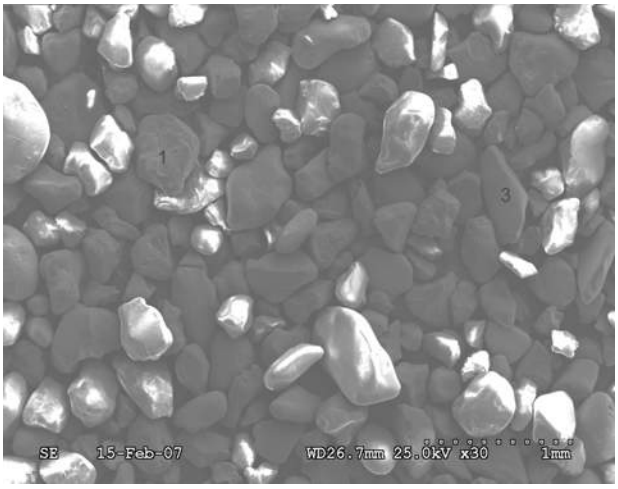

Figure 11. SEM Image of CF Industries Bad Feed Sample.

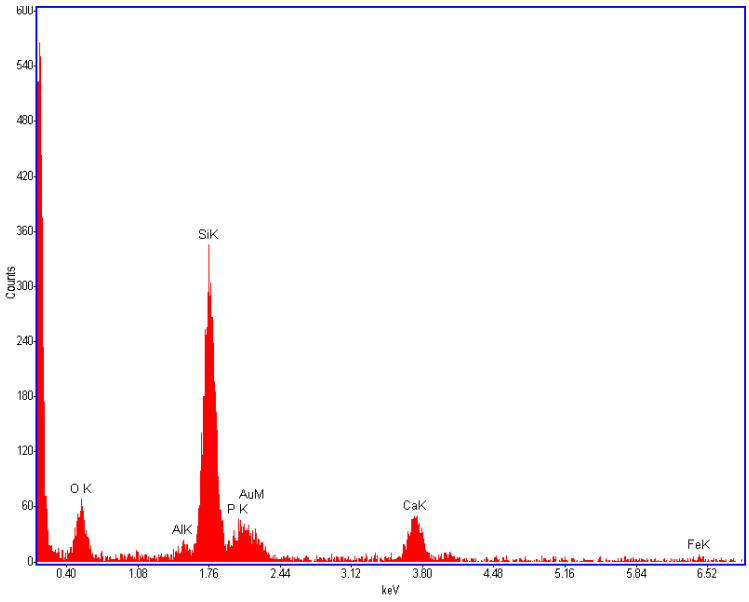

Figure 12. EDS Large Area Spectrum of CF Industries Bad Feed Sample.

Figures 13 to 16 show selected single particles from the CF Industries Bad feed sample together with their elemental composition. Particle 1 can be clearly identified as silica (gangue mineral), while particle 3 is a phosphate particle with only traces of silica present.

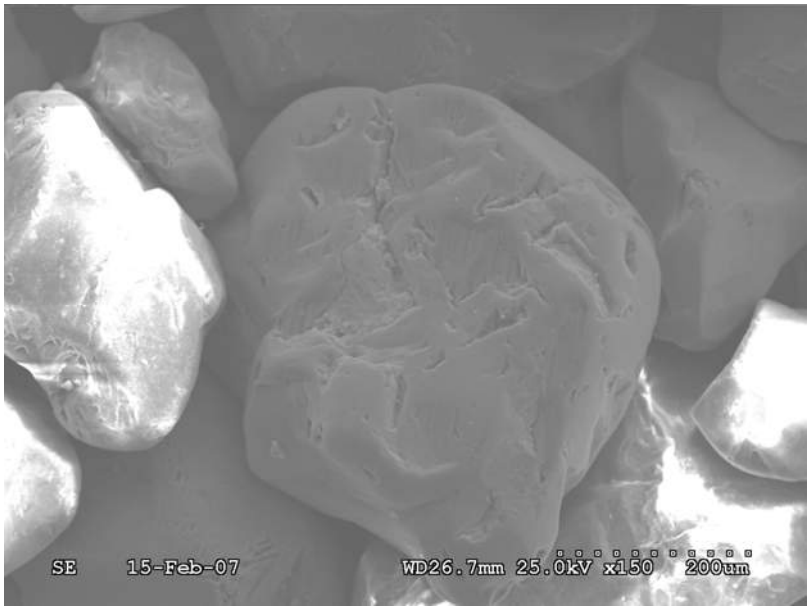

Figure 13. SEM Image of EDS Particle 1 from CF Industries Bad Feed Sample.

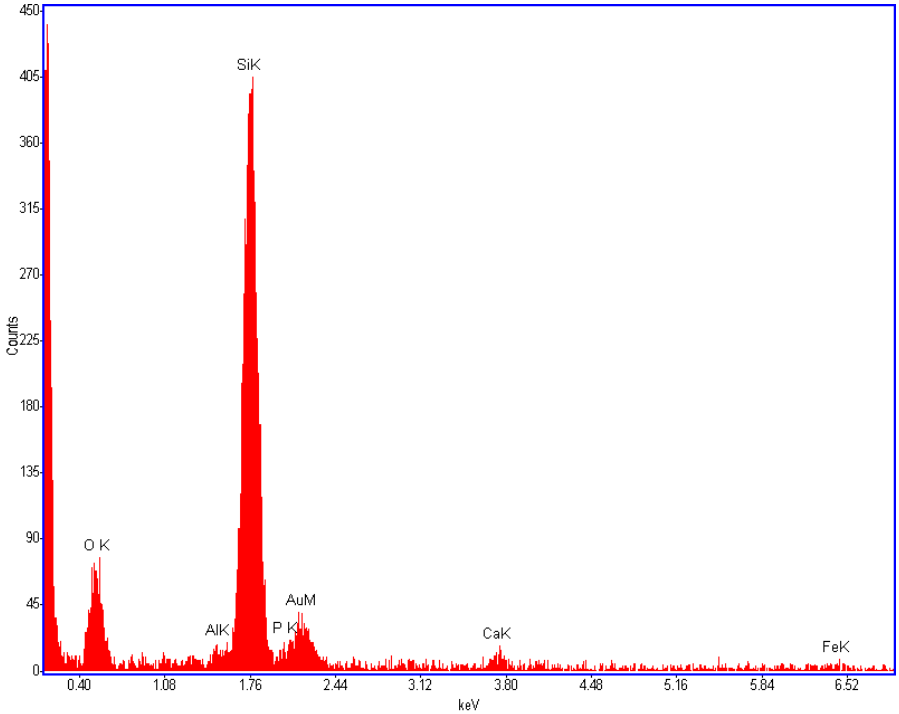

Figure 14. EDS Spot Spectrum of EDS Particle 1 of CF Industries Bad Feed Sample.

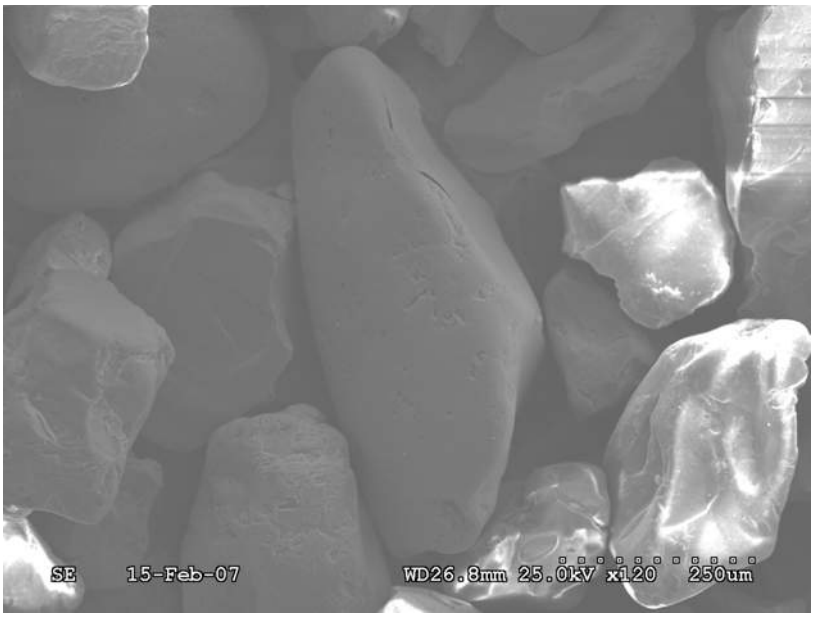

Figure 15. SEM Image of EDS Particle 3 from CF Industries Bad Feed Sample.

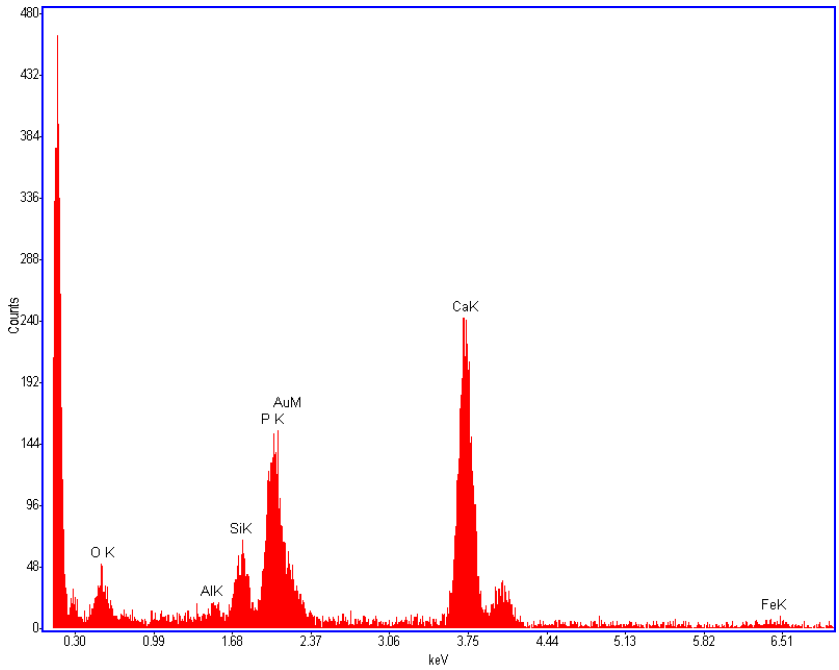

Figure 16. EDS Spot Spectrum of EDS Particle 3 of CF Industries Bad Feed Sample.

Other gangue particles show characteristics of aluminosilicates or calcium carbonates. Further images and results are given in the Appendix. SEM-EDS analysis can be successfully used to characterize the presence of phosphate particles in the sample as well as morphological characteristics of the particles. No clear connection, however,

between the morphology and elemental composition was observed. A systematic study of the samples where the individual particles are analyzed and compared should reveal if any such relationship exists.

Surface Chemistry—X=Ray Photoelectron Spectroscopy (XPS) Analysis

EDS analysis of elemental composition was complemented by surface-sensitive XPS analysis of concentrate and tailing samples from both plants. XPS analysis depends on the interaction of the X-ray beam with the sample surface. During this interaction photoelectrons are emitted from the sample which energy is directly related to the elemental and chemical characteristics of the sample. Since these photoelectrons can escape only from the few top nanometers of the sample material, XPS is a powerful surface analysis technique. Unlike EDS, XPS gives only surface composition information, without the subsurface signal present. It is also very sensitive and allows for quantification of the elements. Modern XPS systems allow for imaging of the sample using an electron gun similar to SEM imaging. This combination allows for collecting signal from the selected single particles of the sample. It is important to mention that the surface characteristics of the sample is a deciding factor during the flotation separation process.

Initial dry samples were screened before the XPS analysis and only the coarse fraction (above 200 µm) was examined in this initial study. Non-quartz looking particles were handpicked for this analysis. The Kratos Axis Ultra DLD XPS system was used, the sample was imaged using an electron gun, and XPS spectra 50 µm by 50 µm were taken. Spectra were quantified and surface elemental compositions of individual selected particles were obtained.

Figures 17 and 18 show the image of a particle from the CF Industries bad concentrate sample and the XPS spectrum of the particle surface, respectively. Elemental composition of the particle surface is given in Table 5. A significant amount of surface phosphorus is evident, suggesting the phosphate character of the particle. As expected most of the analyzed particles in this sample were showing a high phosphorus content at the surface.

Figure 17. Electron Image of XPS Particle 1 from CF Industries Bad Concentrate Sample.

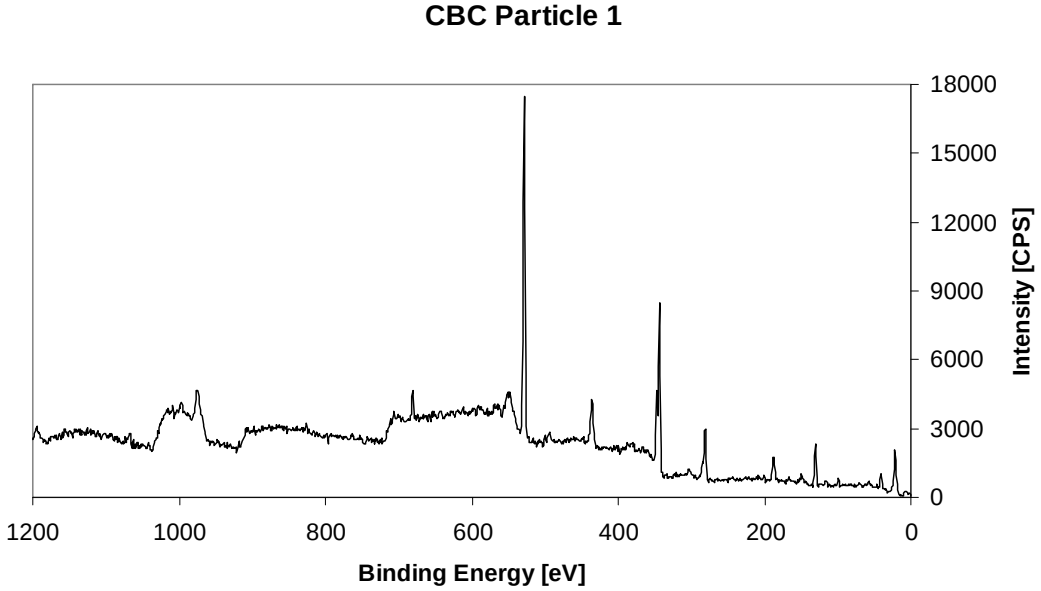

Figure 18. XPS Spectrum XPS Particle 1 from CF Industries Bad Concentrate Sample.

Table 5. Surface Elemental Composition of XPS Particle 1 from CF Industries Bad Concentrate Sample.

Element	Atomic Concentration (%)	Mass Concentration (%)
O	48.04	39.16
Ca	11.86	24.22
C	24.20	14.81
P	7.57	11.95
F	3.37	3.26
Si	1.67	2.39
Al	1.01	1.39
Mg	2.27	2.81

The CF Industries Bad tailings sample was also analyzed and interesting examples are shown in Figures 19 and 20. These figures, as well as Table 6, show a particle from this sample population where the content of phosphorus is very low, the particle obviously being a gangue mineral of calcium carbonate composition.

Figure 19. Electron Image of XPS Particle 2 from CF Industries Bad Tailings Sample.

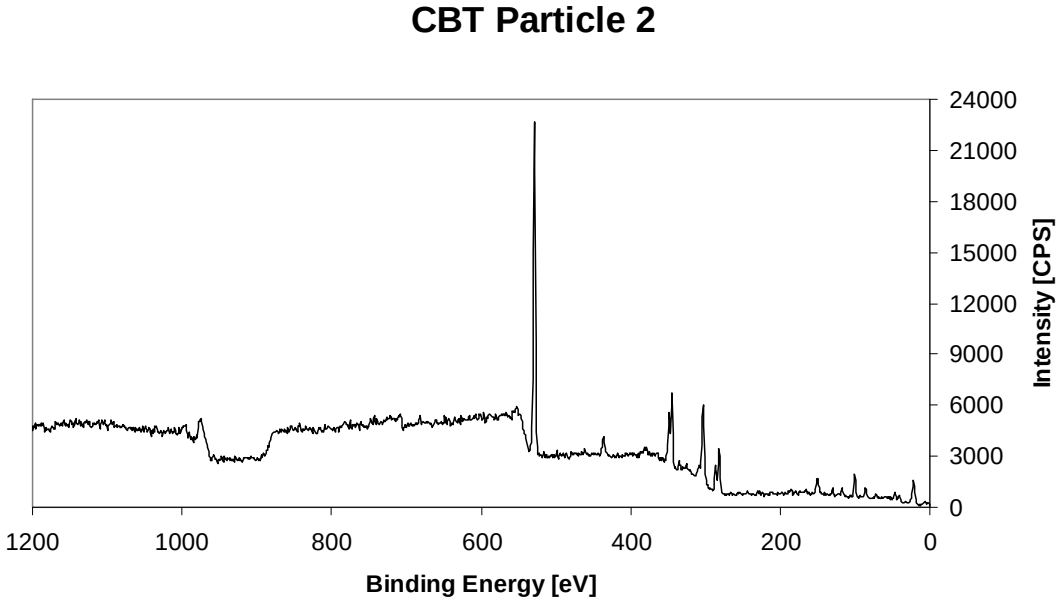

Figure 20. XPS Spectrum of XPS Particle 2 from CF Industries Bad Tailings Sample.

Table 6. Surface Elemental Composition of XPS Particle 2 from CF Industries Bad Tailings Sample.

Element	Atomic Concentration (%)	Mass Concentration (%)
O	46.09	39.18
Ca	6.28	13.38
C	23.44	14.96
P	0.17	0.27
F	0.64	0.65
Si	5.65	8.43
Al	1.66	2.38
Mg	16.07	20.76

However, particles with a high phosphorus concentration were also present in the CF Industries Bad tailings sample, as shown in Figures 21 and 22 and Table 7. The phosphorus surface concentration, while generally lower than that of the concentrate particles, reached 12 mass percent in some cases.

Figure 21. Electron Image of XPS Particle 5 from CF Industries Bad Tailings Sample.

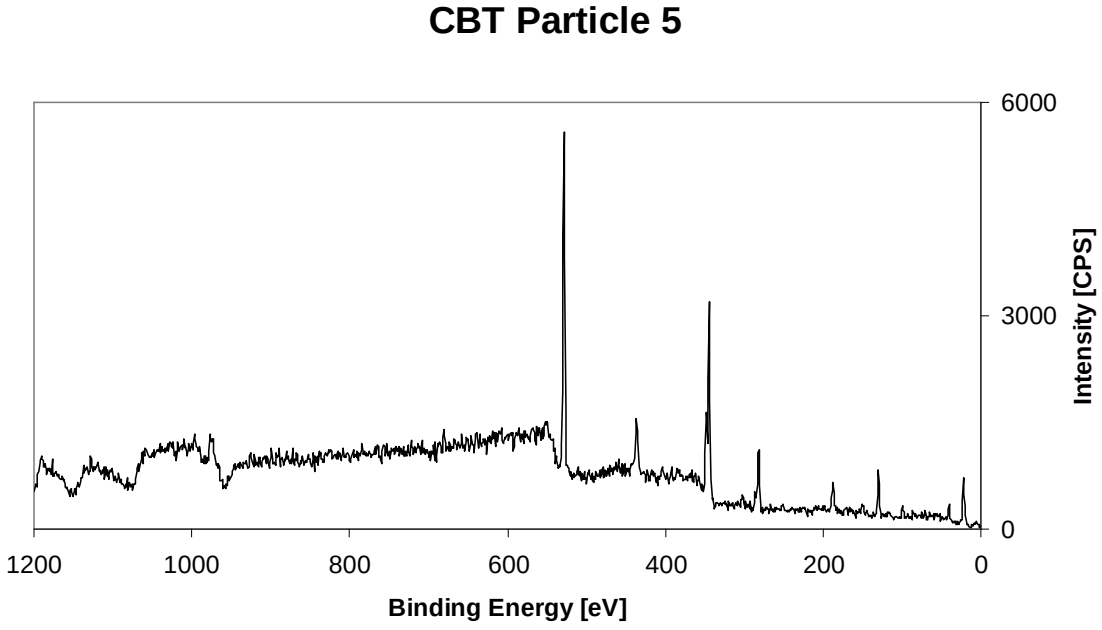

Figure 22. XPS Spectrum of XPS Particle 5 from CF Industries Bad Tailings Sample.

Table 7. Surface Elemental Composition of XPS Particle 5 from CF Industries Bad Tailings Sample.

Element	Atomic Concentration (%)	Mass Concentration (%)
O	47.88	37.78
Ca	13.33	26.35
C	22.42	13.28
P	7.86	12.00
F	1.31	1.23
Si	1.99	2.75
Al	2.69	3.57
Mg	2.53	3.03

X-Ray Microtomography (XMT) Analysis

Modern three-dimensional (3D) image-acquisition techniques, such as X-ray microtomography (XMT), offer a unique imaging capability that can produce high-resolution (a few micrometers) three-dimensional images of the internal structure of multiphase particulate samples. For this reason, high-resolution 3D X-ray microtomography (XMT) was used for the direct determination and analysis of the multiphase particle beds of phosphate samples. X-ray tomographic reconstruction produces a three-dimensional map of the X-ray attenuation coefficients of the irradiated cross-section of the specimen. Differentiation of features within the sample is possible because the linear attenuation coefficient (μ) at each voxel is a function of material density, effective atomic number, and the X-ray energy.

Figure 23 shows the histogram distributions obtained for two different phosphate samples previously scanned by XMT at the University of Utah. It is clear from direct observation of the peaks in the histograms that the mean of the attenuation coefficient is directly related to the density of the material. Three peaks are observed, which represent the air, gangue (silicate) phase, and phosphate phase, as indicated in Figure 23. In general, voxels with an X-ray linear attenuation coefficient of less than 0.07 are considered to represent air. Inset graphs of Figure 23 show volume-rendering images for the different phosphate samples with the gangue phase set as white and phosphate phase set a brown-yellow color. The rich phosphate sample only contains one gangue particle and several locked particles. However, the other sample consists mostly of gangue particles (in white).

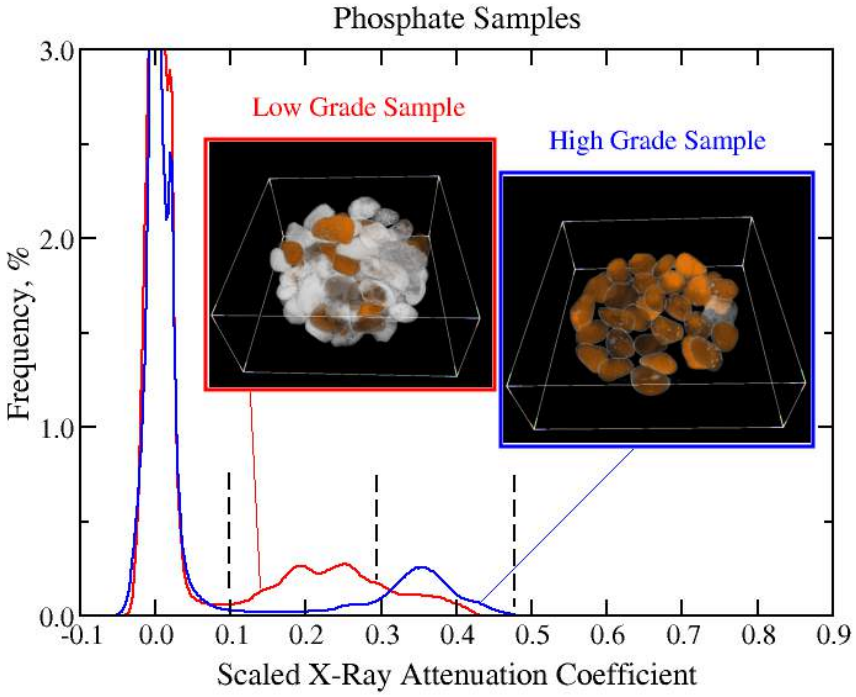

Figure 23. Histograms of Scaled X-ray Attenuation Coefficients for Two Phosphate Samples Previously Examined at the University of Utah.

Based on the these previous results, particles from the bad concentrate and tailings samples from CF Industries and Four Corners were selected and scanned by XMT.

Concentrate and Tailings from the CF Industries Bad Sample

Volume rendering of the 3D reconstructed XMT images for the concentrate and tailings from the CF Industries Bad sample are shown in Figure 24. It is clearly indicated that except for a few particles, most of the phosphate particles (brown-yellow) in the tailings of the CF Industries Bad sample are locked particles. However, as expected, most of the particles in the concentrate are rich in the phosphate phase with a few inclusions of the gangue phase (white).

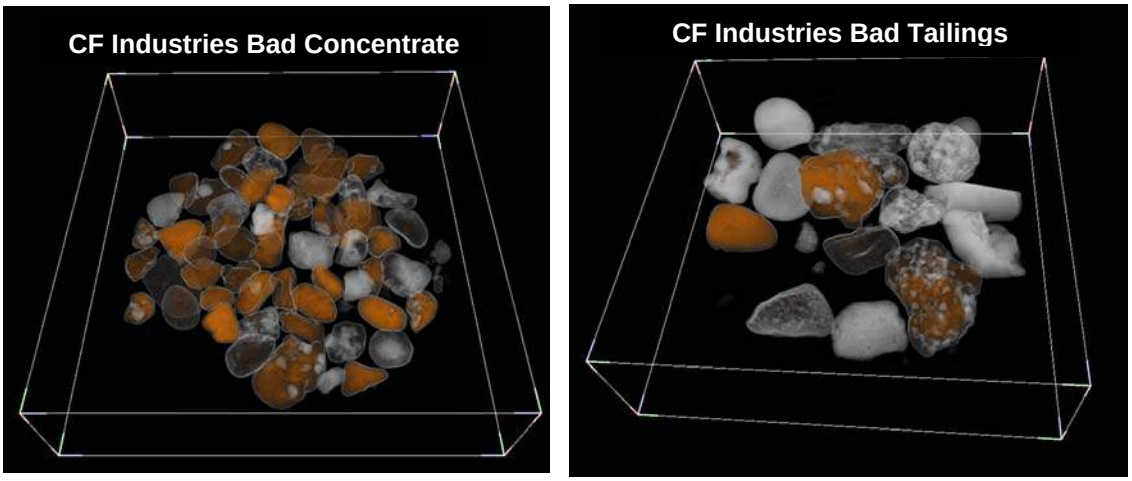

Figure 24. Volume Rendering 3D Reconstructed XMT Images of the Concentrate and Tailings from the CF Industries Bad Sample. Phosphate phase is brown-yellow color and gangue is white.

Individual particles from the tailings of the CF Industries bad sample were segmented and their X-ray linear attenuation coefficient histograms were analyzed. Particles identified by particle number and their corresponding histograms of X-ray linear attenuation coefficients are shown in Figures 25 and 26, respectively. A detailed analysis of each particle is summarized in Table 8.

Table 8. Characterization of Particles from Tailings of CF Industries Bad Sample.

Particle Type	Particle No.	Description
Phosphate	4	Pure phosphate phase
Locked	5,6,14 2,10,15,16,17	Phosphate (dominant), gangue inclusions Gangue (dominant).
Gangue	1,7,8,9,12,13	Pure gangue phase

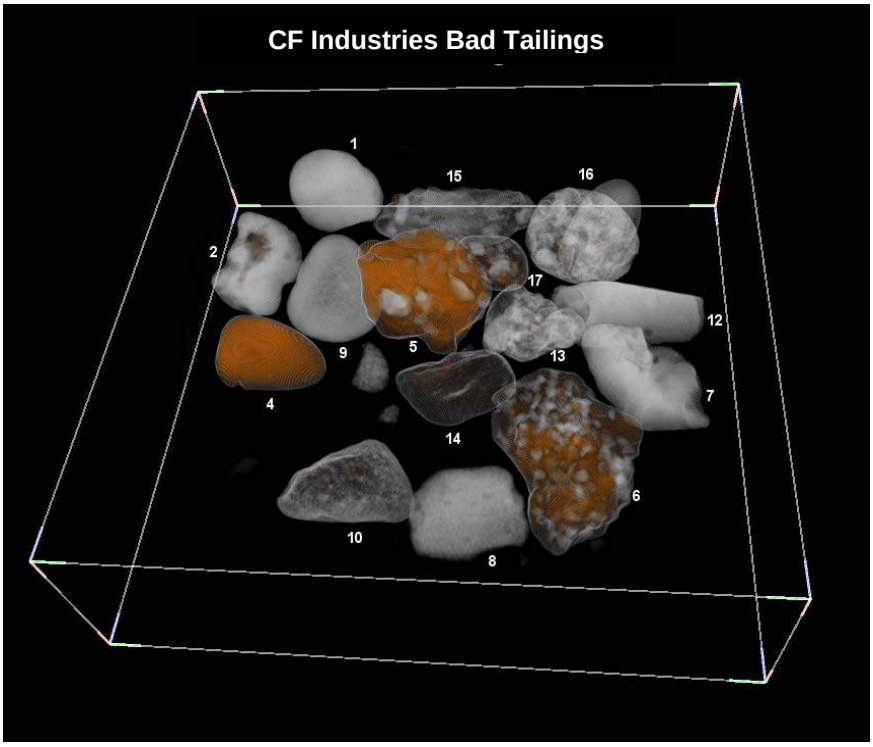

Figure 25. Labeled Particles from CF Industries Bad Tailings Sample.

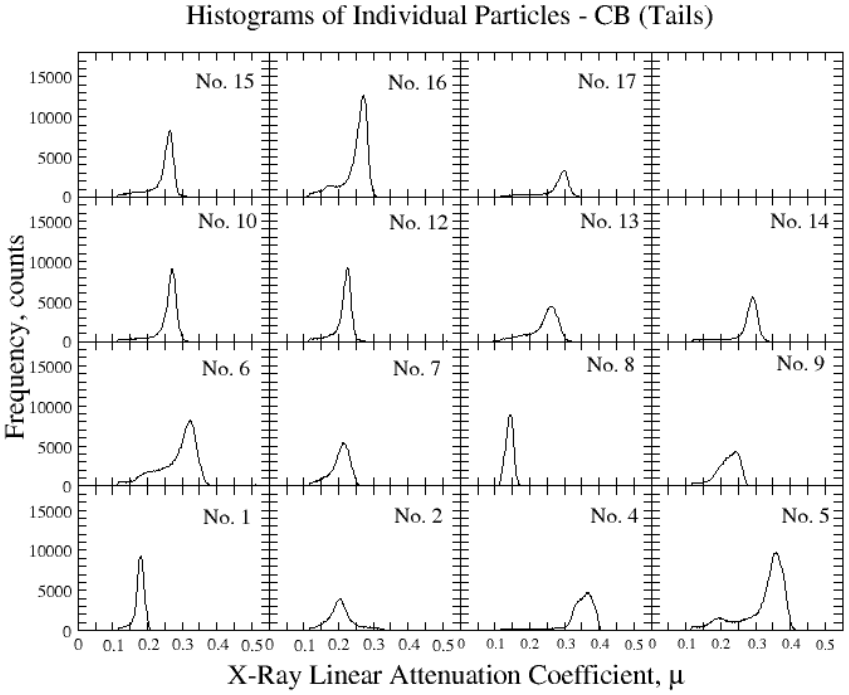

Figure 26. Histograms of Scaled X-ray Attenuation Coefficients of Individual Particles from the Tailings of CF Industries Bad Sample.

Concentrate and Tailings from the Four Corners Bad Sample

Volume rendering of the 3D reconstructed XMT images for the concentrate and tailings from the Four Corners Bad sample are shown in Figure 27.

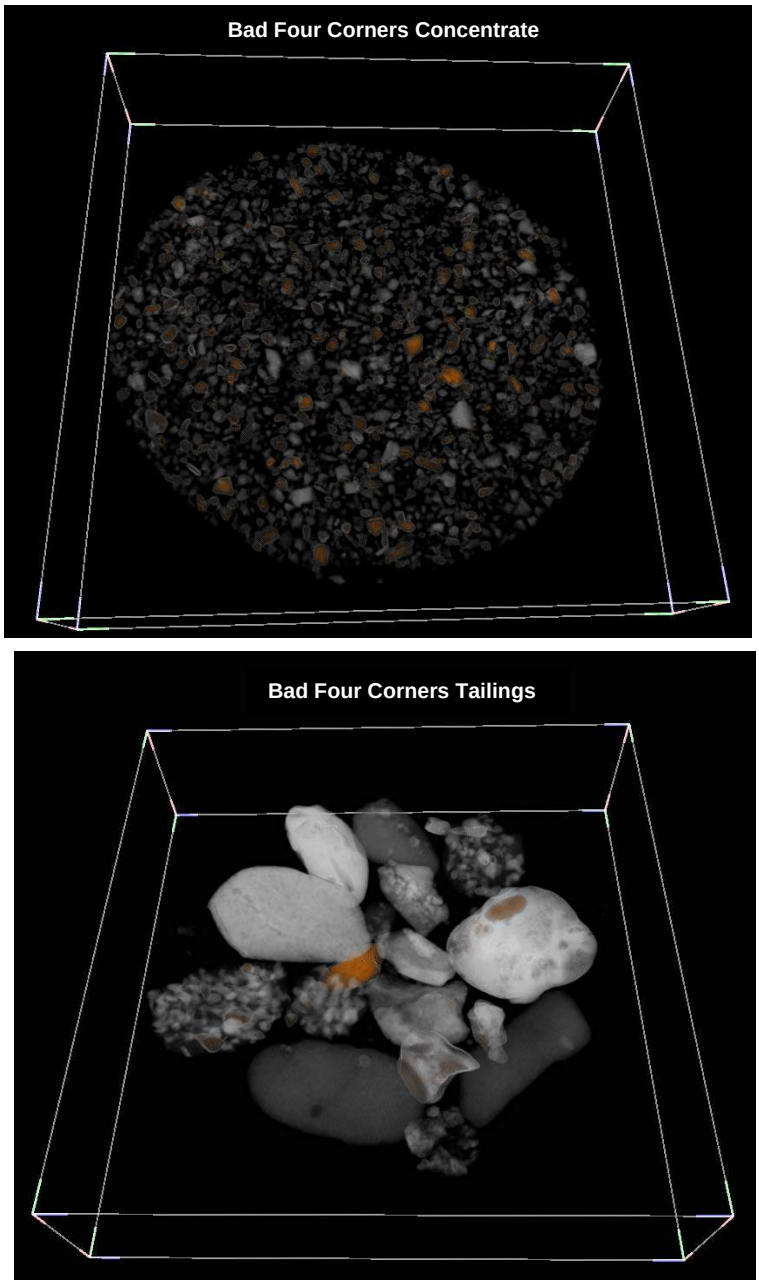

Figure 27. Volume Rendering 3D Reconstructed XMT Images of the Concentrate and Tailings from the Four Corners Bad Sample. Phosphate phase is brown-yellow color and gangue is white.

Individual particles from the tailings of the bad Four Corners sample were segmented and their X-ray linear attenuation coefficient histograms were analyzed. The particles identified by particle number and their corresponding histograms of X-ray linear attenuation coefficients are shown in Figures 28 and 29, respectively. A detailed analysis of each particle is summarized in Table 9.

Table 9. Characterization of Particles from Tailings of the Four Corners Bad Sample.

Particle Type	Particle No.	Description
Phosphate	13	Pure phosphate phase
Locked	1,8,10,11,15	Gangue (dominate).
Gangue	2,3,4,5,6,7,14,15,16	Pure gangue phase

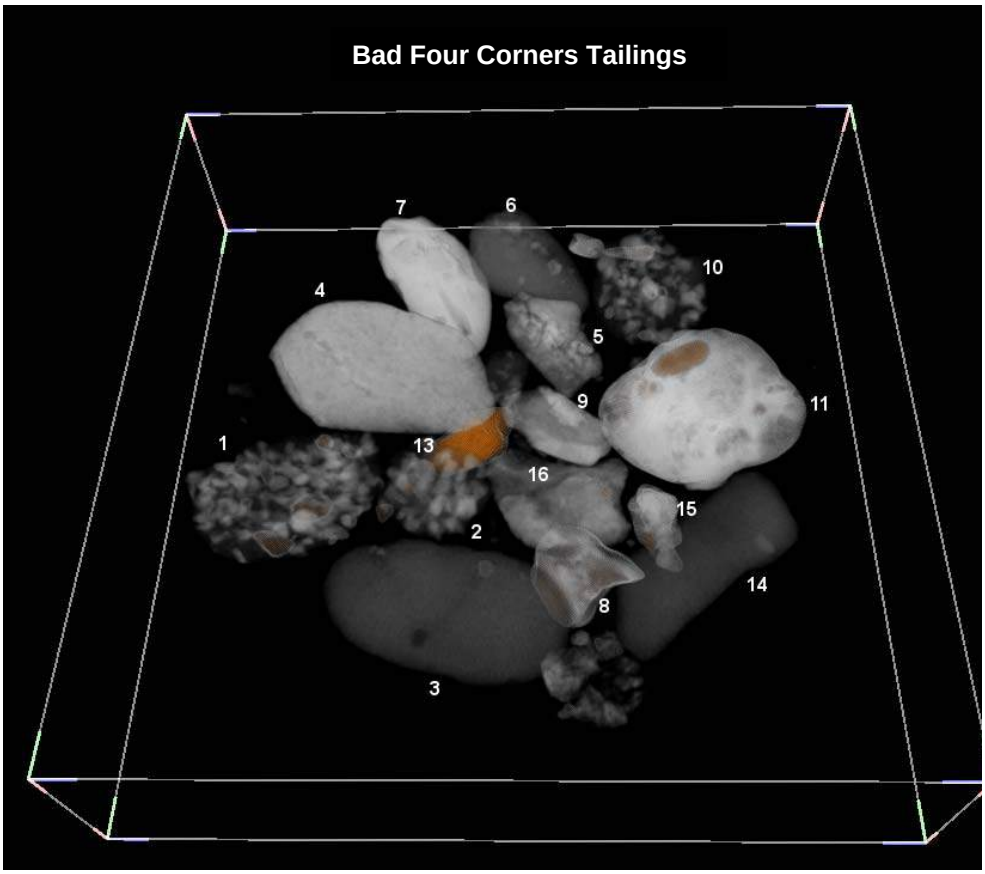

Figure 28. Labeled Particles from Four Corners Bad Tailings Sample.

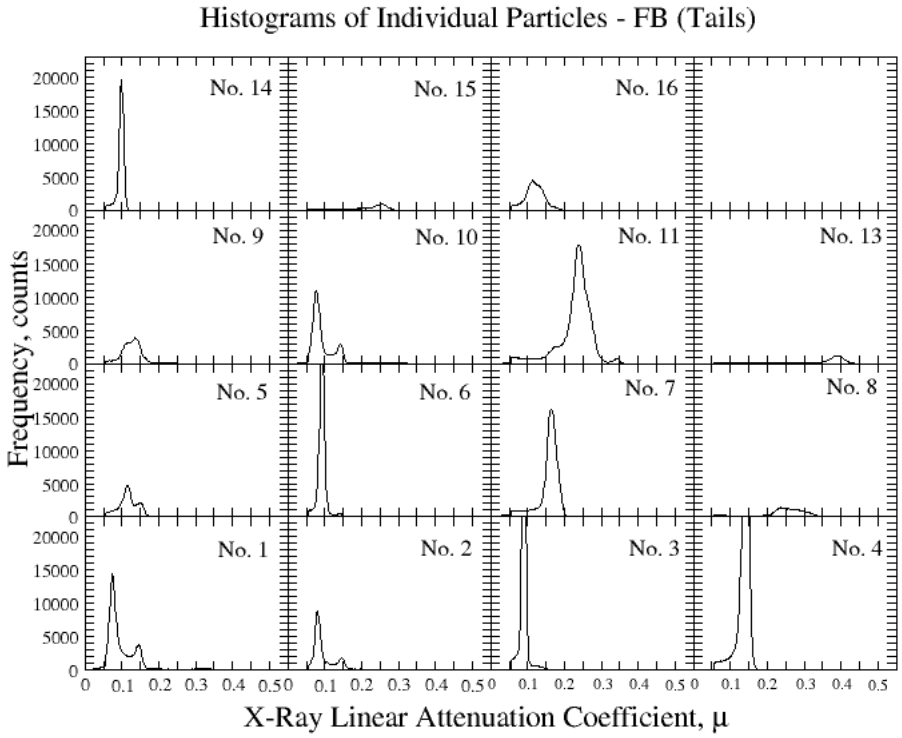

Figure 29. Histograms of Scaled X-Ray Attenuation Coefficients of Individual Particles from the Tailings of Four Corners Bad Sample.

The XMT scans clearly indicated that most of the phosphate particles (brown-yellow) in the tailings of the CF Industries Bad and Four Corners Bad samples are locked particles. Furthermore, most of the phosphate particles in the concentrate are rich in the phosphate phase with few inclusions of the gangue phase. However, not only the amount of locked particles but also their type is of great importance.

Correlation of CT Data with Chemical Analysis

A number of samples from different Florida phosphate deposits were analyzed by chemical analysis (wt. % BPL) and by XMT at 50 kV and 20 micron resolution (vol. % phosphate mineral). The samples are characterized by a phosphate mineral phase of varying microporosity. The density of nonporous apatite (single crystal) is reported to be between 3.1-3.3 g/cm^3, and this corresponds to an attenuation coefficient (μ) value of 0.53. However due to porosity considerations a lower average attenuation coefficient corresponds to the collophanite phosphate mineral present in these Florida samples. In the case of the CF samples, the average attenuation coefficient for collophanite is 0.3 and on this basis the correlation of the chemical analysis (wt. % BPL) with the volume percent phosphate mineral determined by XMT is presented in Figure 30. The

relationship predicted from Equation 1 was based on a gangue mineral density of 2.65 g/cm^3 and a phosphate mineral of 1.75 g/cm^3, as estimated from the CT data.

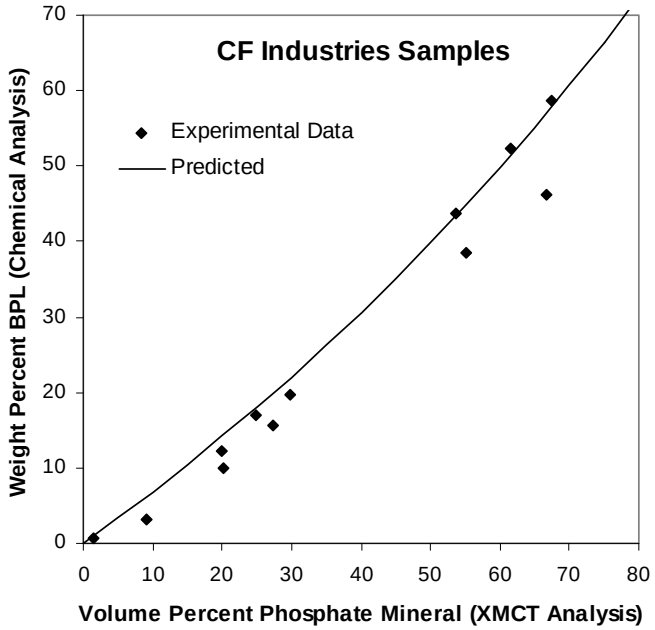

Figure 30. Correlation between Chemical Analysis Data in Weight Percent BPL and Volume Percent Phosphate Mineral from XMT Data for the CF Industries Samples from Florida Phosphate Operations. The solid line is the predicted relationship calculated from equation 1, with gangue mineral density = 2.65 g/cm^3 and phosphate mineral density = 1.75 g/cm^3, as estimated from CT data.

Micro CT Analysis, Liberation-Limited Grade Recovery Curves

As mentioned before, the mineral liberation analyses were carried out using XMT data to classify the sample constituent particles into twelve grade classes based on phosphate areal grade percent (2D liberation analysis) and phosphate volume grade percent (3D liberation analysis). The grade classes are as follows: 0%, 5%, 15%, 25%, 35%, 45%, 55%, 65%, 75%, 85%, 95% and 100% phosphate. These analyses were carried out for the feed and flotation products of samples from Four Corners Bad, Four Corners Good, CF Industries Bad and CF Industries Good samples received in 2007.

Grade/recovery curves limited only by the liberation characteristics were constructed from Micro CT scans of feed samples in each case. The grades of each feed sample and flotation products (concentrate and tailings) were calculated from XMT data and the recovery of phosphate in the concentrate was then calculated using the two-product formula (Equation 1). A summary with respect to recovery limitation for each of the 2007 samples is presented in Table 10.

Table 10. Recovery Limitations as Revealed by Micro CT Analysis of the 2007 Samples.

Sample	Micro CT			Flotation @ 1Lb./T, 180s	Limitation to Recovery
	No. of Particles Analyzed	Grade [%]	Recovery (%)	Recovery (%)	
Four Corners Feed (Bad)	25122	15.97	38.42	~23	Other Factors Major Effect
Four Corners Concentrate (Bad)	32826	37.94			
Four Corners Tailings (Bad)	19610	11.73			
Four Corners Feed (Good)	20928	12.88	92.73	~92.5	Liberation
Four Corners Concentrate (Good)	33243	53.34			
Four Corners Tailings (Good)	20177	1.21			
CF Industries Feed (Bad)	5994	29.72	80.23	~89	Other Factors to Some Extent
CF Industries Concentrate (Bad)	3723	67.40			
CF Industries Tailings (Bad)	1757	9.10			
CF Industries Feed (Good)	7690	27.25	95.12	~97	Liberation
CF Industries Concentrate (Good)	9869	55.10			
CF Industries Tailings (Good)	15094	1.46			

It is evident from this detailed CT analysis that improved separation cannot be achieved for the Four Corners Good and CF Industries Good samples unless improved liberation of the feed is achieved by size reduction (Figures31B and 31D). On the other hand, in the case of the CF Industries Bad sample some slight improvement in efficiency might be achieved by improved flotation conditions. For example, in the best case recovery could be increased from 80% to ~95% at the same grade (Figure 31C). In the case of the Four Corners Bad sample, considerable improvement in recovery and grade should be possible by improved flotation conditions (Figure A). In this case it is clear that efficiency is limited by factors other than liberation, such as slime coatings, surface structure, surface composition, etc.

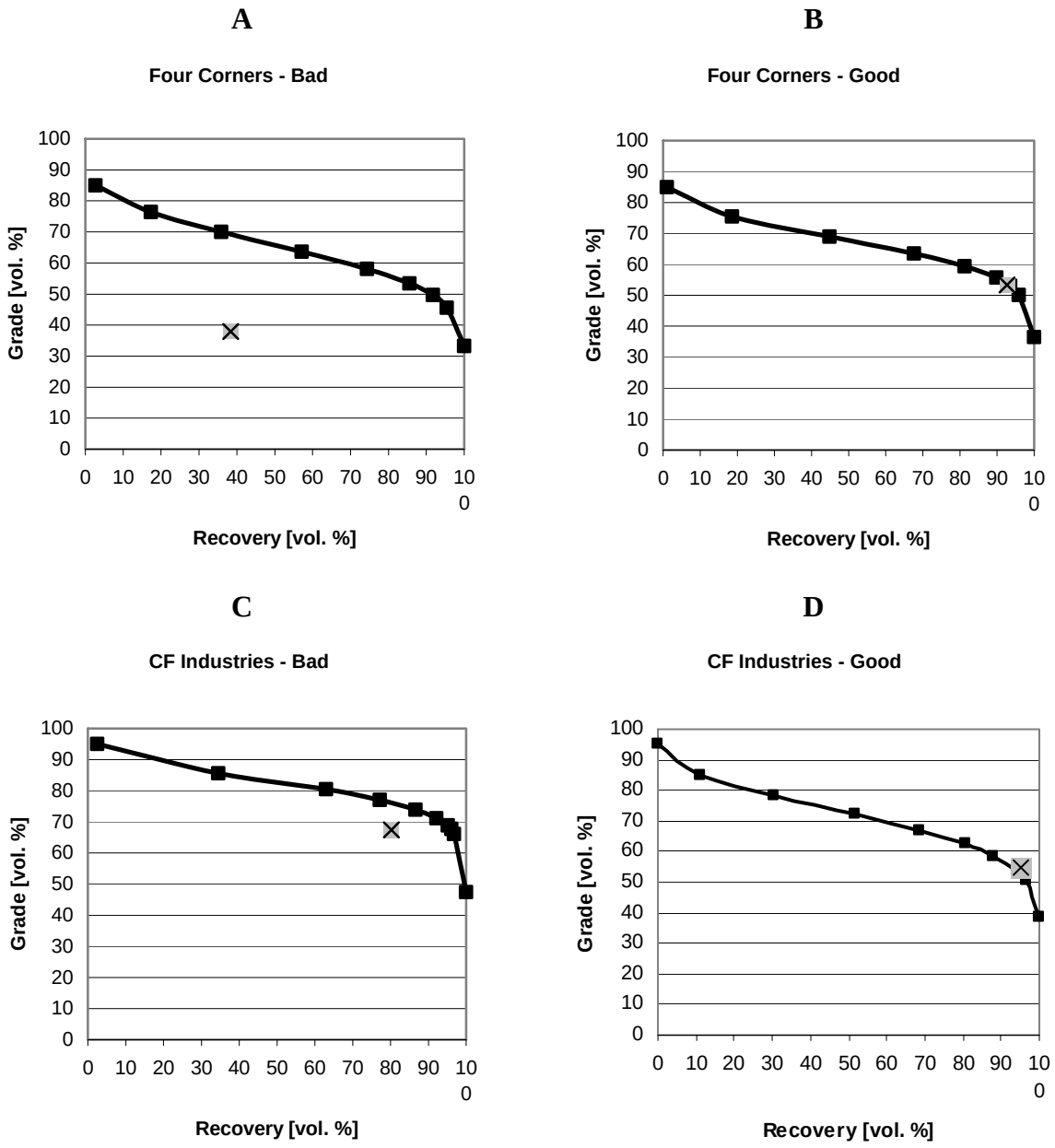

Figure 31. Liberation-Limited Grade/Recovery Curves for the 2007 Samples. Actual recoveries are marked with a cross on a gray background. Key: A - Liberation-limited grade/recovery curve for the Four Corners Bad feed; B - Liberation-limited grade/recovery curve for the Four Corners Good feed; C - Liberation-limited grade/recovery curve for the CF Industries Bad feed; D - Liberation-limited grade/recovery curve for the CF Industries Good feed.

CHARACTERIZATION OF 2008 SAMPLES

Mineralogical Analysis by X-Ray Diffraction (XRD)

Hole 1862 Split 2

The mineralogical analysis (Figure 32 and Table 11) of the 1862-S2 feed indicates that the feed is composed essentially of quartz (52.66%) and apatite (44.84%) with small percentages of calcite, dolomite, gypsum and kaolinite. The flotation results show that there is no effective separation where all constituent minerals are represented in both concentrate and tailings products.

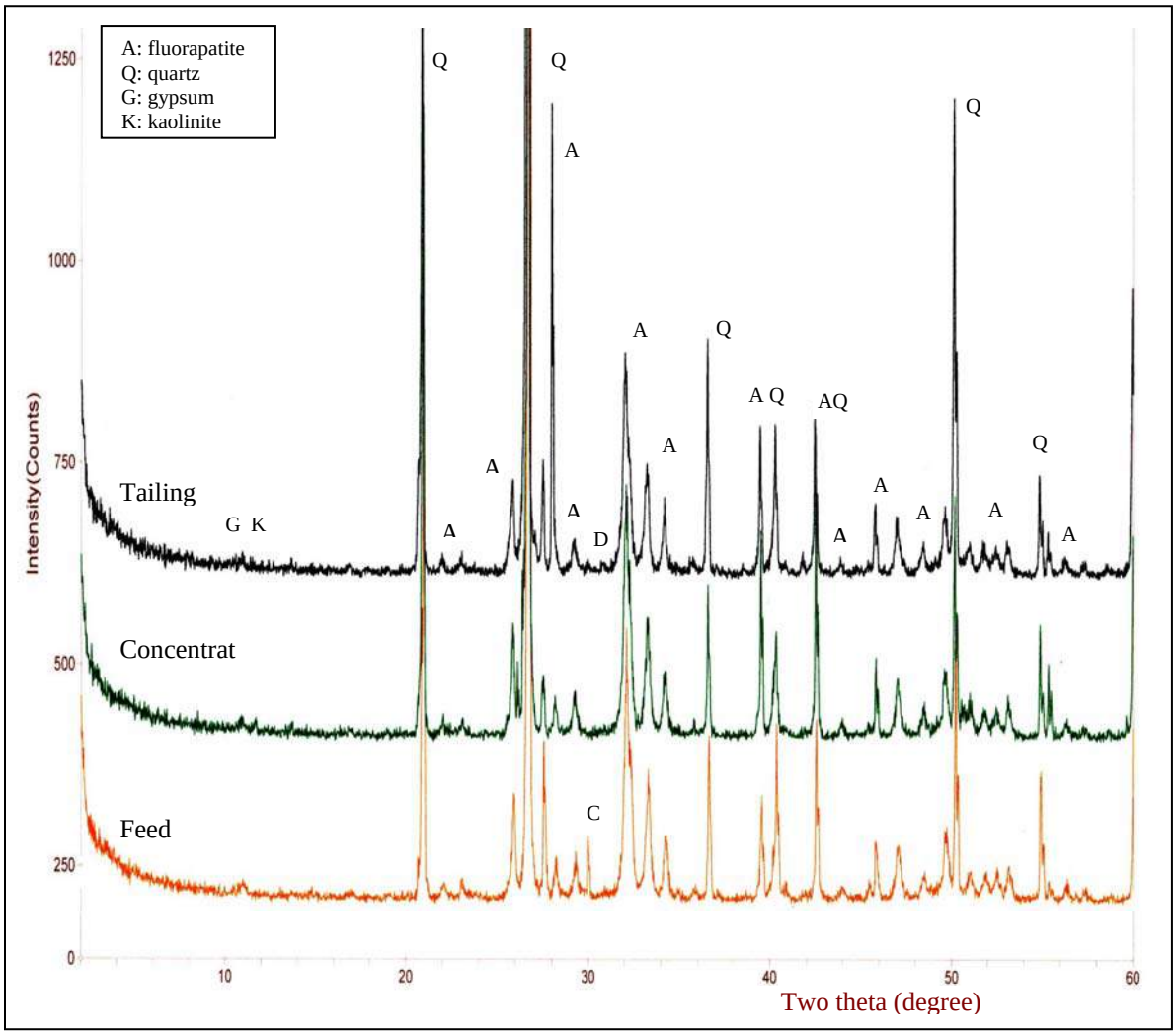

Figure 32. X-Ray Diffraction Patterns of the 1862-S2 Feed, Concentrate and Tailings.

Table 11. Mineral Composition of 1862-S2 Feed and Flotation Products.

Sample	Mineral Composition (%)				
	Quartz	Apatite	Clays	Carbonate	Gypsum
Feed	52.66	44.84	0.58	0.58	1.38
Concentrate	47.56	51.23	0.05	0.10	0.81
Tailings	59.92	39.44	0.83	0.64	1.32

Hole 464 Split 1

X-ray diffraction patterns (Figure 33) and microscopic investigation (Table 12) of the 464-S1 feed indicate that the feed is composed essentially of quartz (79.11%) and apatite (17.97%) with small percentages of gypsum and kaolinite. These patterns show that there is no effective separation where all constituent minerals are represented in both concentrate and tailings products.

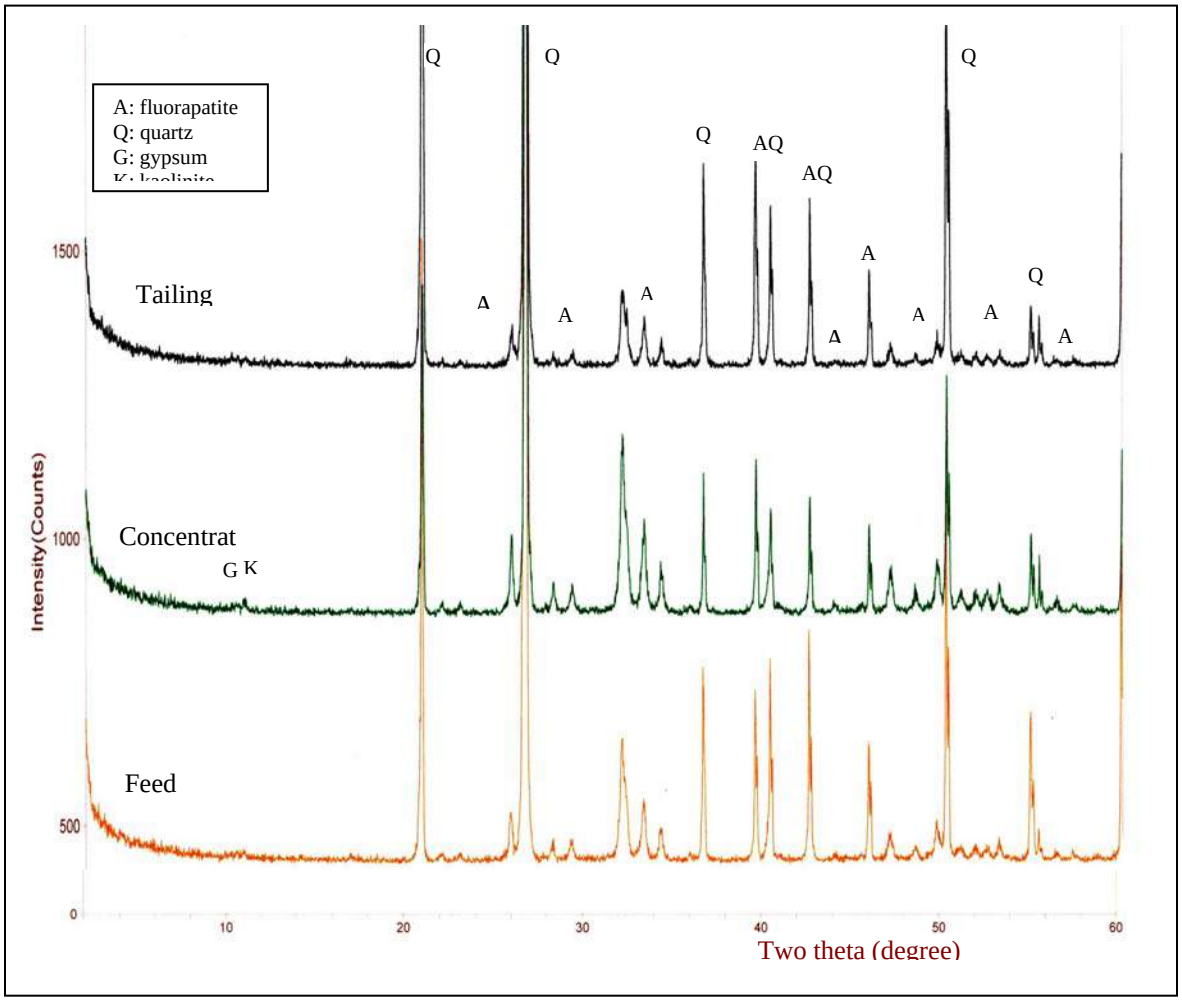

Figure 33. X-Ray Diffraction Patterns of the 464-S1 Feed, Concentrate and Tailings.

Table 12. Mineral Composition of 464-S1 Feed and Flotation Products.

Sample	Mineral Composition (%)				
	Quartz	Apatite	Clays	Carbonate	Gypsum
Feed	79.11	17.97	1.62	0.0	1.29
Concentrate	75.59	22.09	1.37	0.0	1.16
Tailings	84.87	14.48	1.02	0.0	0.32

Hole 464 Split 2

The mineralogical analysis (Figure 34 and Table 13) indicate that the 464-S2 feed sample is composed essentially of quartz (71.75%), apatite (27.83%) in addition to small percentage of gypsum and kaolinite. Quartz is still present at a good percentage in the concentrate (41%) and the phosphate grade of the tailings is 7%. Kaolinite and gypsum are also separated with the concentrate.

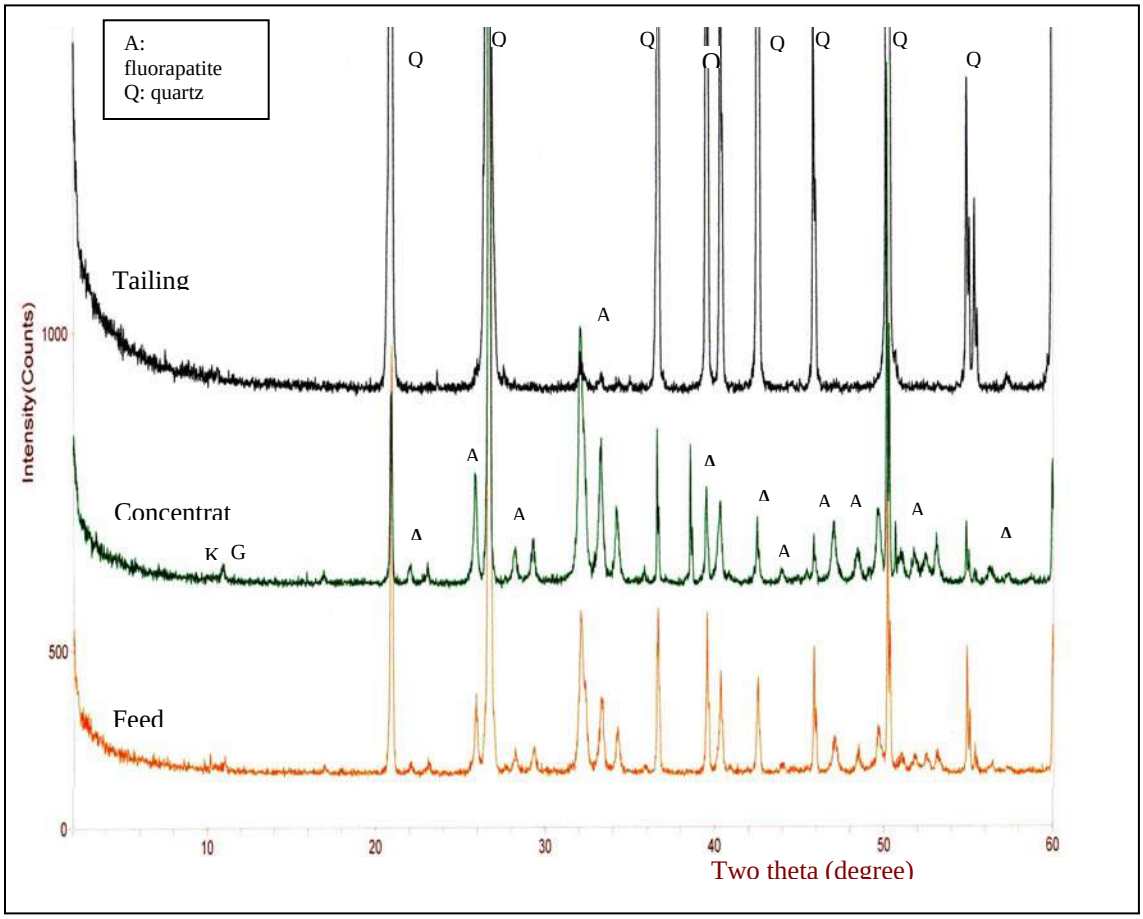

Figure 34. X-Ray Diffraction Patterns of the Hole 464 Split 2 Feed, Concentrate and Tailings.

Table 13. Mineral Composition of Hole 464 Split 2 Feed and Flotation Products.

Sample	Mineral Composition (%)				
	Quartz	Apatite	Clays	Carbonate	Gypsum
Feed	71.75	27.33	0.41	0.0	0.53
Concentrate	40.80	57.50	0.72	0.0	0.97
Tailings	92.87	7.12	0.0	0.0	0.0

CF Combined

The mineralogical analysis (Figure 35 and Table 14) of the CF Combined feed indicates that the feed is composed essentially of quartz (75.51%) and apatite (23.72%), with small percentages of dolomite, gypsum and clay minerals. The clay minerals are represented by kaolinite, montmorillonite and illite. These patterns show that there is effective separation where most of the phosphate is separated in the concentrate and most of the quartz is separated in the tailings, and the phosphate content does not exceed 1.5% in the tailings. Kaolinite and gypsum are separated in the concentrate, while dolomite is distributed in both the concentrate and tailings.

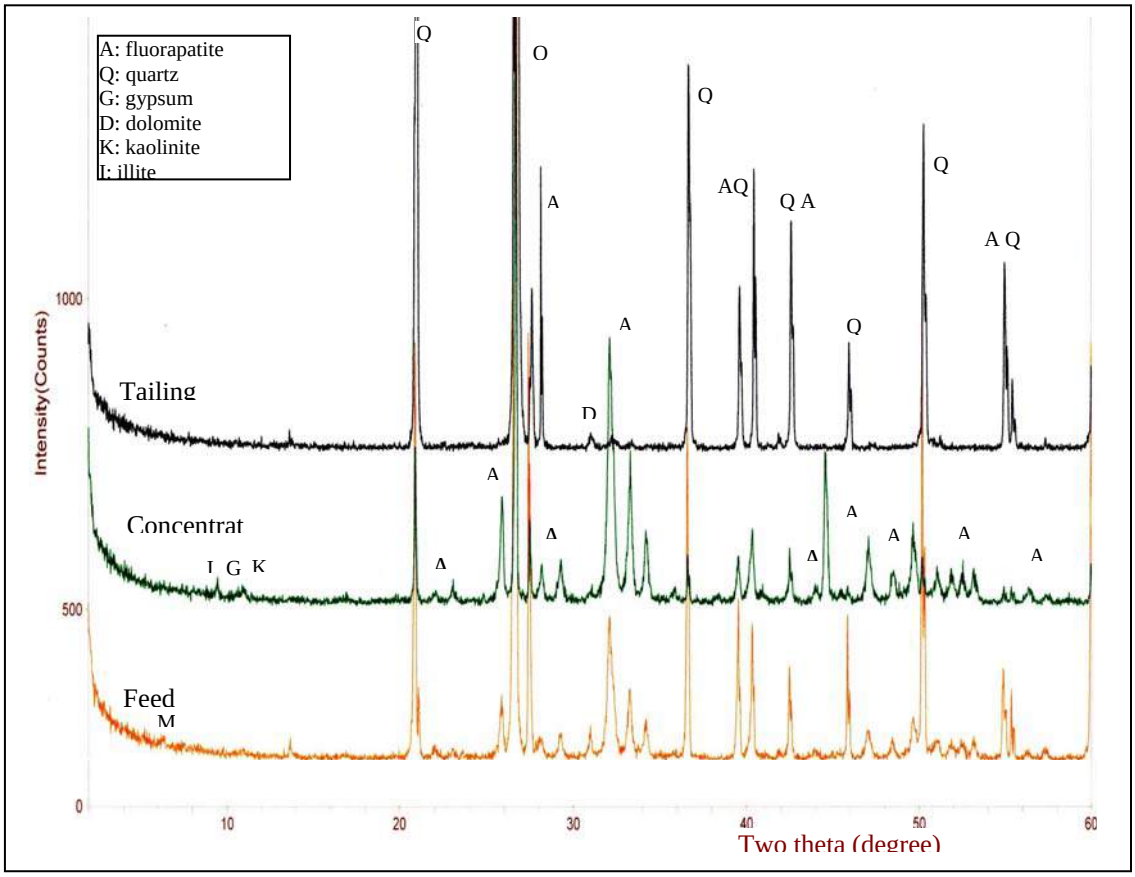

Figure 35. X-Ray Diffraction Patterns of the CF Combined Feed, Concentrate and Tailings.

Table 14. Mineral Composition of CF Combined Feed and Flotation Products.

Sample	Mineral Composition (%)				
	Quartz	Apatite	Clays	Dolomite	Gypsum
Feed	75.5	23.7	~1	~0.5	0.10
Concentrate	31.00	66.50	1.5	0.7	0.3
Tailing	98.08	1.48	0.0	0.24	0.0

CF West Pit

X-ray diffraction analysis (Figure 36) and thin-section investigation (Table 15) of the CF West Pit feed indicates that the feed is composed essentially of quartz (~75%) and apatite (~22%), with a small percentage (~3%) of dolomite, gypsum and clays. The clay minerals are represented by kaolinite, montmorillonite and illite. These results show that there is effective separation by fatty acid flotation where most of the phosphate is separated into the concentrate containing 63% apatite, and most of the quartz is separated into the tailings containing 97% apatite. Kaolinite and gypsum are separated in the concentrate, while dolomite is distributed in both the concentrate and tailings.

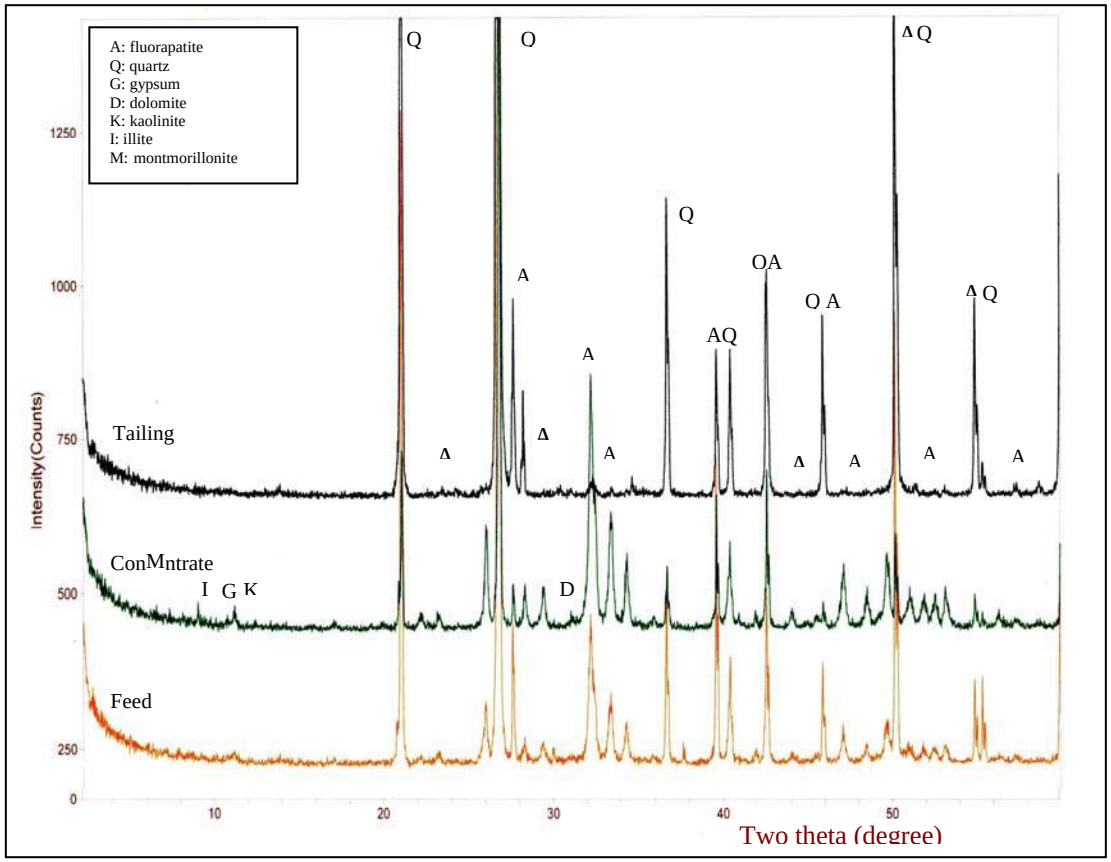

Figure 36. X-Ray Diffraction Patterns of the CF West Pit Feed, Concentrate and Tailings.

Table 15. Mineral Composition of CF West Pit Feed and Flotation Products.

Sample	Mineral Composition (%)				
	Quartz	Apatite	Clays	Dolomite	Gypsum
Feed	75	22	~1	~1	<0.5
Concentrate	36	63	0.5	~1	<0.5
Tailing	97.5	1.5	<0.5	<0.5	-

CF East Pit

The mineralogical analysis (Figure 37, Table 16) of the CF East Pit feed indicates that the feed is composed essentially of quartz (85.5%) and apatite (13%), with small percentages of dolomite and kaolinite. These results show that there is effective separation where almost all the phosphate is separated in the concentrate and containing 76% apatite, while most of the quartz is separated in the tailings product, analyzing 98.5% quartz. Kaolinite is mostly separated in the concentrate, while dolomite is mostly separated in the tailings.

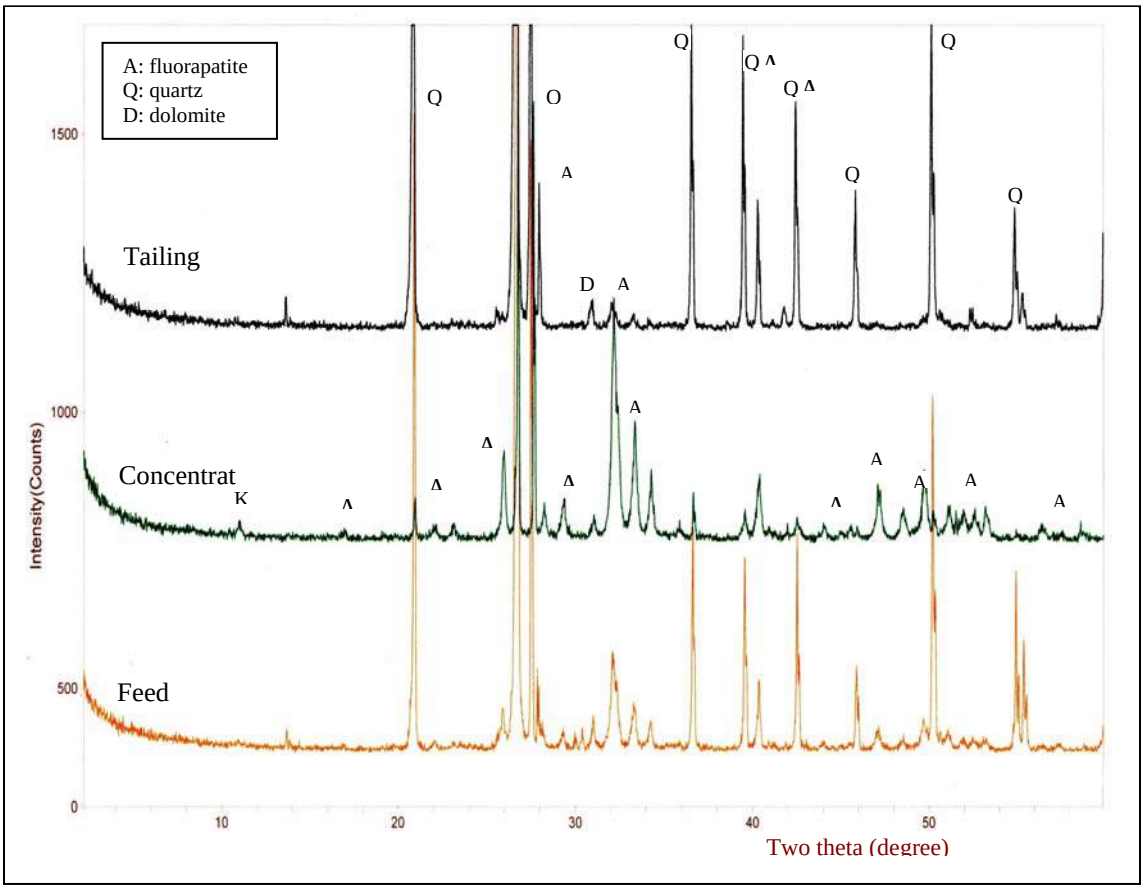

Figure 37. X-Ray Diffraction Patterns of the CF East Pit Feed, Concentrate and Tailings.

Table 16. Mineral Composition of CF East Pit Feed and Flotation Products.

Sample	Mineral Composition (%)				
	Quartz	Apatite	Clays	Dolomite	Gypsum
Feed	85.5	13	<0.5	1	0.0
Concentrate	21	76	0.5	2.5	0.0
Tailing	98.5	1.0	0.0	0.5	0.0

Summary

The present studies indicate that the feed phosphate samples are composed essentially of quartz and apatite in variable percentages. In addition, subordinate amounts of clay minerals (kaolinite, illite, and montmorillonite), gypsum and carbonate minerals (mainly dolomite) are found except for the 464-S1 and 464-S2 feed samples, which are free of carbonate minerals. On flotation separation almost all phosphate minerals are transferred into the concentrates for the good feeds and the phosphate mineral percentage in the good tailings does not exceed 1.5%. In contrast, for the bad feeds there is no great difference between the grade of the concentrates and tailings, except 464-S2 where the concentrate grade was found to be about 58% phosphate and the tailings grade about 7% phosphate.

Surface Chemistry—SEM and EDS Analyses

SEM, in conjunction with energy dispersion spectroscopy (EDS), was performed using a Quanta FEG Model 600, which gives a unique opportunity to analyze the shape of particles as well as their surface and subsurface elemental composition. The EDS signal is collected from a depth of several micrometers, thus giving an idea about the bulk composition rather than the surface composition. As shown in this report, it is possible to obtain information about the elemental composition of a large population of particles, and subsequently focus on individual particles. In turn, the characteristic texture and elemental composition enable us to determine the mineralogy of the particle surface.

Scanning electron microscopy also was used to analyze the particle shape. Additionally, analysis of the elemental composition of the sample was performed using energy dispersion spectroscopy (EDS). Bad and good feed samples from four different streams (1862-S2, 464-S1, CF Combined and CF West) were analyzed using a Quanta FEG Model 600 SEM and an EDAX EDS analyzer at 25 kV and 26 mm working distance. Overall, a small magnification image was taken for each sample with the corresponding large area EDS scan showing the overall elemental composition of the observed image. Subsequently, SEM images and EDS spectra and maps of selected particles were taken.

Hole 1862 Split 2

SEM micrographs of the 1862-S2 feed (Figures 38-42) show a wide range of particle sizes and phosphate particles of elongated and spherical shapes, but the elongated shape is more common. The phosphate particles are mostly coarse in size and are coarser than the associated quartz particles. This feed is rich in gypsum; sometimes gypsum is precipitated in the form of cylindrical crystals around phosphate particles and sometimes it is aggregated in coarse particles. Gypsum is a source of calcium that may interfere in the flotation process. The concentrate (Figures 43-47) is relatively homogenous in particle size, and the presence of gypsum in it is also recorded. In the tailings (Figures 48-52), the phosphate particles are one of the following types: coarse, highly porous, coated with kaolinite, or unliberated. In addition, the phosphate particles in the tailings are more porous than those in the concentrate. The particle shape seems to have some effect on the separation, where elongated and oval particles are common in the concentrate and spherical particles are common in the tailings.

Hole 1862 Split 2 Feed

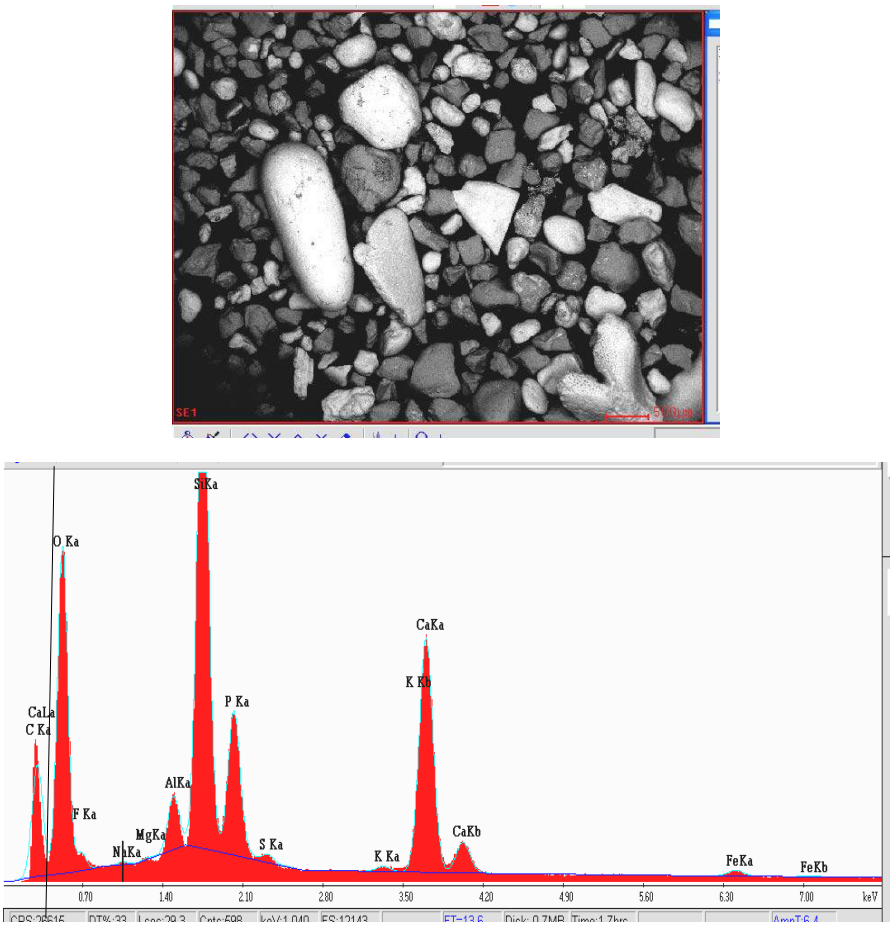

Figure 38. SEM Micrograph of the Hole 1862 Split 2 Feed Showing Heterogeneous Particle Size, and Phosphate Particles (light color) Mostly Coarser Than Quartz Particles (gray color), and EDS Spectrum of Large Area.

Hole 1862 Split 2 Feed

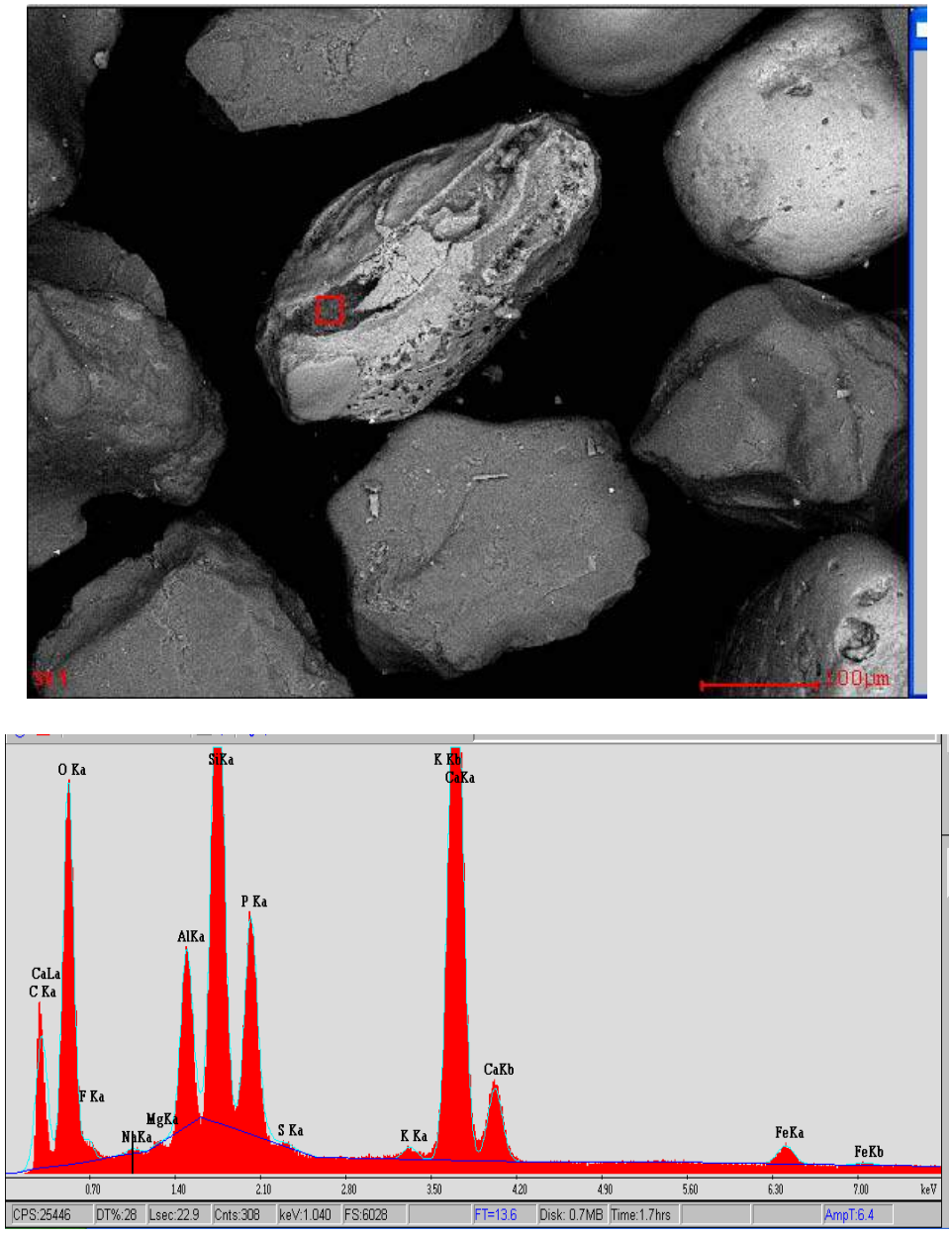

Figure 39. SEM Micrograph of the Hole 1862 Split 2 Feed Showing Phosphate Particle with Clay Minerals and the Corresponding EDS Spectrum for the Clay Minerals.

Hole 1862 Split 2 Feed

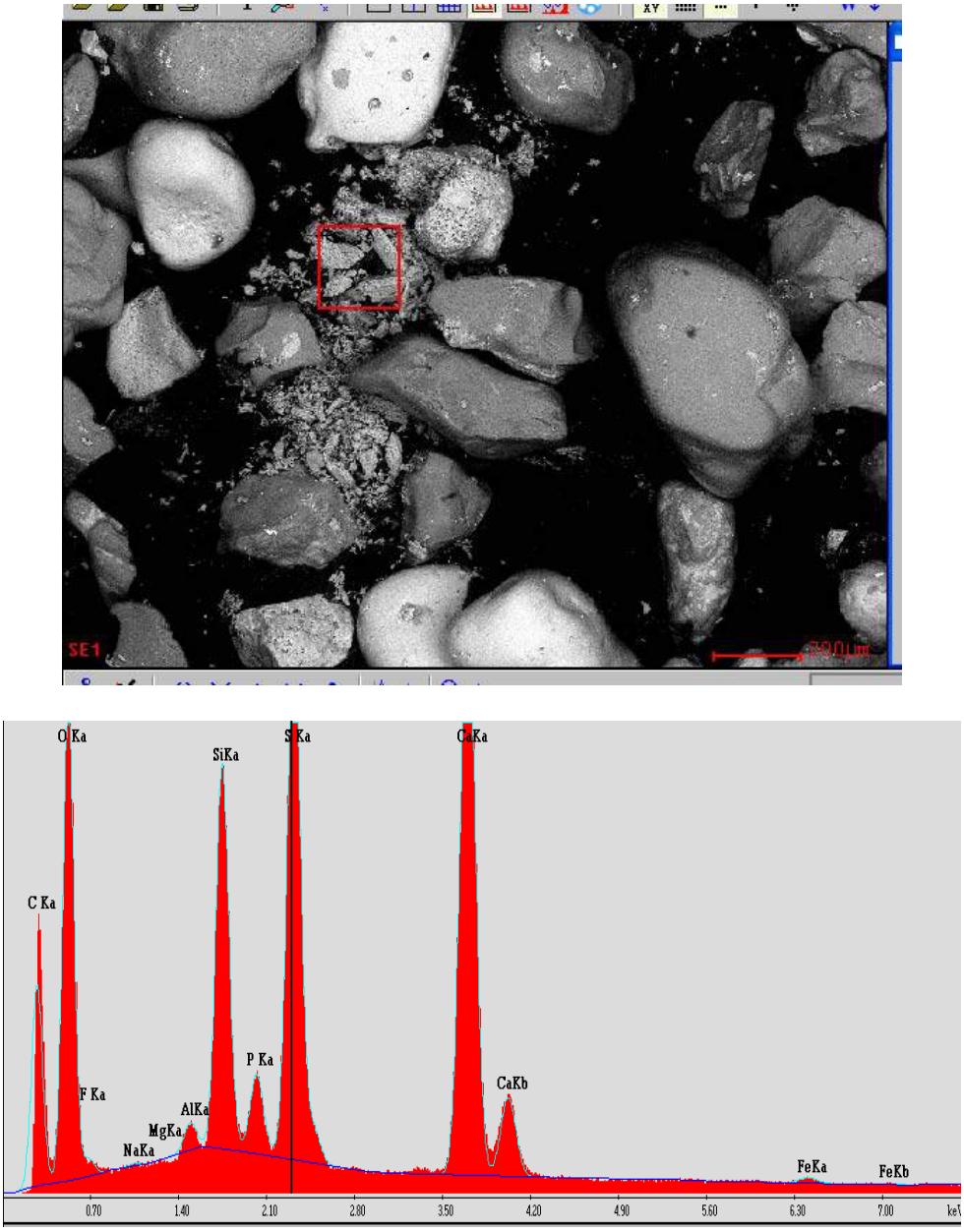

Figure 40. SEM Micrograph of the Hole 1862 Split 2 Feed Showing Soft Gypsum Crystals Fragmented during Sampling for SEM, and Its EDS Spectrum.

Hole 1862 Split 2 Feed

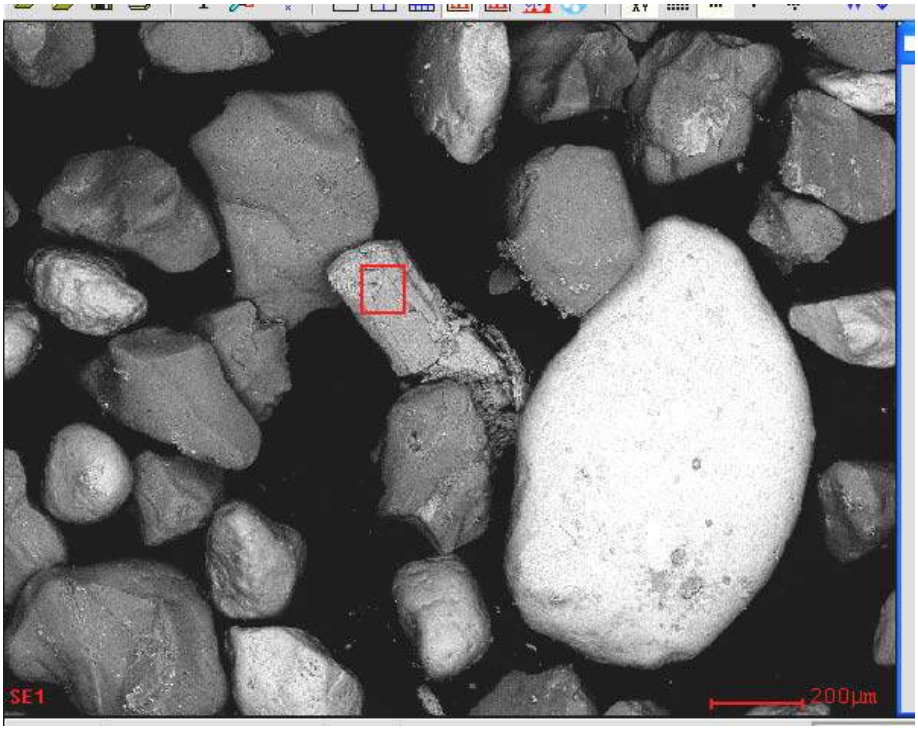

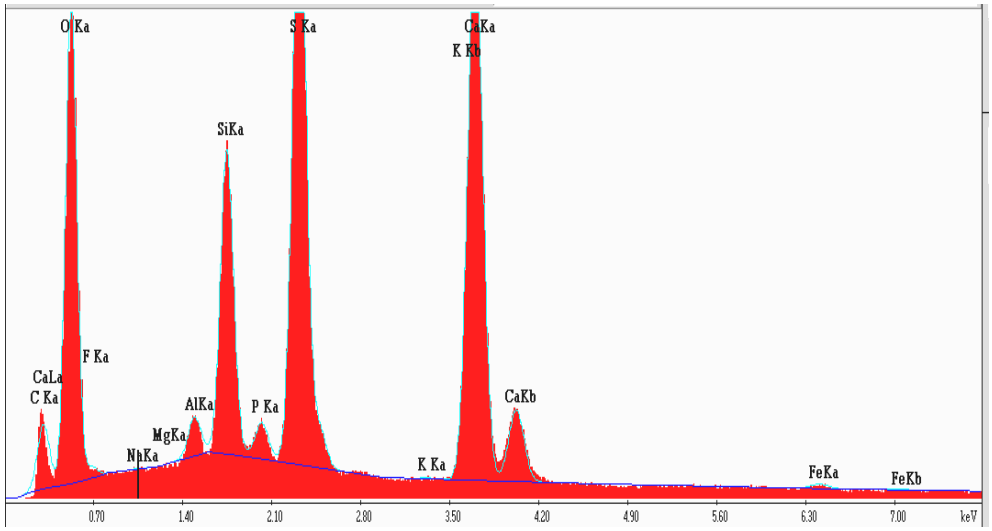

Figure 41. SEM Micrograph of the Hole 1862 Split 2 Feed Showing Cylindrical Gypsum Crystals Surrounding Phosphate Particle and Its EDS Spectrum.

Hole 1862 Split 2 Feed

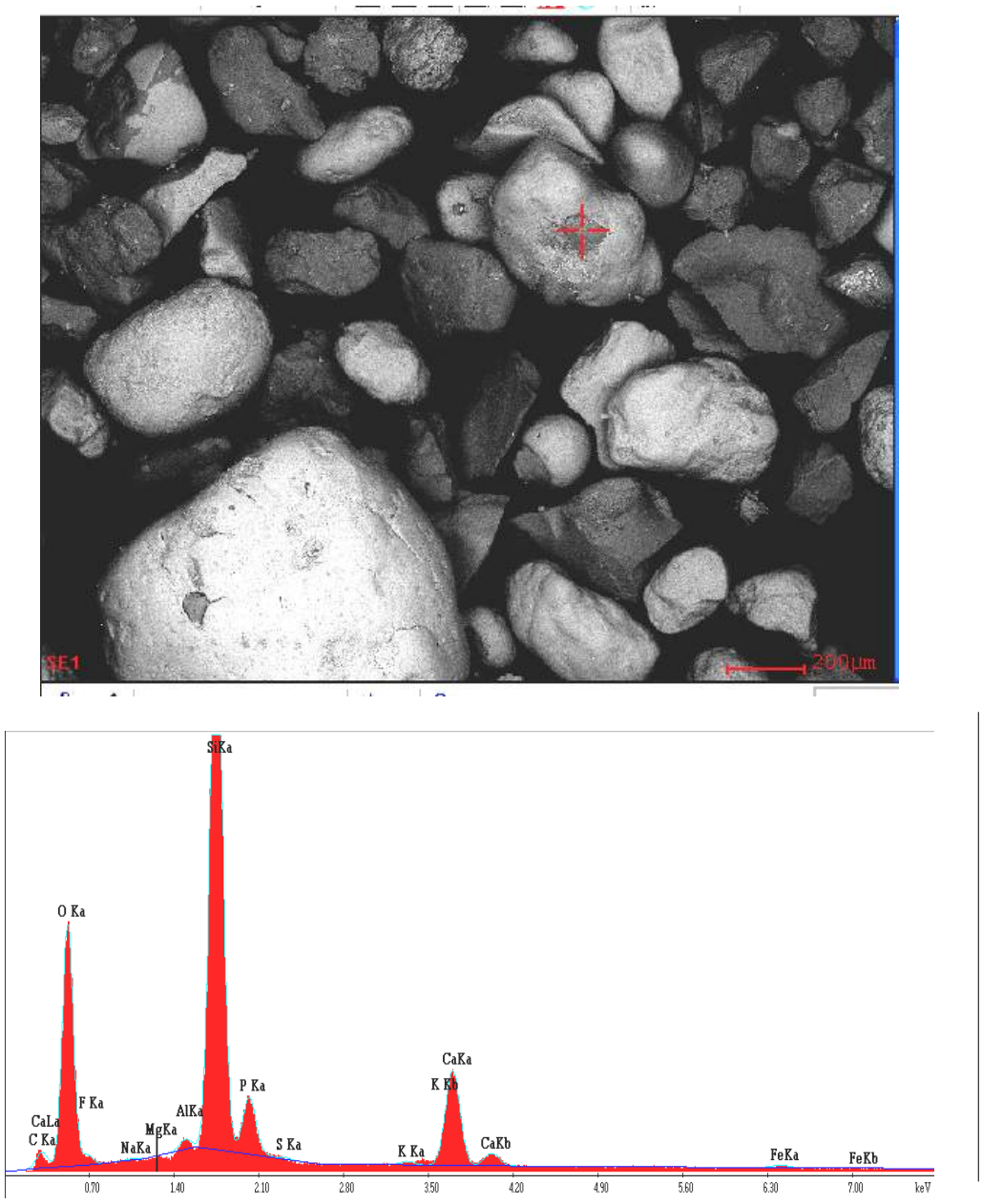

Figure 42. SEM Micrograph of the Hole 1862 Split 2 Feed Showing Silica Attached to Phosphate Particle and Its EDS Spectrum.

Hole 1862 Split 2 Concentrate

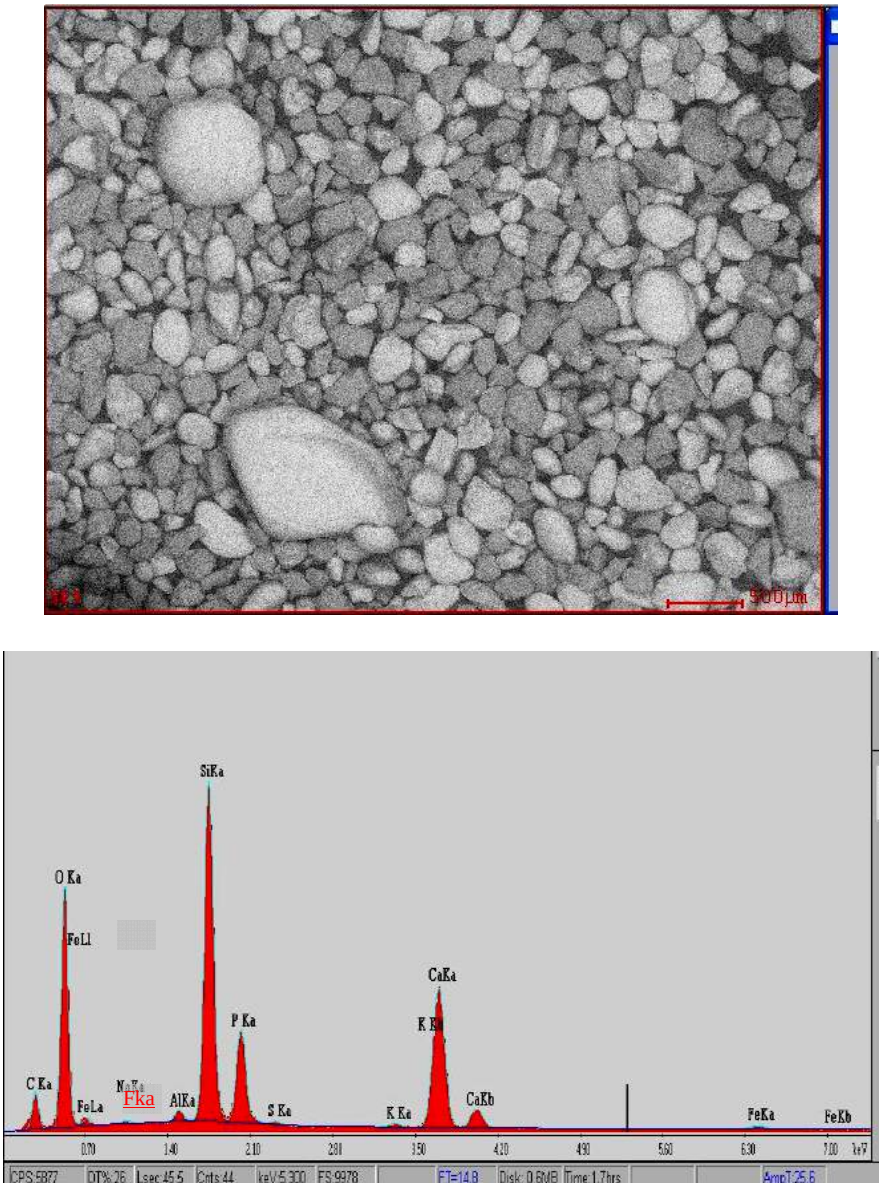

Figure 43. SEM Micrograph of Hole 1862 Split 2 Concentrate Showing Narrow Particle Size Range Except a Few Coarse Phosphate Particles and EDAX of Large Area. Phosphate (white), quartz (gray)

Hole 1862 Split 2 Concentrate

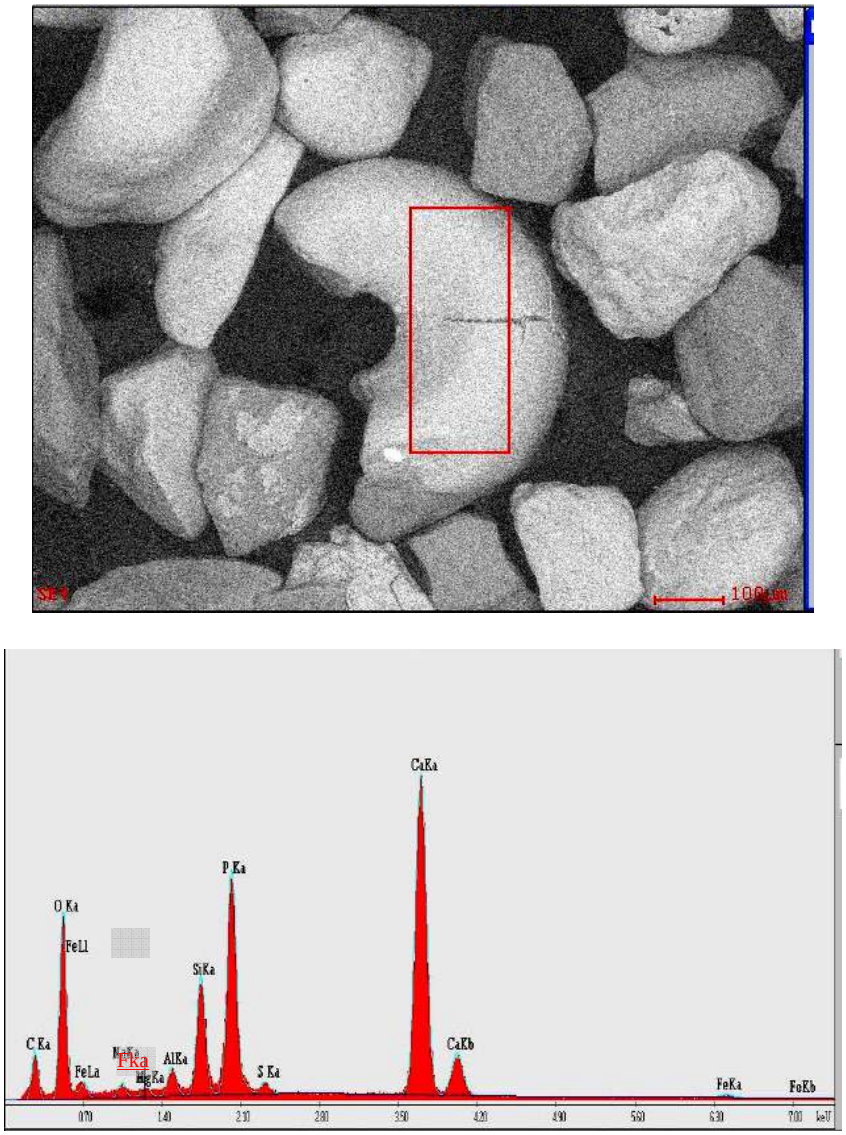

Figure 44. SEM Micrograph of Hole 1862 Split 2 Concentrate Showing Phosphatized Fossil Fragment Surrounded by Phosphate (white) and Quartz (gray) Particles, and Its EDS Spectrum.

Hole 1862 Split 2 Concentrate

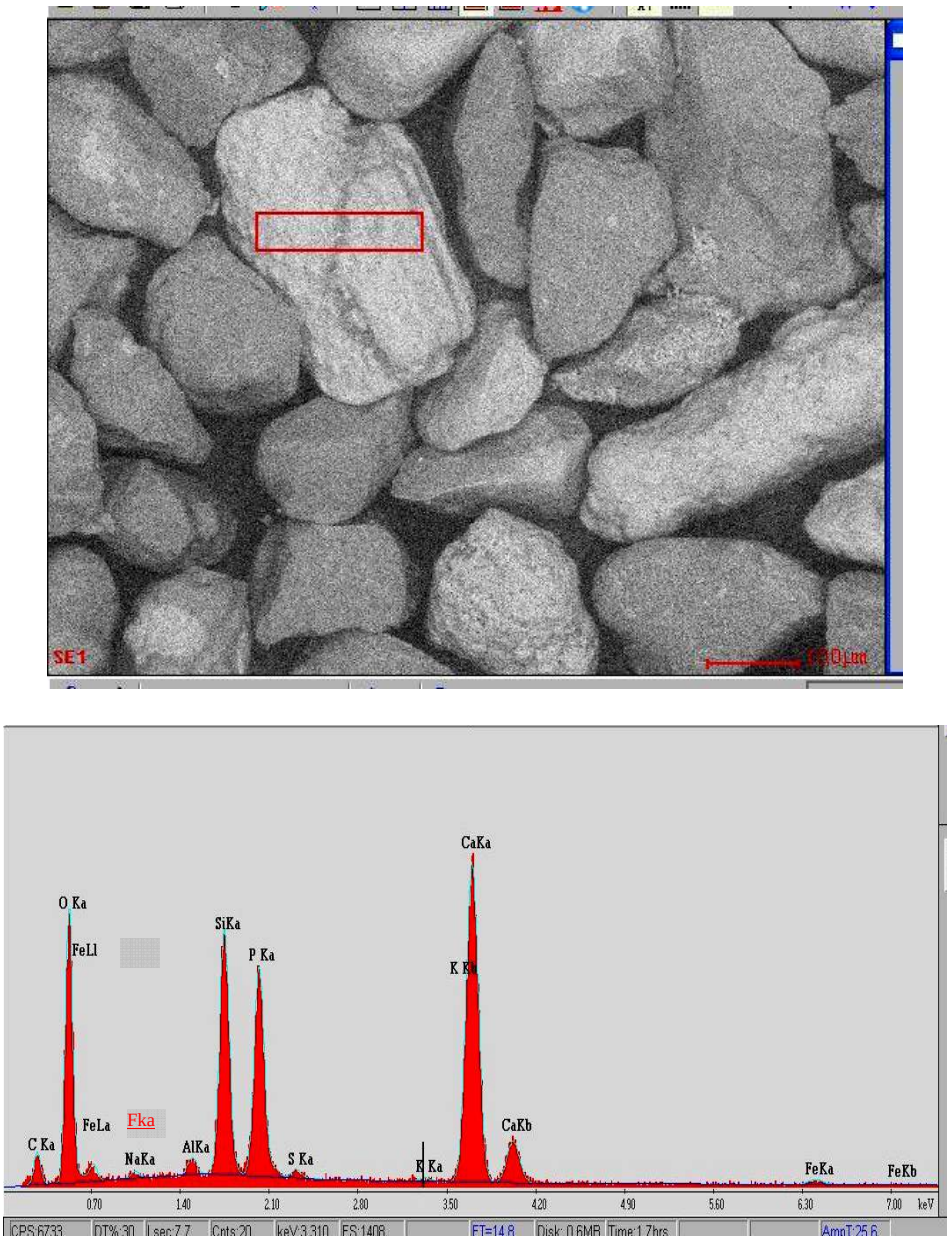

Figure 45. SEM Micrograph of Hole 1862 Split 2 Concentrate Showing Elongated Phosphate Particles and an Ornamented Phosphate Plate and Its EDS Spectrum.

Hole 1862 Split 2 Concentrate

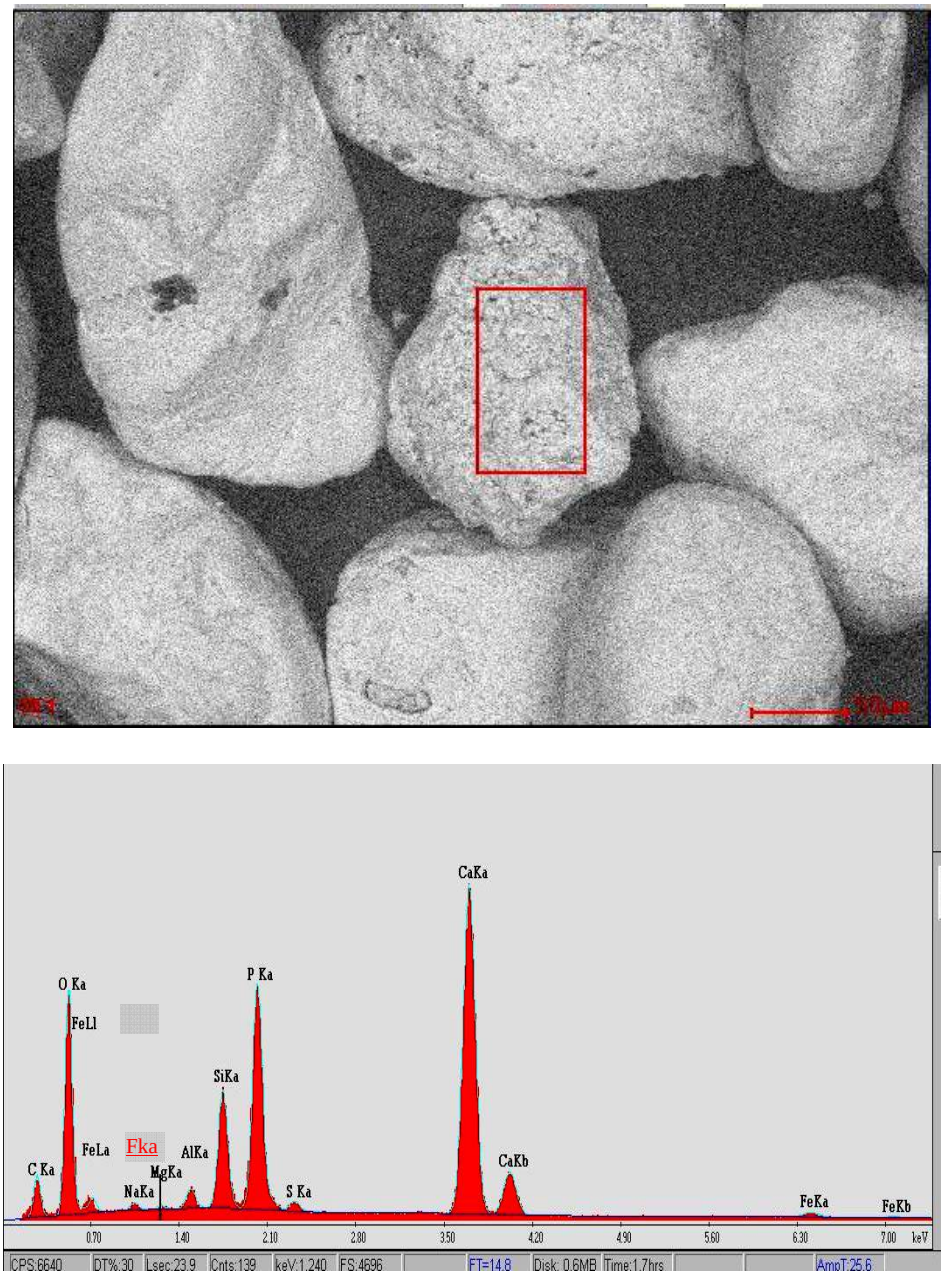

Figure 46. SEM Micrograph of Hole 1862 Split 2 Concentrate Showing the Elongated and Rarely Porous Phosphate Particles and EDS Spectrum of the Marked Particle.

Hole 1862 Split 2 Concentrate

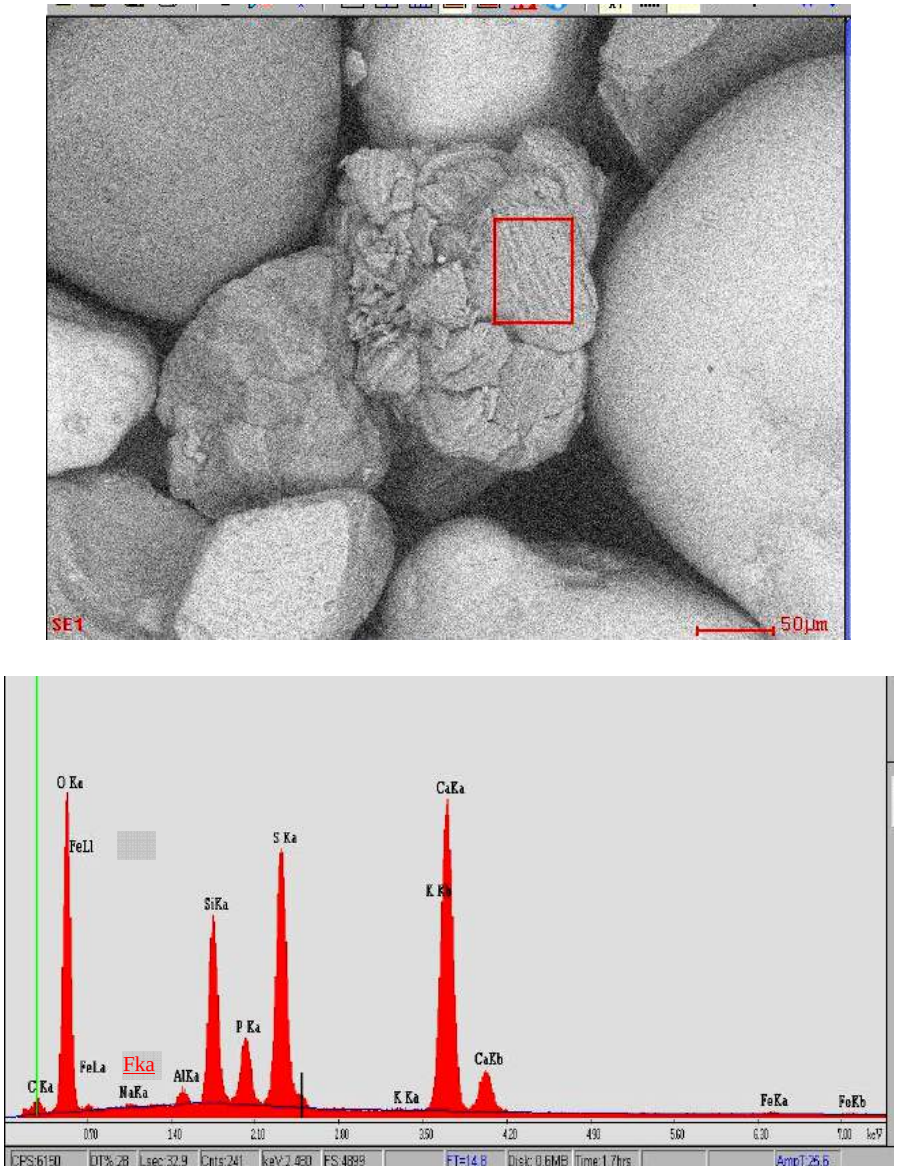

Figure 47. SEM Micrograph of Hole 1862 Split 2 Concentrate Showing Aggregate of Gypsum Striated Plates with Some Silica and Phosphate in between, and EDS Spectrum of One Plate.

Hole 1862 Split 2 Tailings

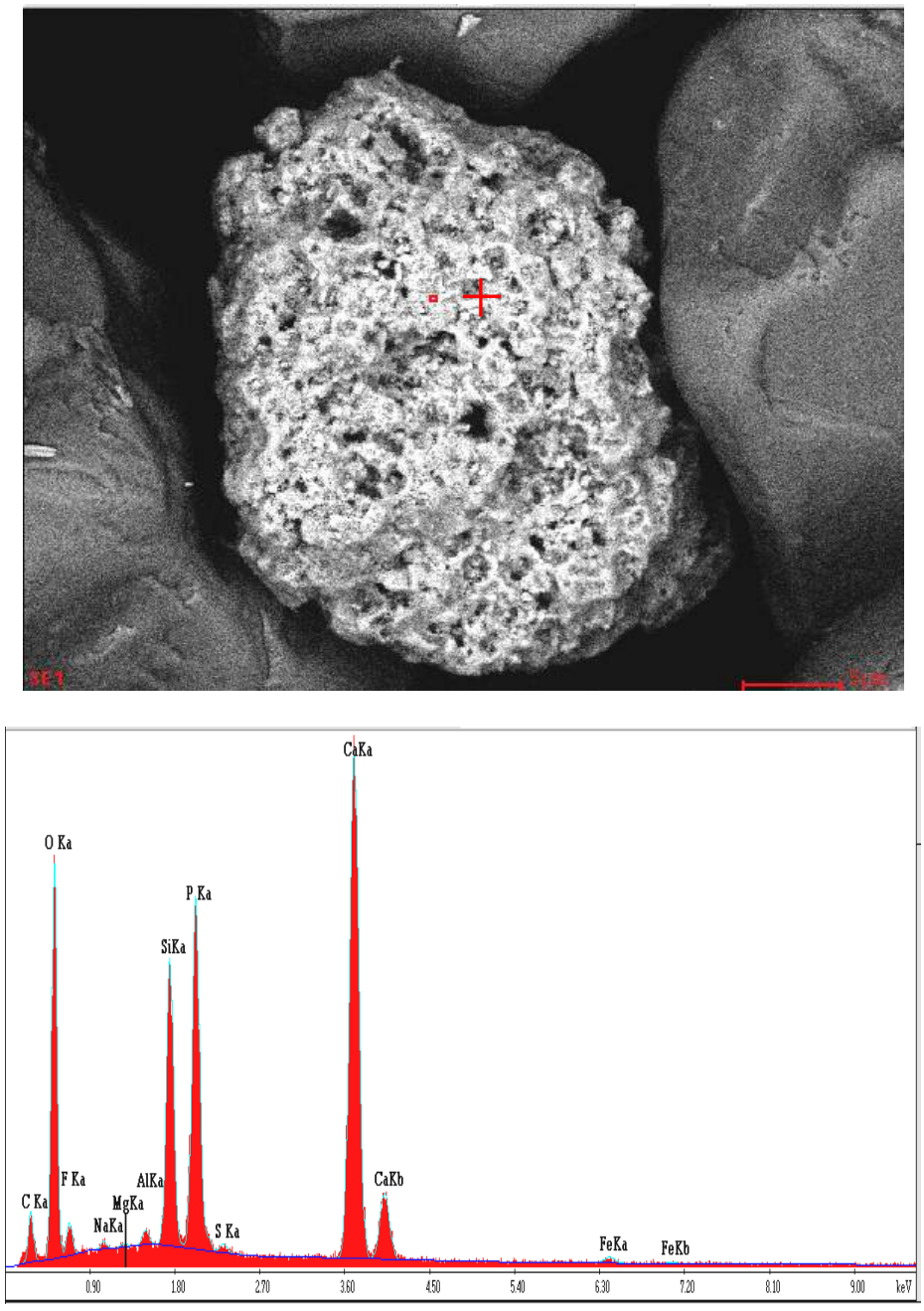

Figure 48. SEM Micrograph of Hole 1862 Split 2 Tailings Showing Highly Porous Phosphate Particle and Local EDS Spectrum of That Particle.

Hole 1862 Split 2 Tailings

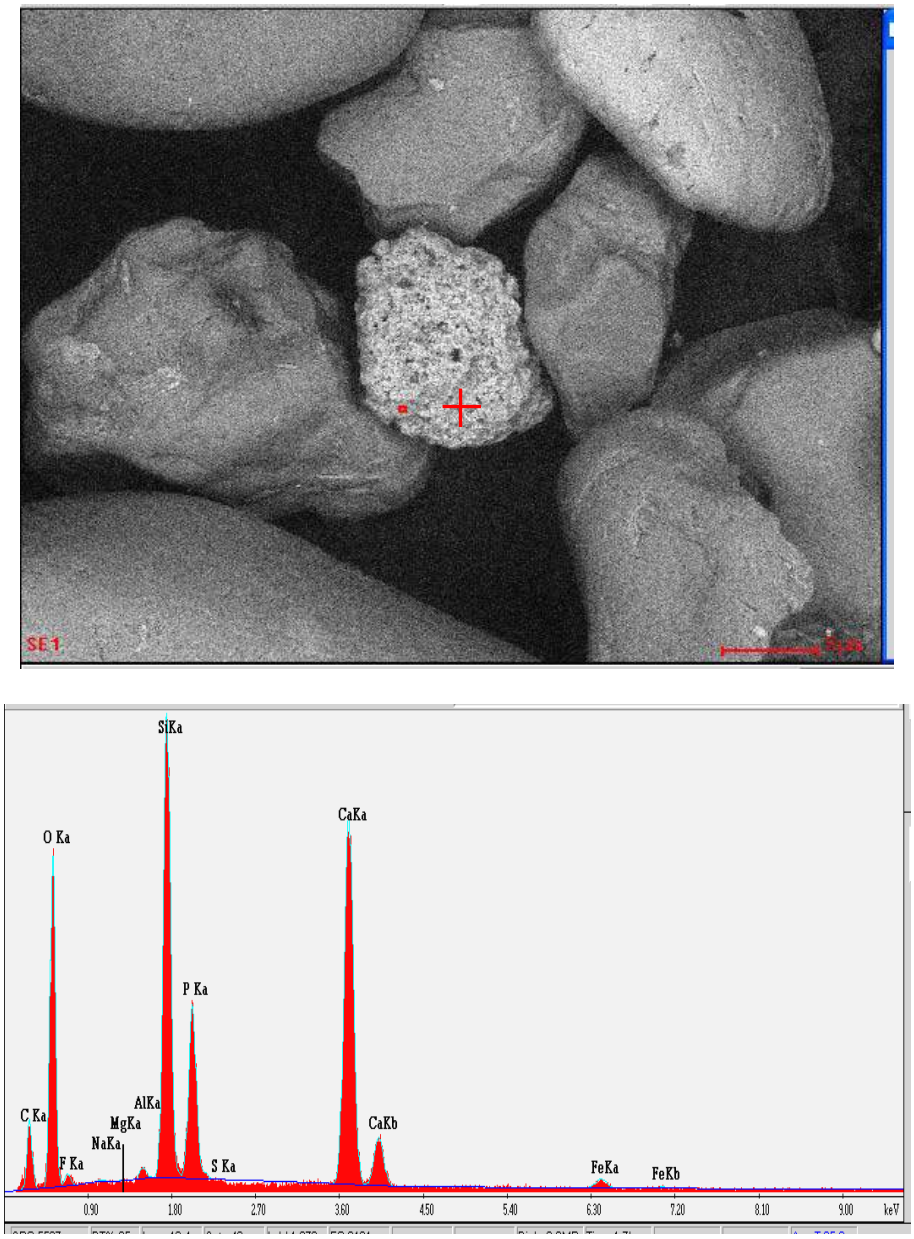

Figure 49. SEM Micrograph of Hole 1862 Split 2 Tailings Showing Silica Associated with the Highly Porous Phosphate Particle and Local EDS Spectrum of That Particle.

Hole 1862 Split 2 Tailings

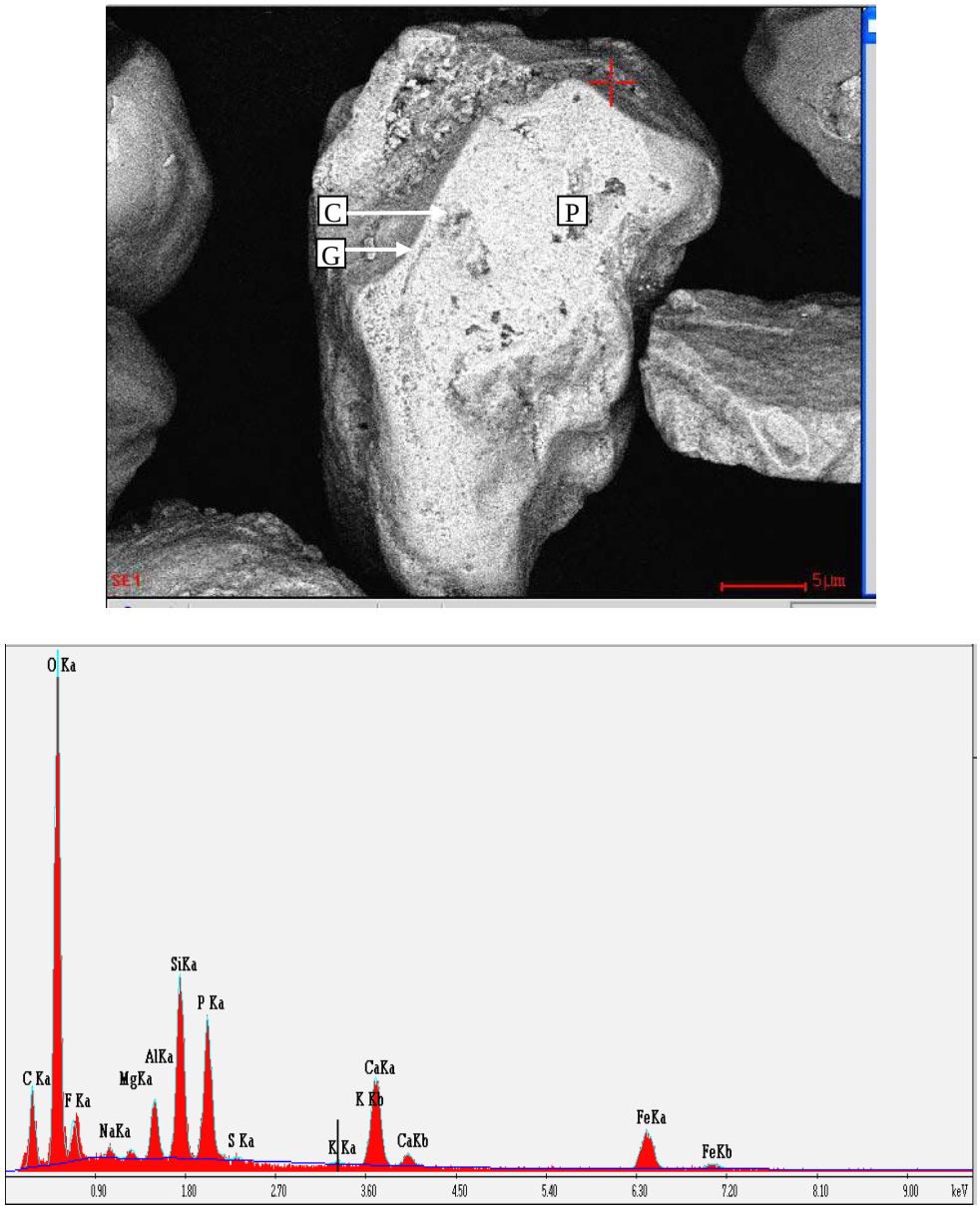

Figure 50. SEM Micrograph of Hole 1862 Split 2 Tailings Showing Phosphate Particle Partially Coated with Clay Minerals (C) and Prismatic Gypsum Crystals (G), and Local EDS Spectrum of That Particle.

Hole 1862 Split 2 Tailings

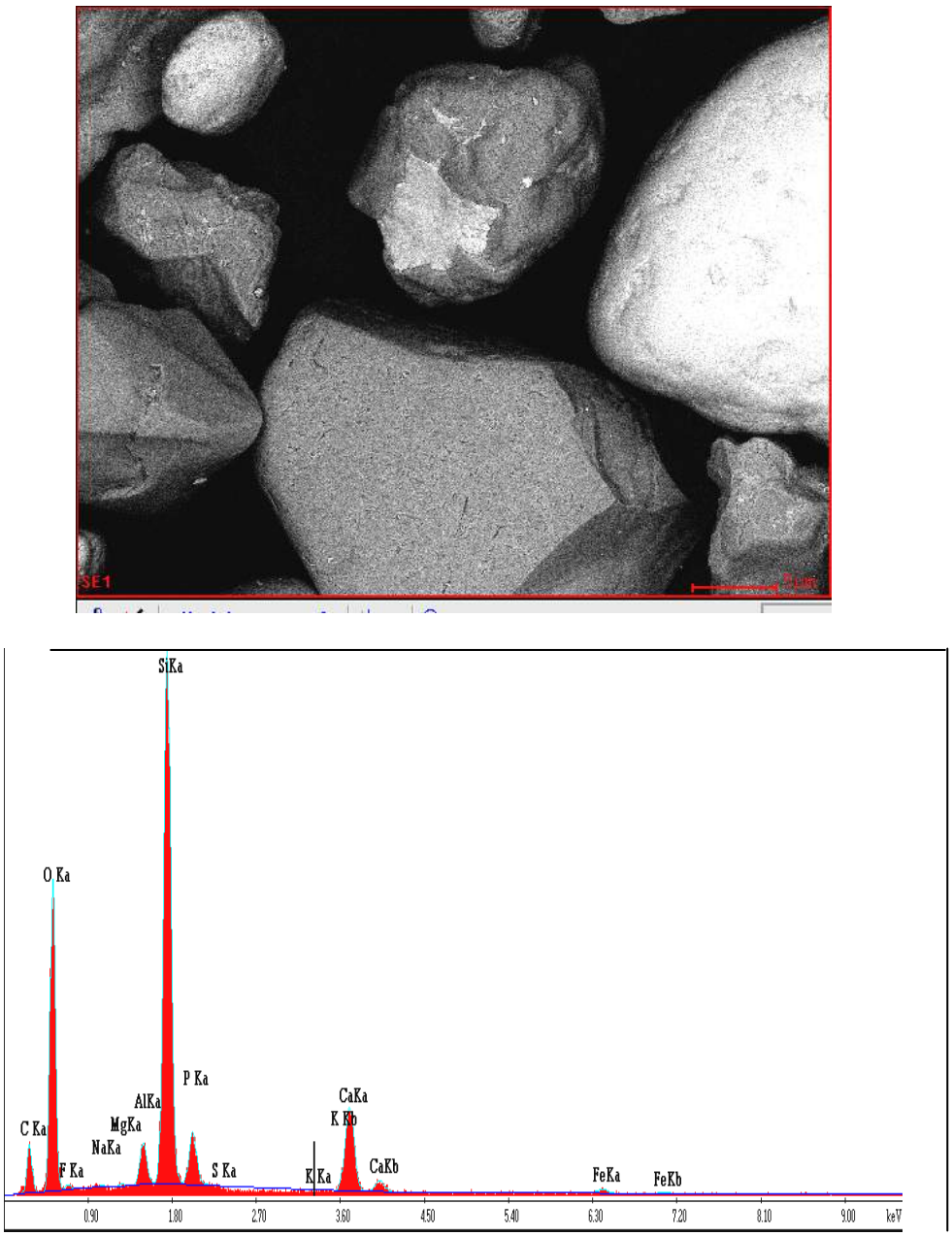

Figure 51. SEM Micrograph of Hole 1862 Split 2 Tailings Showing Interlocked Quartz-Phosphate Particle and Coarse Phosphate Particle, and EDS Spectrum of Large Area.

Hole 1862 Split 2 Tailings

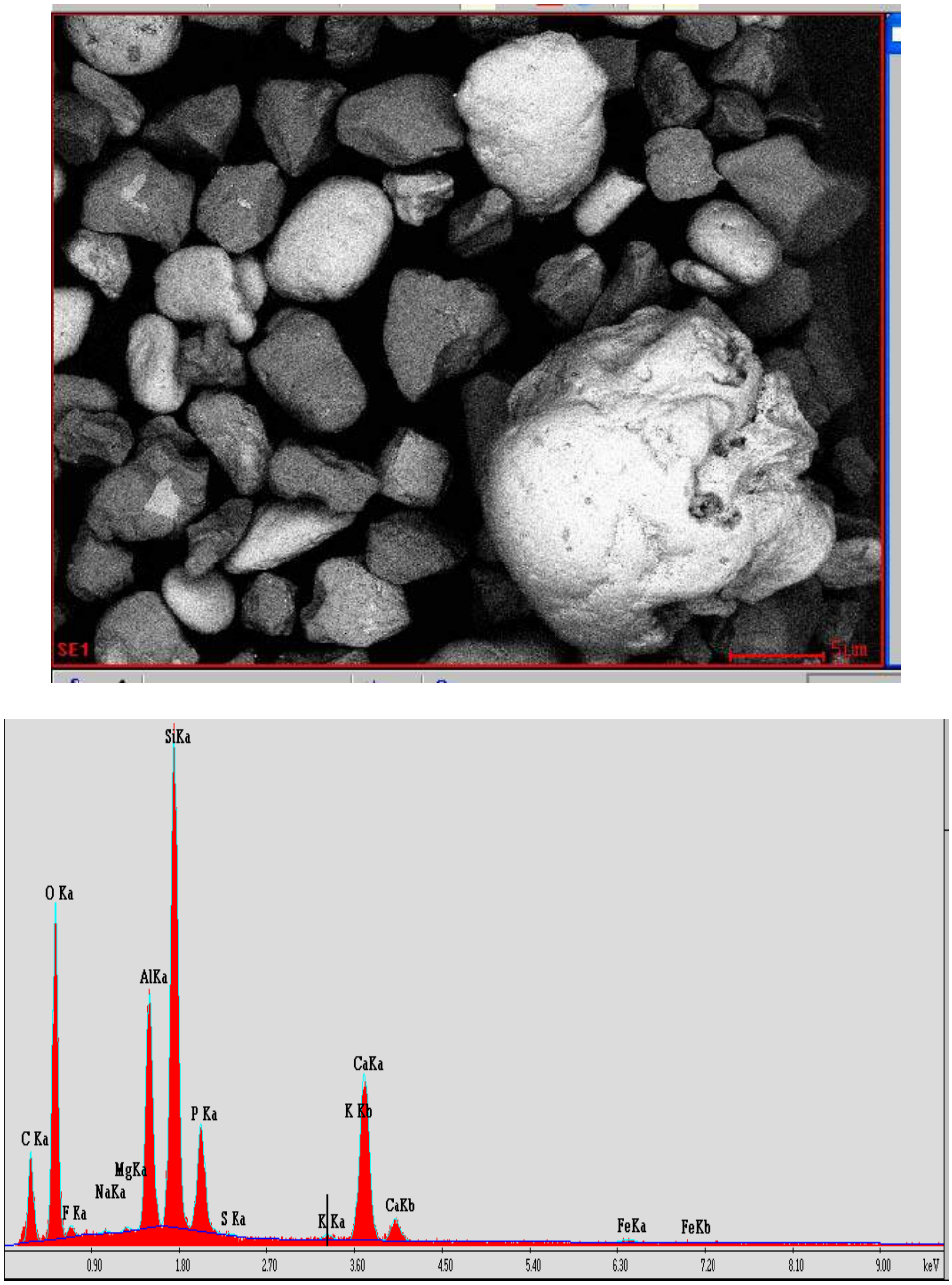

Figure 52. SEM Micrograph of Hole 1862 Split 2 Tailings Showing Coarse Phosphate Particles Compared to all Quartz Particles, and EDS Spectrum of Large Area.

Hole 464 Split 1

SEM analysis of the feed of 464-S1 (Figures 53-58) revealed that it is composed of particles with a wide size range, especially phosphate particles that are extremely large

in comparison to the others. Some phosphate particles show high porosity. As in the other phosphate samples, the phosphate particles are elongated (rods or oval) and spherical or irregular. This feed is rich in clay minerals, especially kaolinite, which is present in the shape of worms, rods or ropes attached or stained on the surface of both phosphate and quartz particles; sometimes the kaolinite forms a shell around the quartz particles. Also this feed is rich in gypsum. Kaolinite is mostly separated in the concentrate (Figures 59-63), but the SEM micrographs show some kaolinite separated in the tailings (Figures 64-67). These kaolinite particles act as a binding material for some particles. The phosphate particles in 464-S1 tailings (Figures 64-67) are very coarse, and are unliberated or attached to quartz particles by kaolinite mineral. In this case, the elongated phosphate particles are more common in the concentrate than in the tailings.

Hole 464 Split 1 Feed

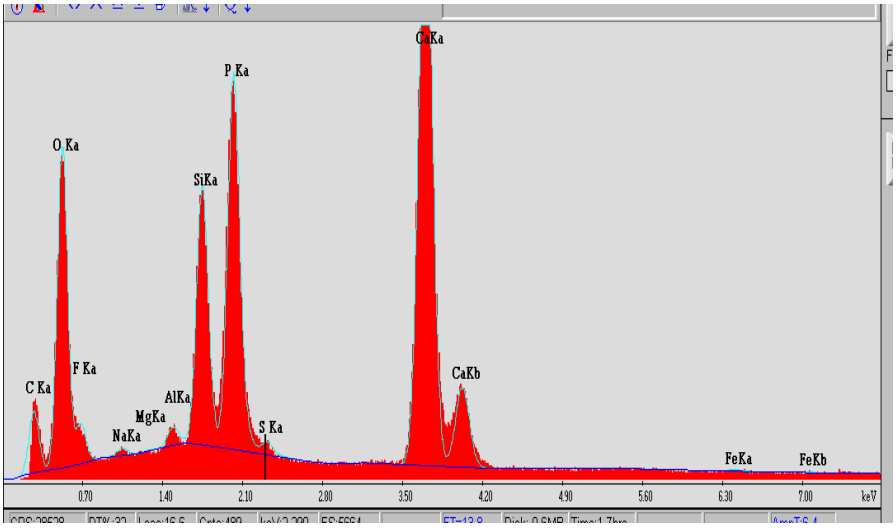

Figure 53. SEM Micrograph of the Hole 464 Split 1 Feed Showing Porous Phosphate Particle and Its EDS Spectrum.

Hole 464 Split 1 Feed

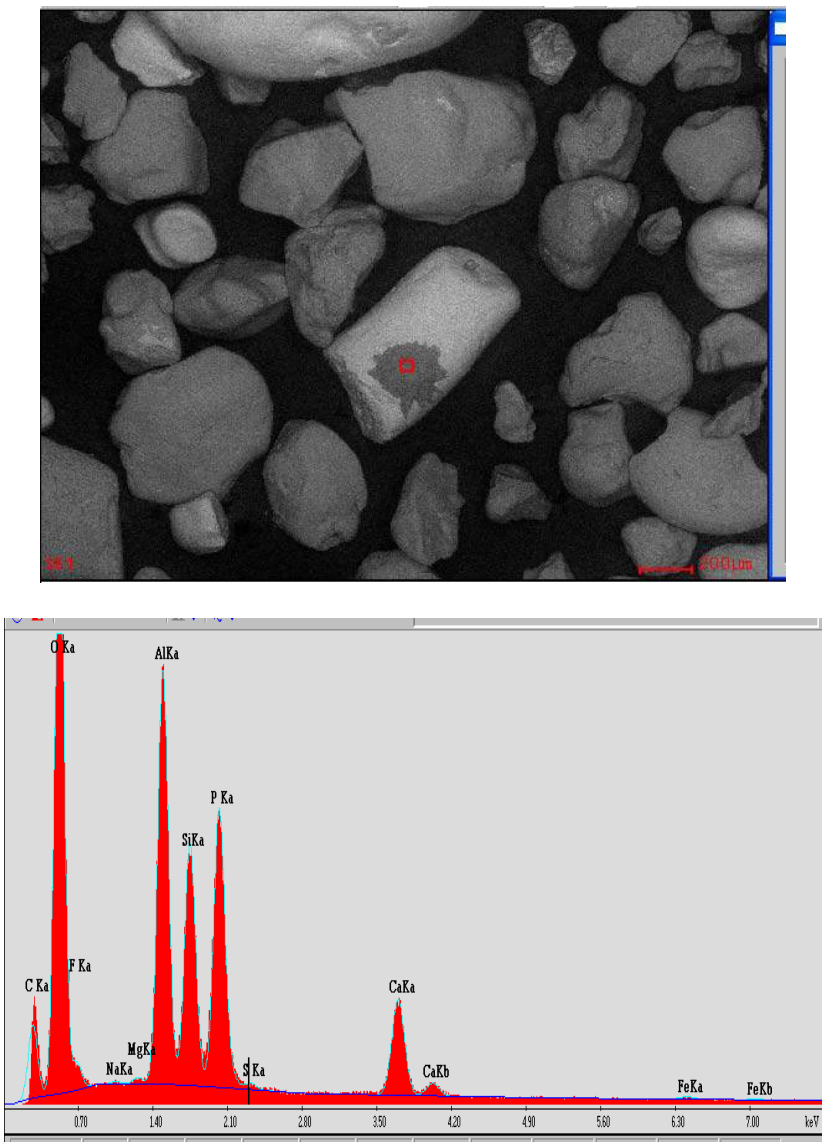

Figure 54. SEM Micrograph of the Hole 464 Split 1 Feed Showing Kaolinite Attached to Phosphatic Rod-Like Particle.

Hole 464 Split 1 Feed

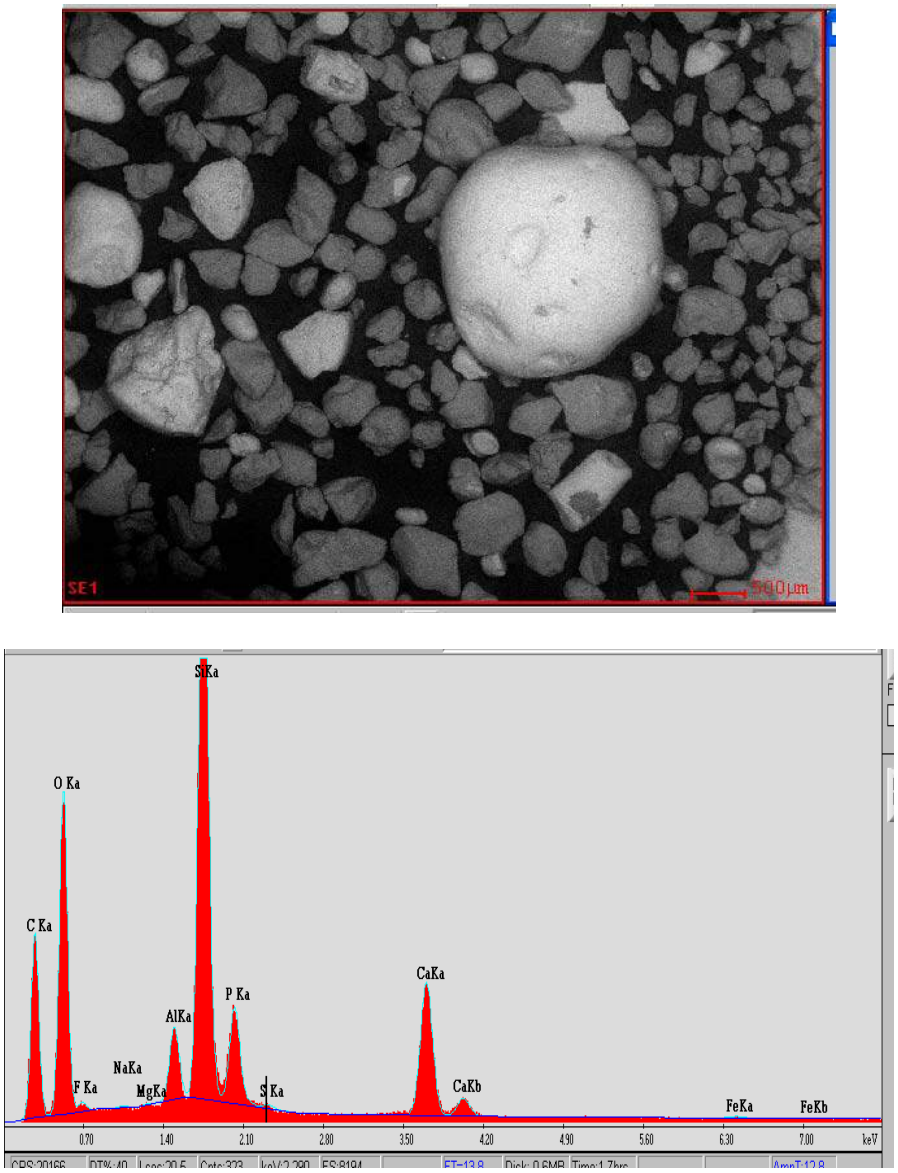

Figure 55. SEM Micrograph of the Hole 464 Split 1 Feed Showing Particles of Wide Size Range Where the Phosphate Particles Are Coarser than Quartz Particles; EDAX Analysis of Large Area.

Hole 464 Split 1 Feed

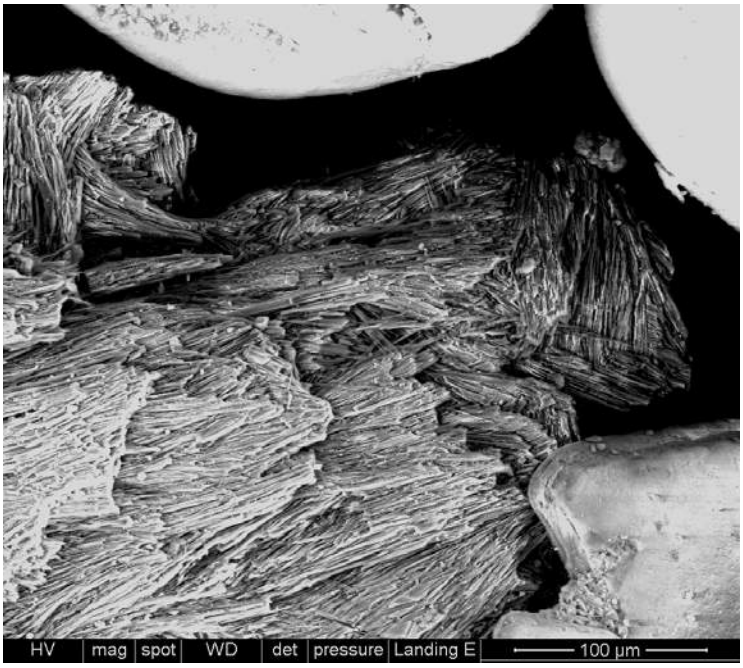

Figure 56. SEM Micrograph of the Hole 464 Split 1 Feed Showing the Kaolinite in Rope-Like Structure and Another Vermicular Kaolinite Strongly Attached to Phosphate Particle in the Lower Right Corner.

Hole 464 Split 1 Feed

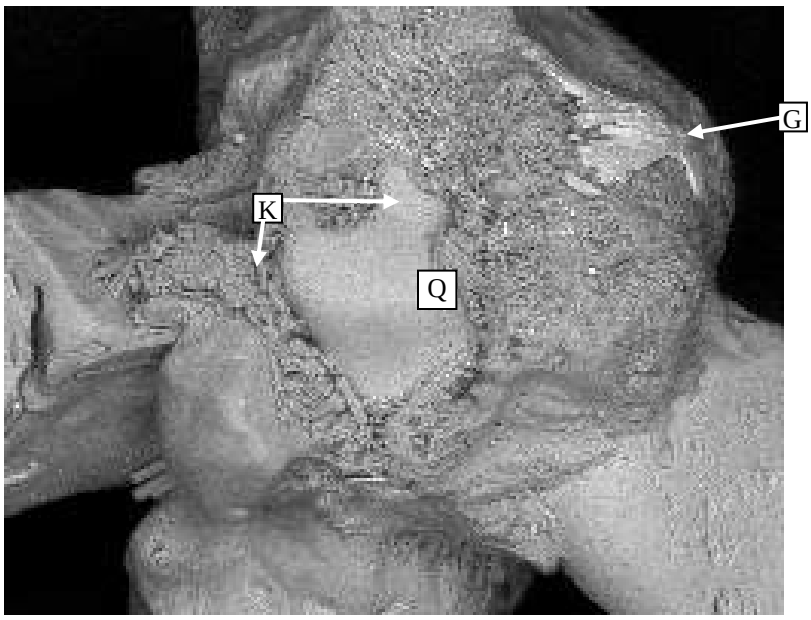

Figure 57. SEM Micrograph of the Hole 464 Split 1 Feed Showing a Composite Particle of Quartz (Q) in the Center Coated with Two Layers of Kaolinite (K) Followed by Gypsum (G) with Some Phosphates. Kaolinite has rod shape and gypsum of radial structure (Hole 464 Split 1 Feed).

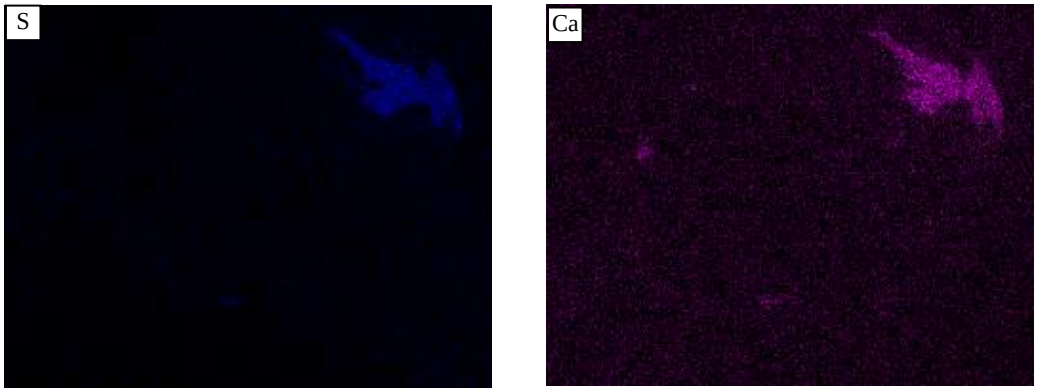

Figure 58. EDS Chemical Maps of the Previous Particle.

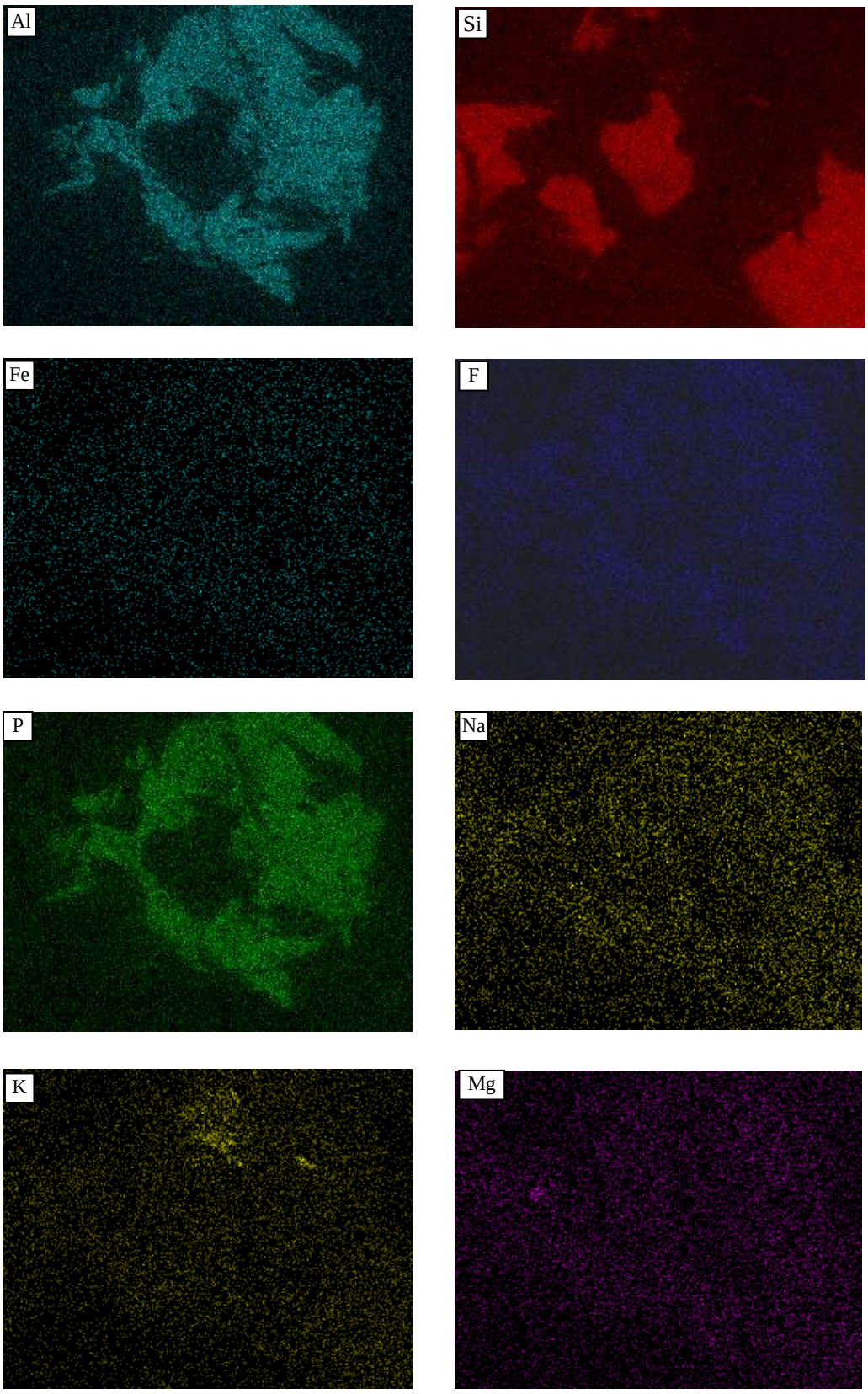

Figure 58 (Cont.). EDS Chemical Maps of the Previous Particle.

Hole 464 Split 1 Concentrate

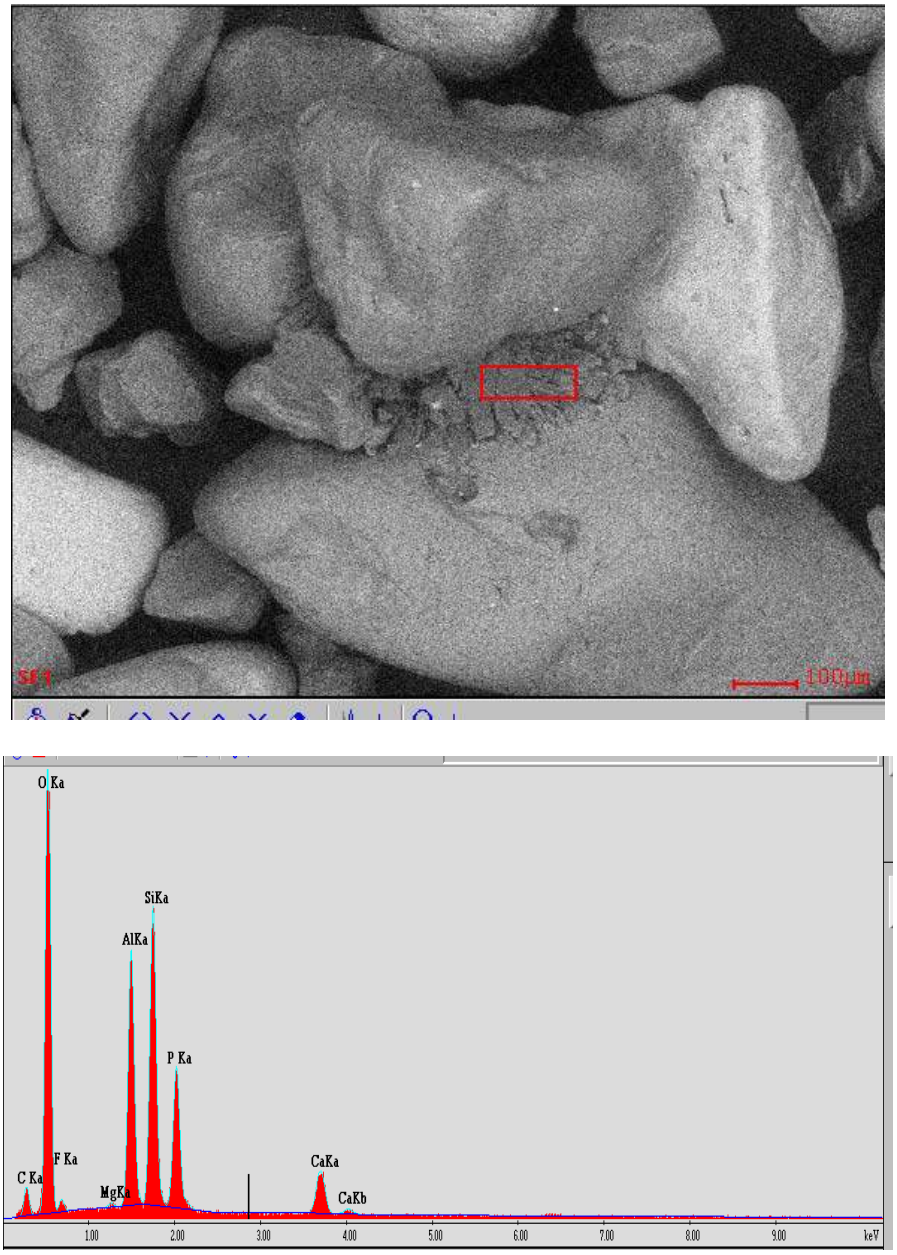

Figure 59. SEM Micrograph of the Concentrate of Hole 464 Split 1 Showing Kaolinite Fragments in between Different Grains, and Their EDS Spectrum.

Hole 464 Split 1 Concentrate

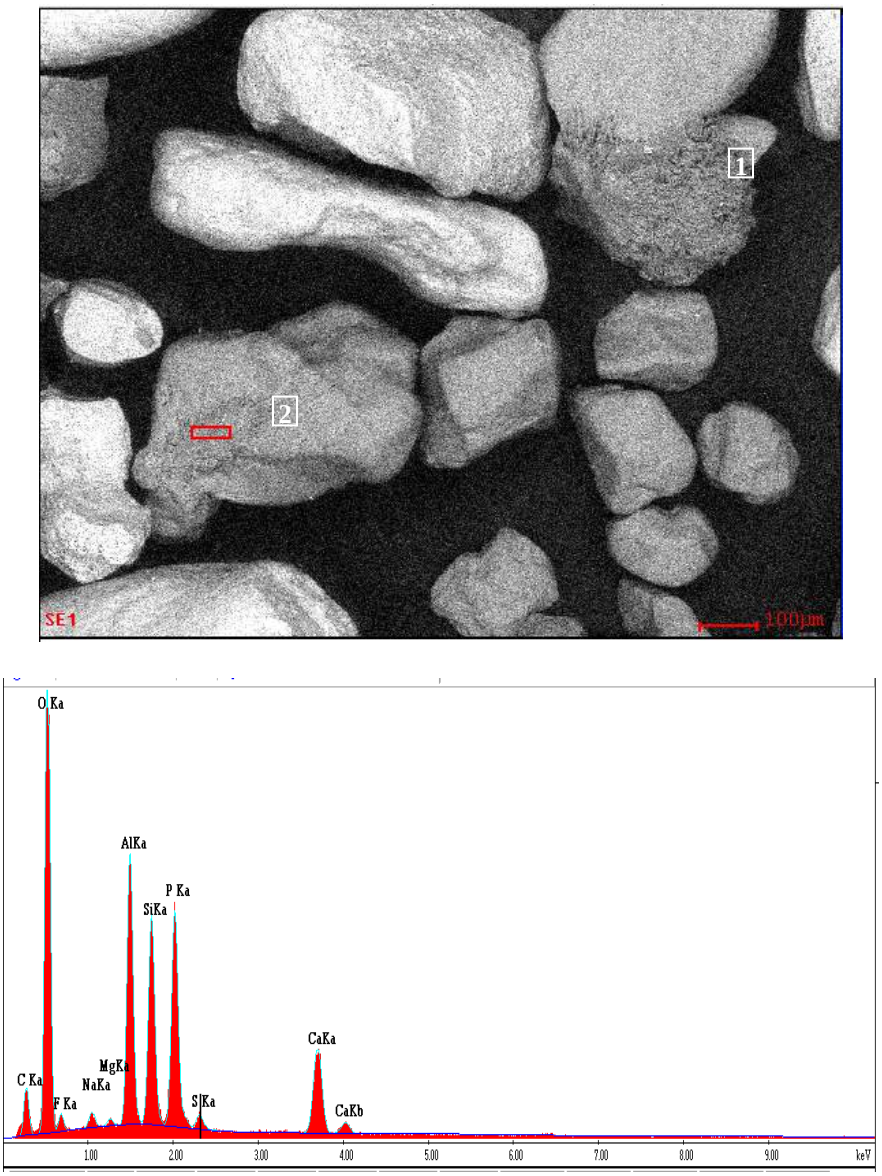

Figure 60. SEM Micrograph of the Concentrate of Hole 464 Split 1 Showing Particles of Narrow Size Range and Kaolinite Particles of Vermicular Shape Attached to Phosphate (1) and Quartz (2) Particles. Note that most of the phosphate particles are elongated particles. The EDS spectrum is of the marked clays on a silica particle.

Hole 464 Split 1 Concentrate

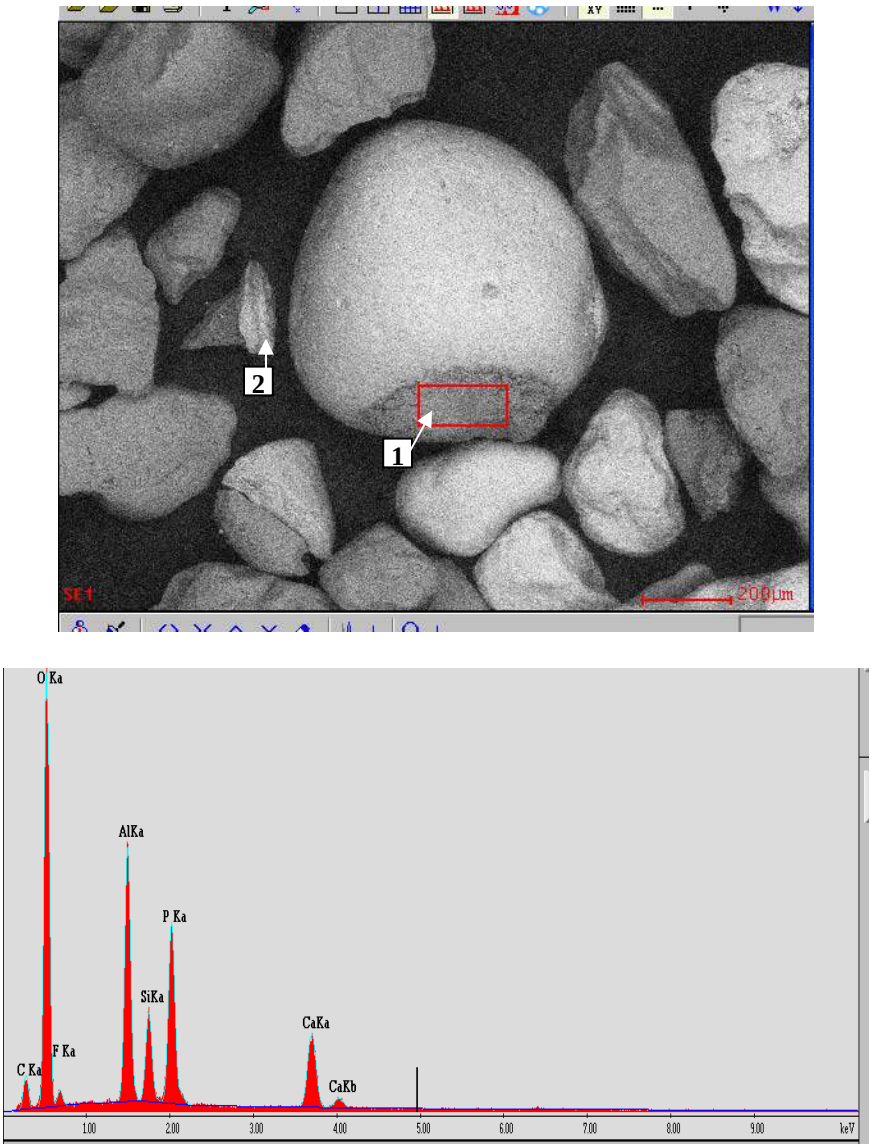

Figure 61. SEM Micrograph of the Concentrate of Hole 464 Split 1 Showing the Kaolinite Particles of Vermicular Structure Attached to the Coarse (1) and Fine (2) Phosphate Particles and Their Analysis.

Hole 464 Split 1 Concentrate

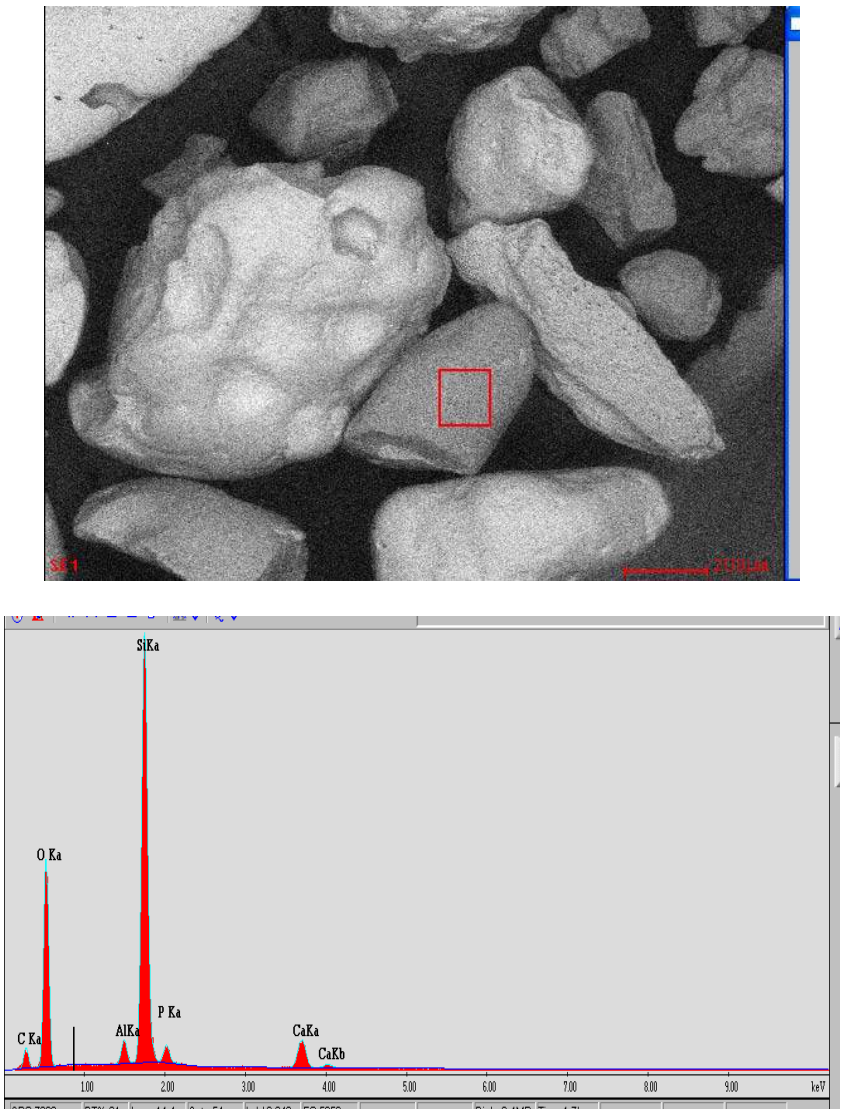

Figure 62. SEM Micrograph of the Concentrate of Hole 464 Split 1 Showing the Analysis of Quartz Particle with Inclusions of Phosphate that Extend to the Surface. To the right is a long phosphate particle affected by slightly thick layer of kaolinite on the surface. To the left is phosphate particle affected by traces of kaolinite on the surface.

Hole 464 Split 1 Concentrate

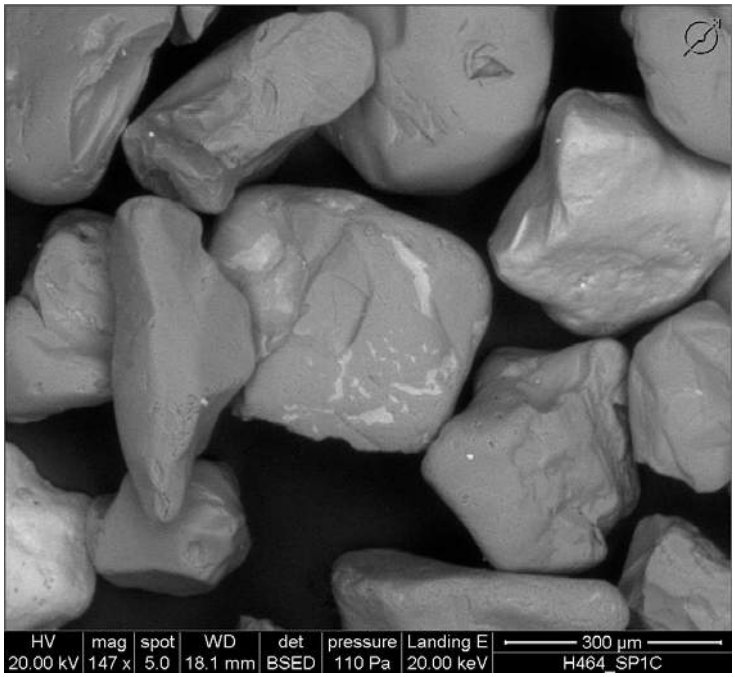

Figure 63. SEM Micrograph of the Concentrate of Hole 464 Split 1 Showing the Abundance of Quartz Particles with Phosphate Inclusions That Extend to the Surface.

Hole 464 Split 1 Tailings

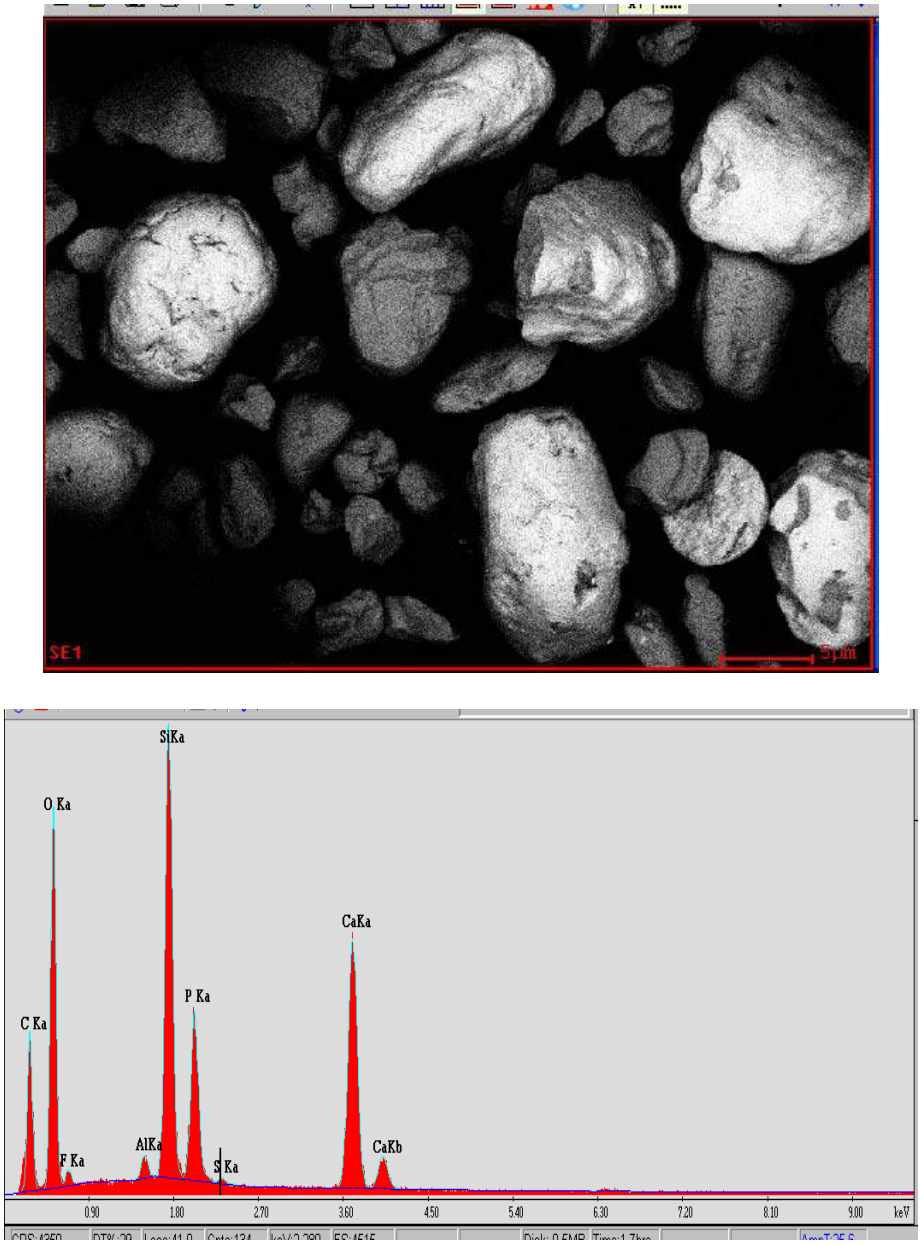

Figure 64. SEM Micrograph of Hole 464 Split 1 Tailings in Which the Phosphate Particles Are Coarser than Quartz Particles, and EDS Spectrum of Large Area.

Hole 464 Split 1 Tailings

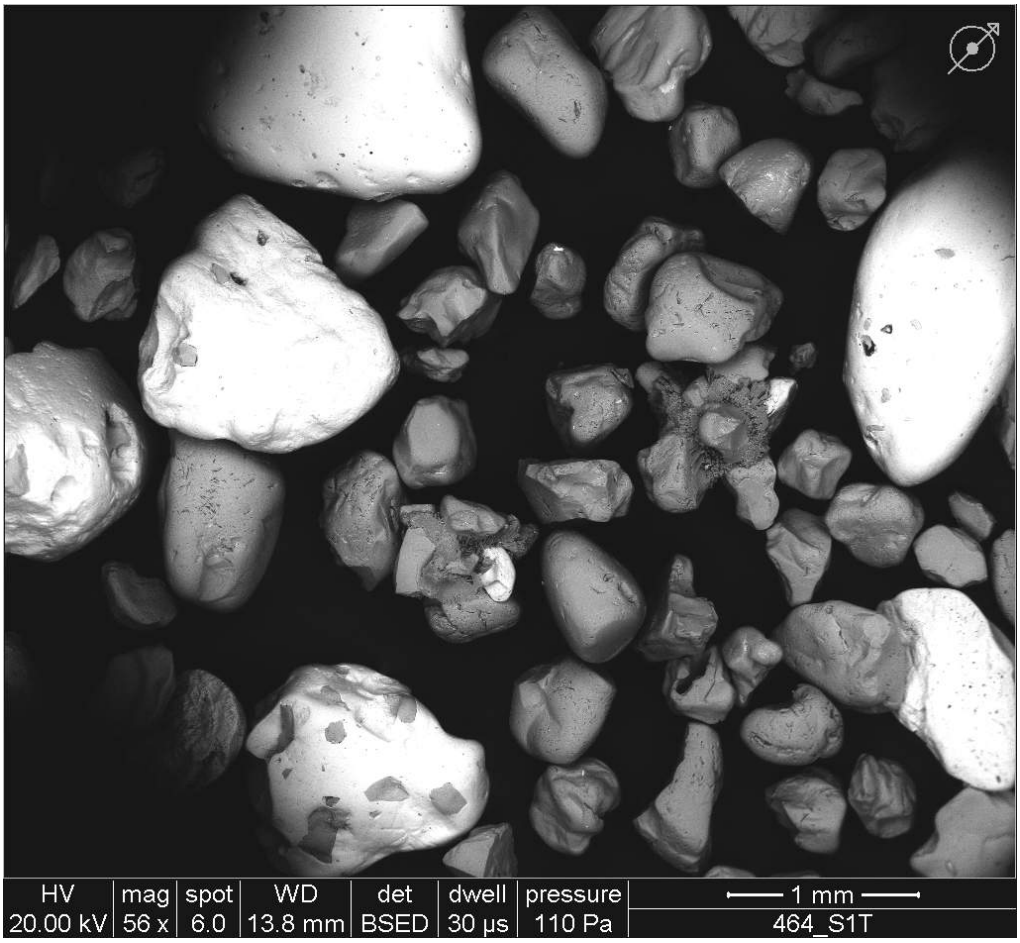

Figure 65. SEM Micrograph of Hole 464 Split 1 Tailings in Which the Phosphate Particles Are Coarse, Unliberated and/or Attached to Quartz Particles by Kaolinite Mineral. Note that spherical or semispherical phosphate particles are common.

Hole 464 Split 1 Tailings

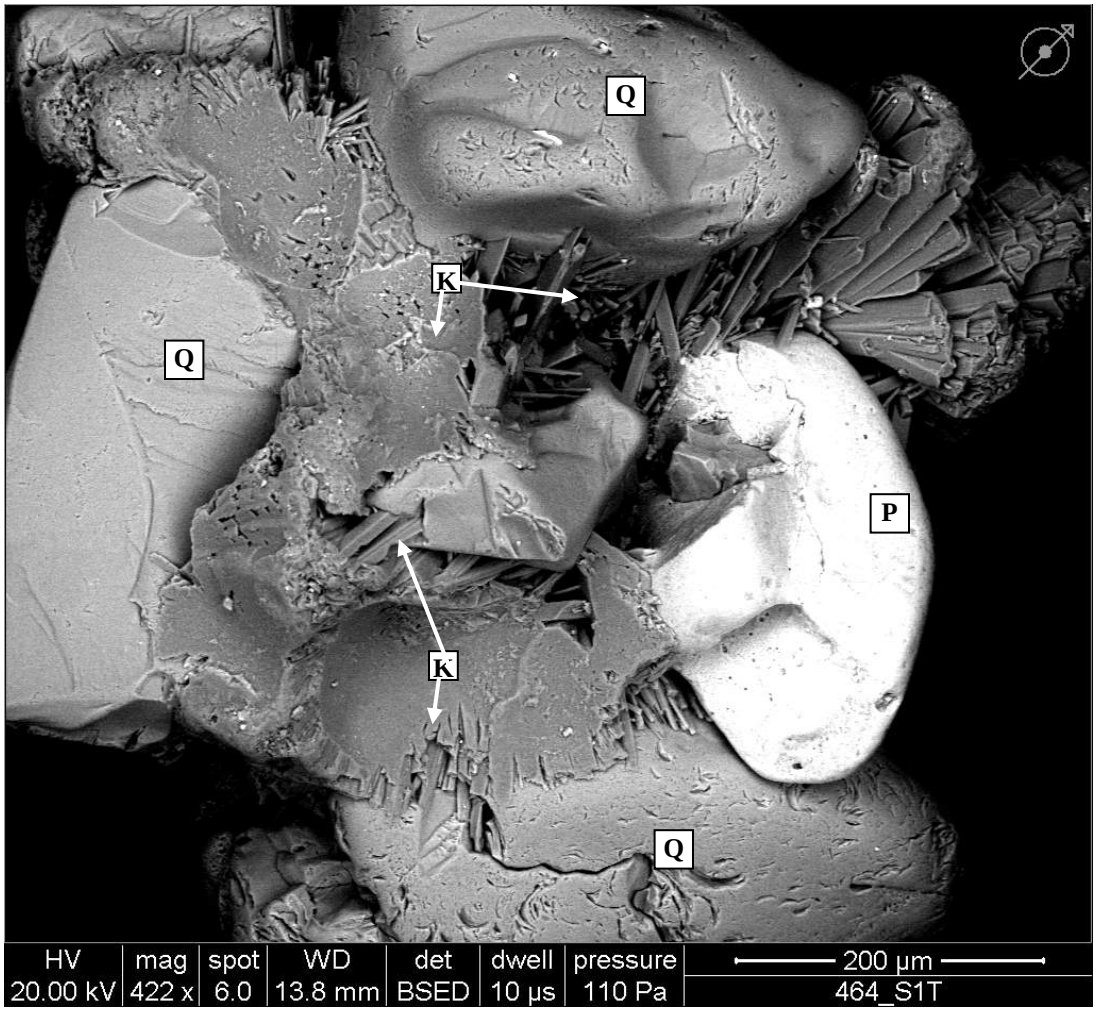

Figure 66. SEM Micrograph of Hole 464 Split 1 Tailings in Which the Phosphate Particle Is Attached to Quartz Particles by Crystalline and Noncrystalline Kaolinite Mineral.

Hole 464 Split 1 Tailings

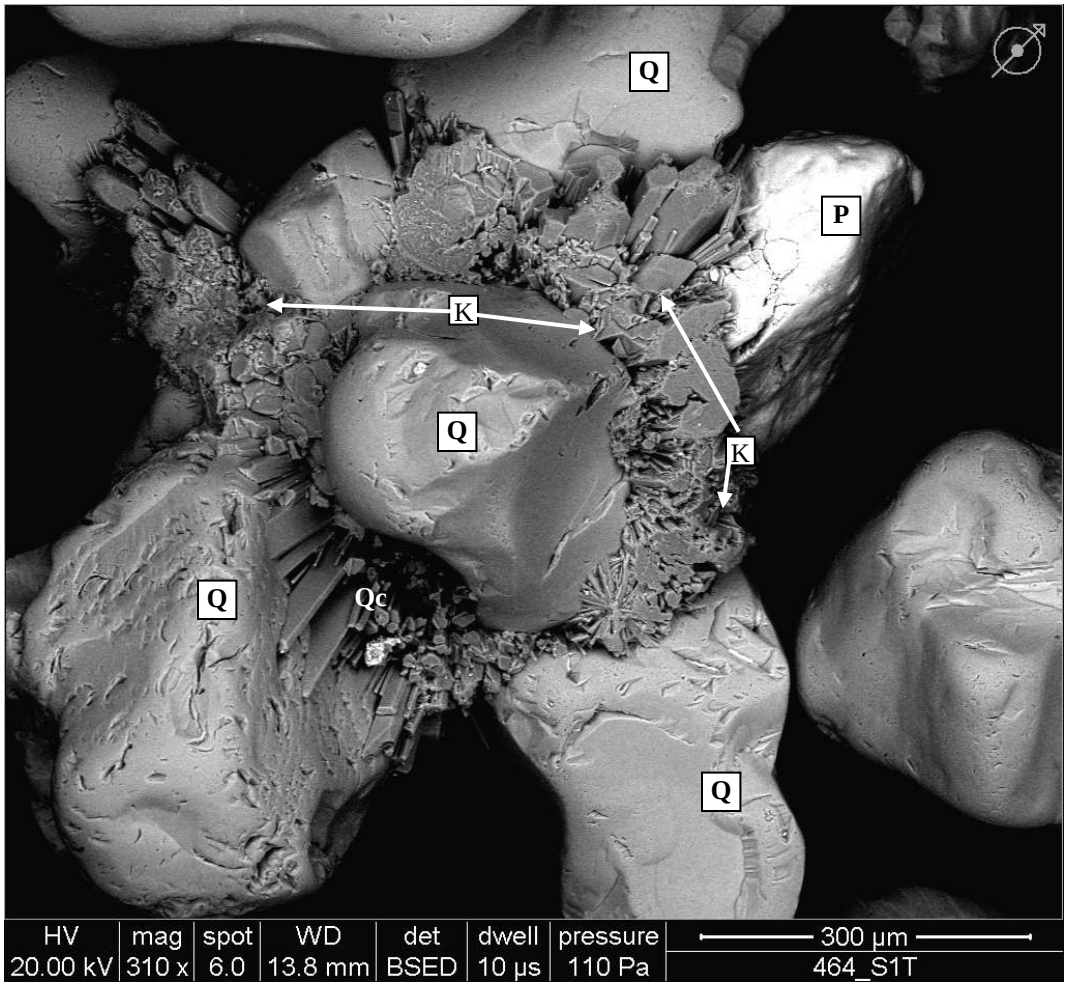

Figure 67. SEM Micrograph of Hole 464 Split 1 Tailings in Which the Phosphate (P) Particle Is Attached to Quartz (Q) Particles by Kaolinite (K) Mineral and Platy Crystalline Silica (Qc).

CF Combined

SEM micrographs of CF Combined feed (Figures 68-69) indicated that it had a narrow particle size distribution and good liberation. There were no clay particles on the surface of phosphate particles, in spite of the presence of the clayey particles of kaolinite and montmorillonite. Also rare dolomite particles were recorded. Those results were revealed before by X-ray diffraction data. Most of the clay particles floated with the concentrate, as was confirmed by the XRD results. The concentrate was of fixed particle size. The phosphate particles in the concentrate were mostly elongated or oval in shape and had a good degree of liberation (Figures 70-77).

CF Combined Feed

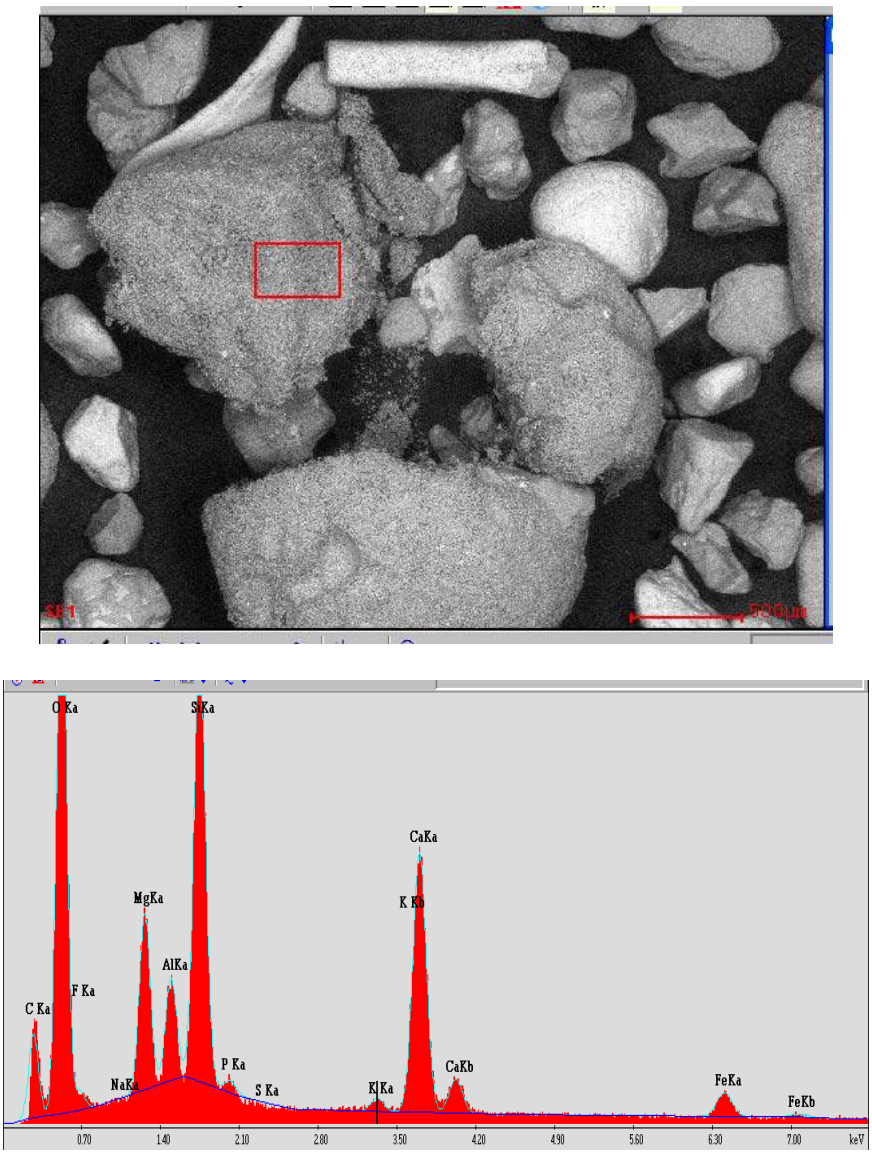

Figure 68. SEM Micrograph of CF Combined Feed Showing Ca-Mg Montmorillonite Particle Fragmented During Sampling for SEM, and Its EDS Spectrum.

CF Combined Feed

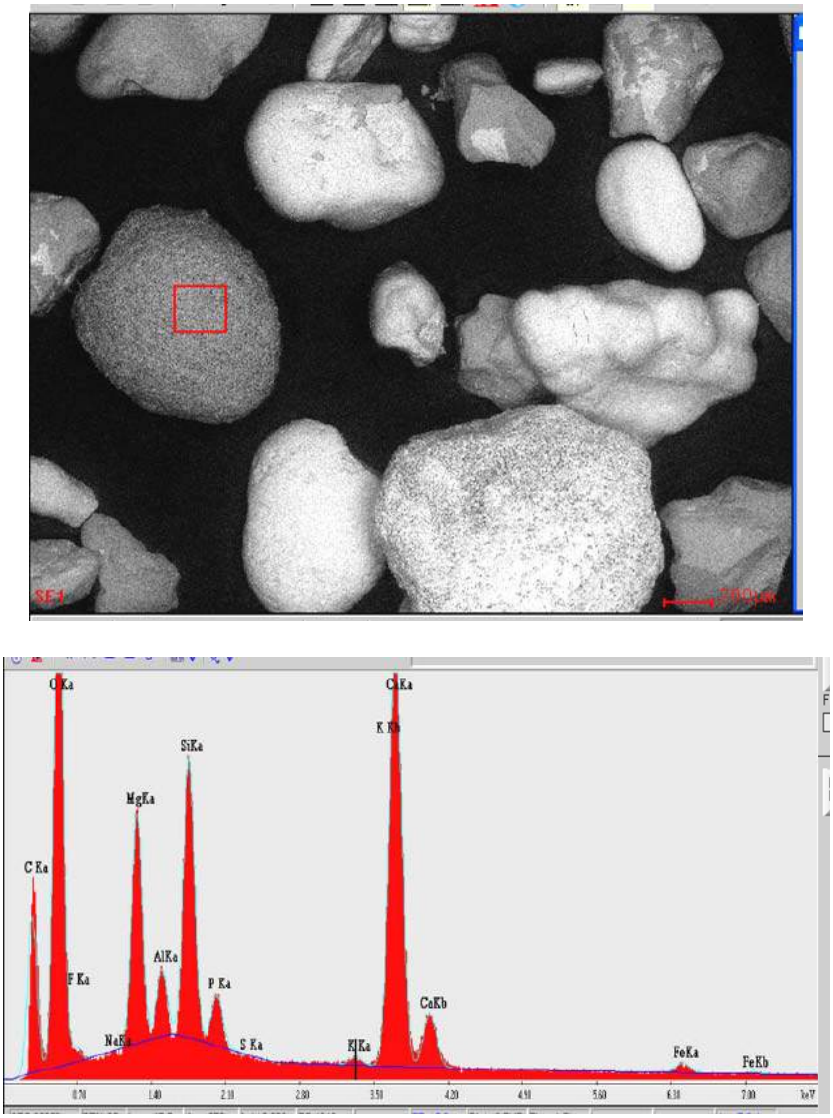

Figure 69. SEM Micrograph of CF Combined Feed Showing Clayey Dolomite Particle, and Its EDS Spectrum.

CF Combined Concentrate

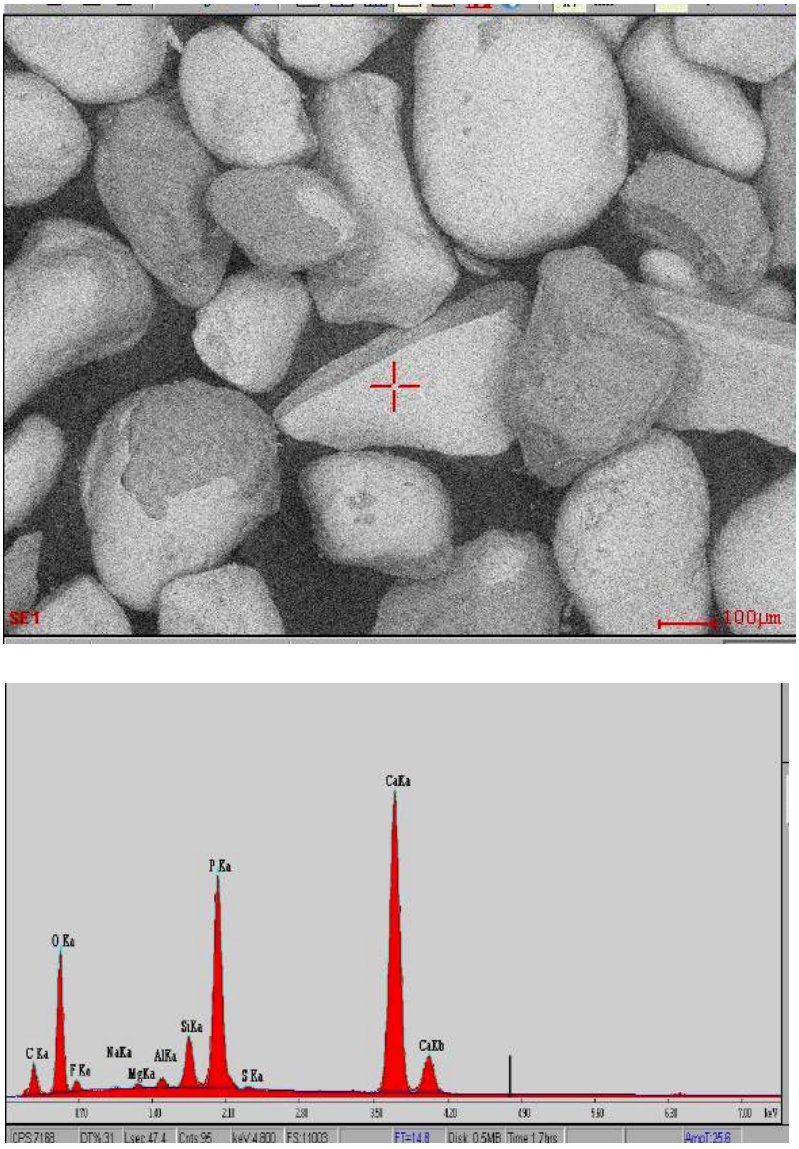

Figure 70. SEM Micrograph of CF Combined Concentrate Showing Narrow Particle Size Distribution, Some Interlocked Phosphate Particles, and EDS Spectrum of One Phosphate Particle. Note the abundance of oval and elongated particles.

CF Combined Concentrate

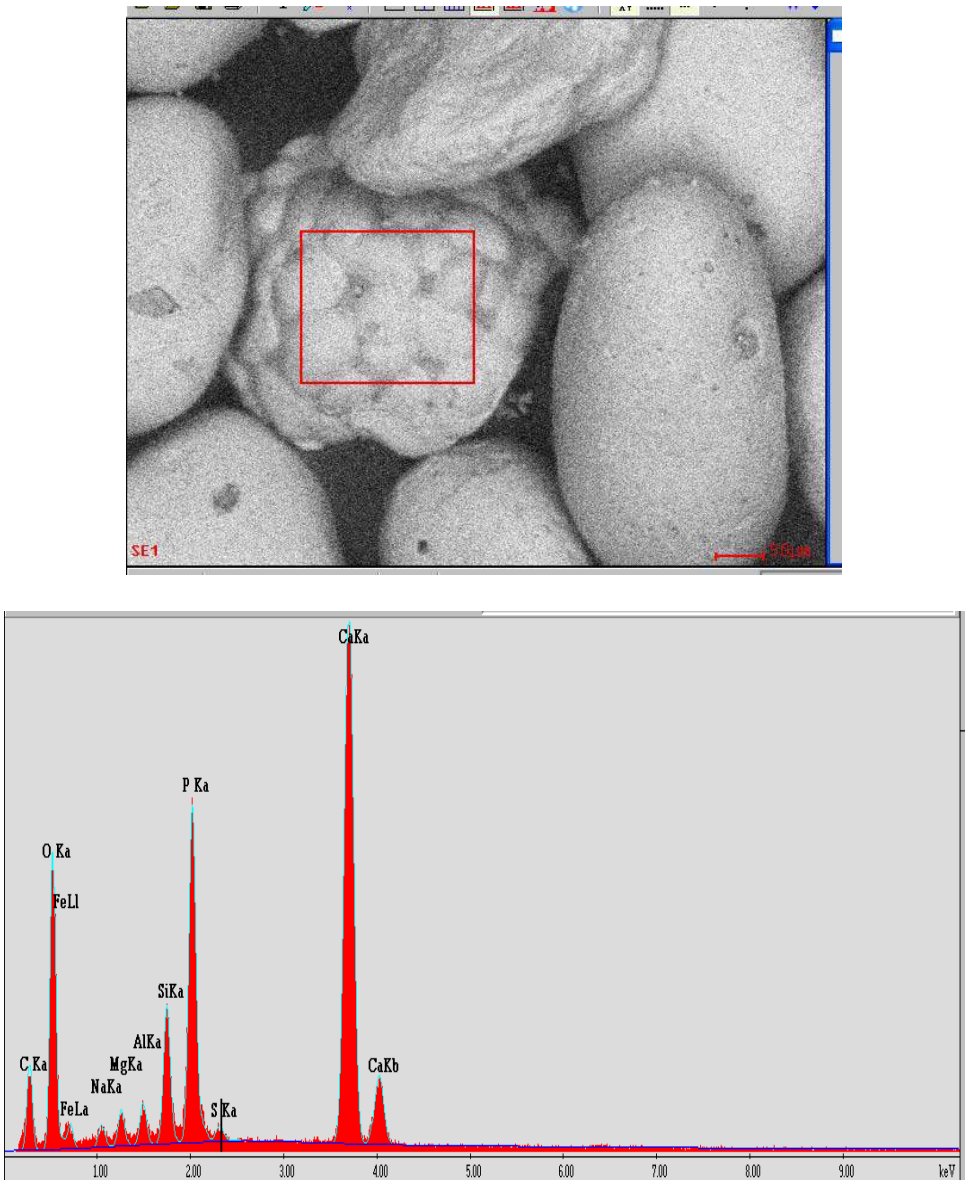

Figure 71. SEM Micrograph of CF Combined Concentrate Showing a Fixed Particle Size, Oval Shape of Phosphate Particles, and a Composite Phosphate Particle of Small Phosphate Aggregates Cemented by Silica and Clays. The EDS spectrum is of the latter particle.

CF Combined Concentrate

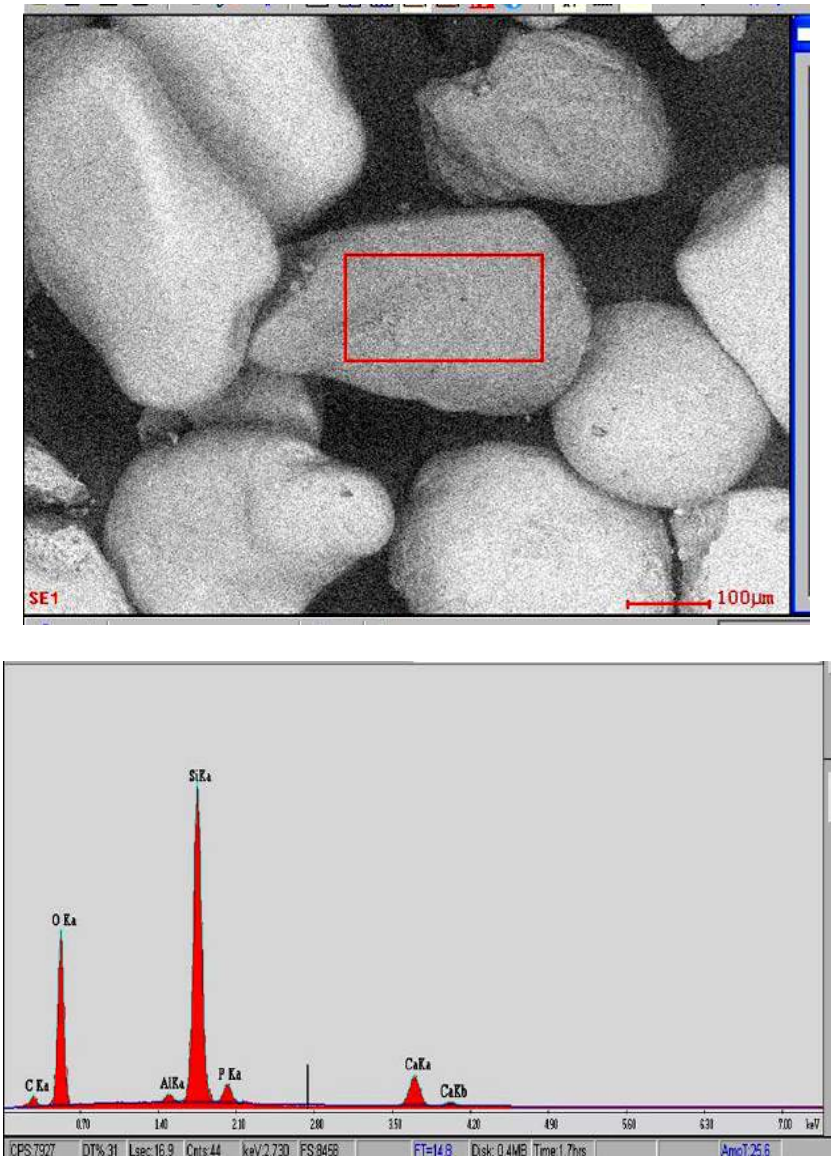

Figure 72. SEM Micrograph of CF Combined Concentrate Showing Elongated and Oval Phosphate Particles (white). The EDS spectrum is of an elongated quartz particle (gray).

CF Combined Concentrate

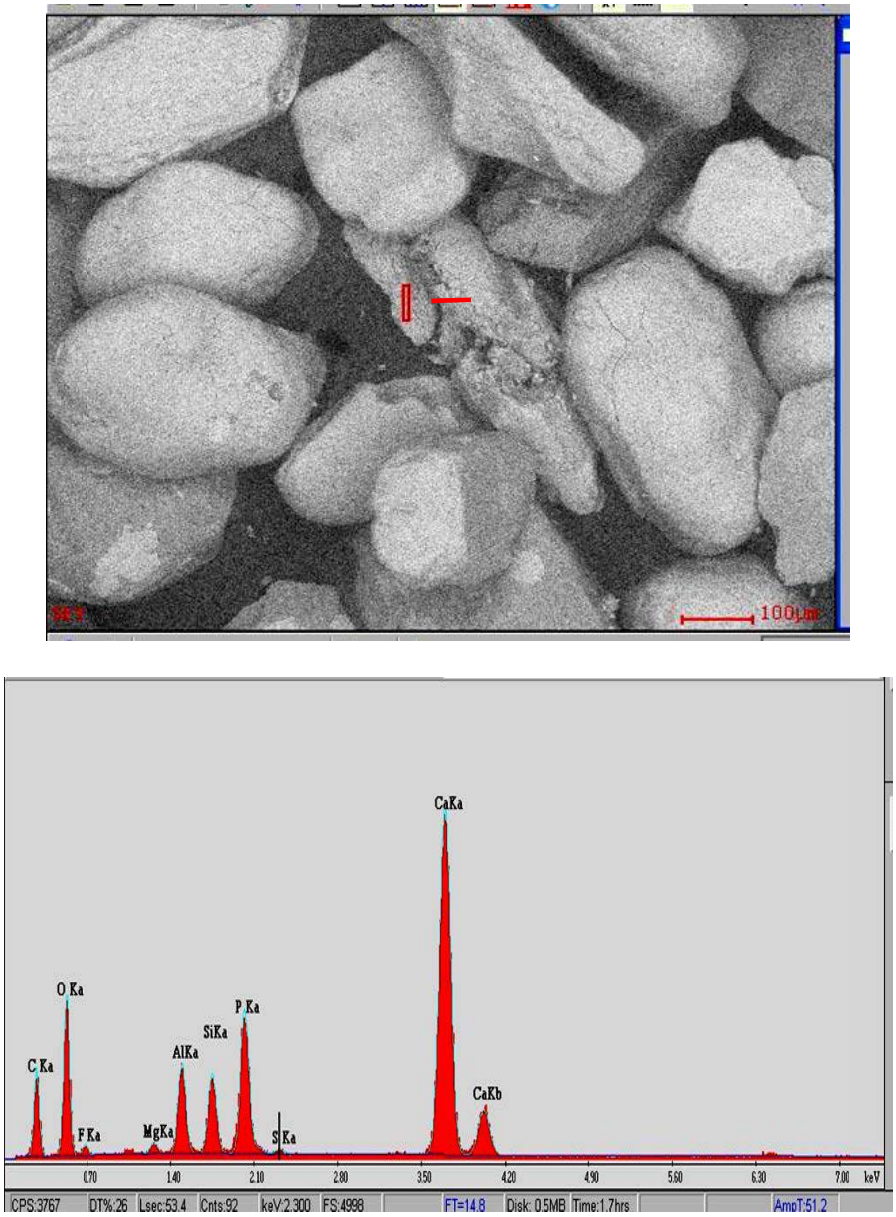

Figure 73. SEM Micrograph of CF Combined Concentrate Showing Fragmented Clayey Phosphate Particle and Its EDS Spectrum. Note that the elongated or oval phosphate particles are common.

CF Combined Concentrate

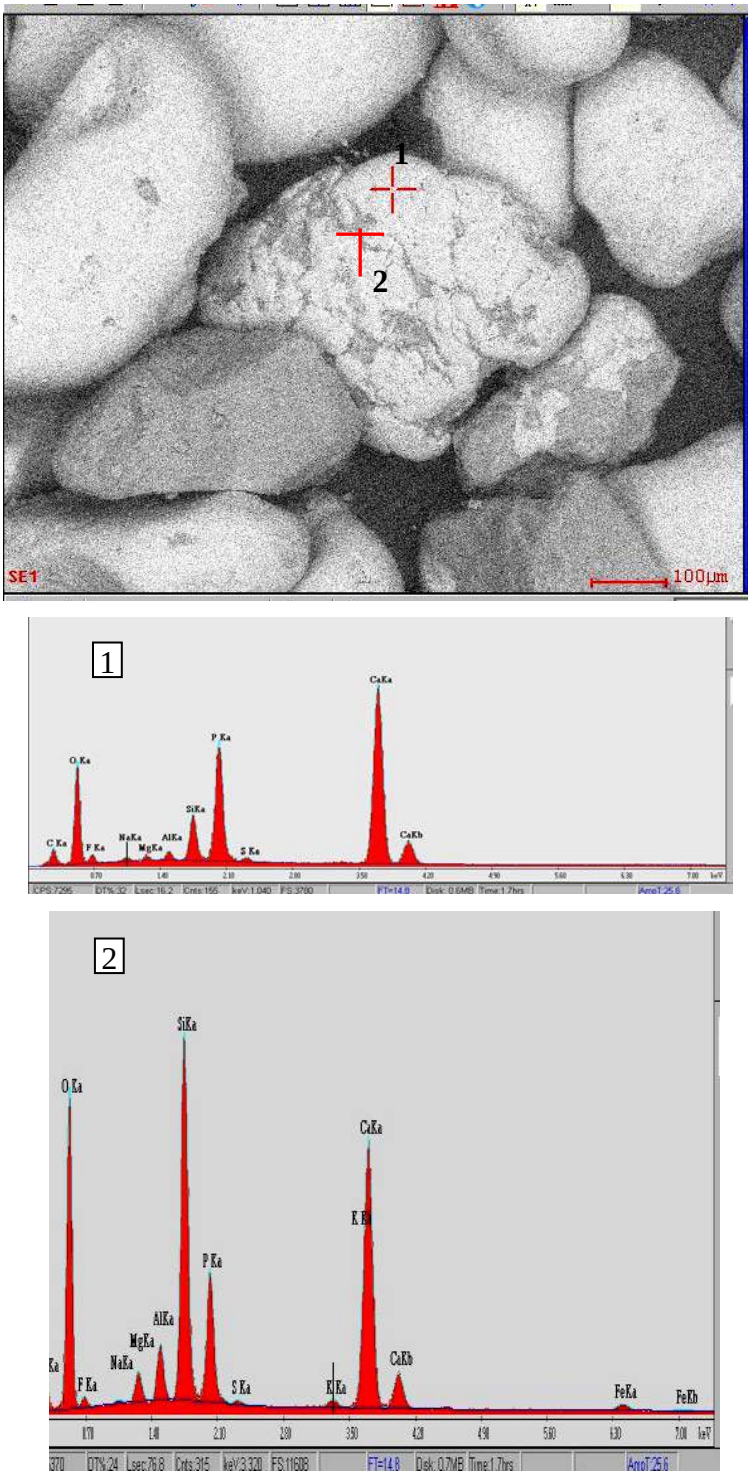

Figure 74. SEM Micrograph of CF Combined Concentrate with Unliberated Phosphate Particles, and EDS Spectra of the Phosphate Particle at Different Spots 1 and 2.

CF Combined Concentrate

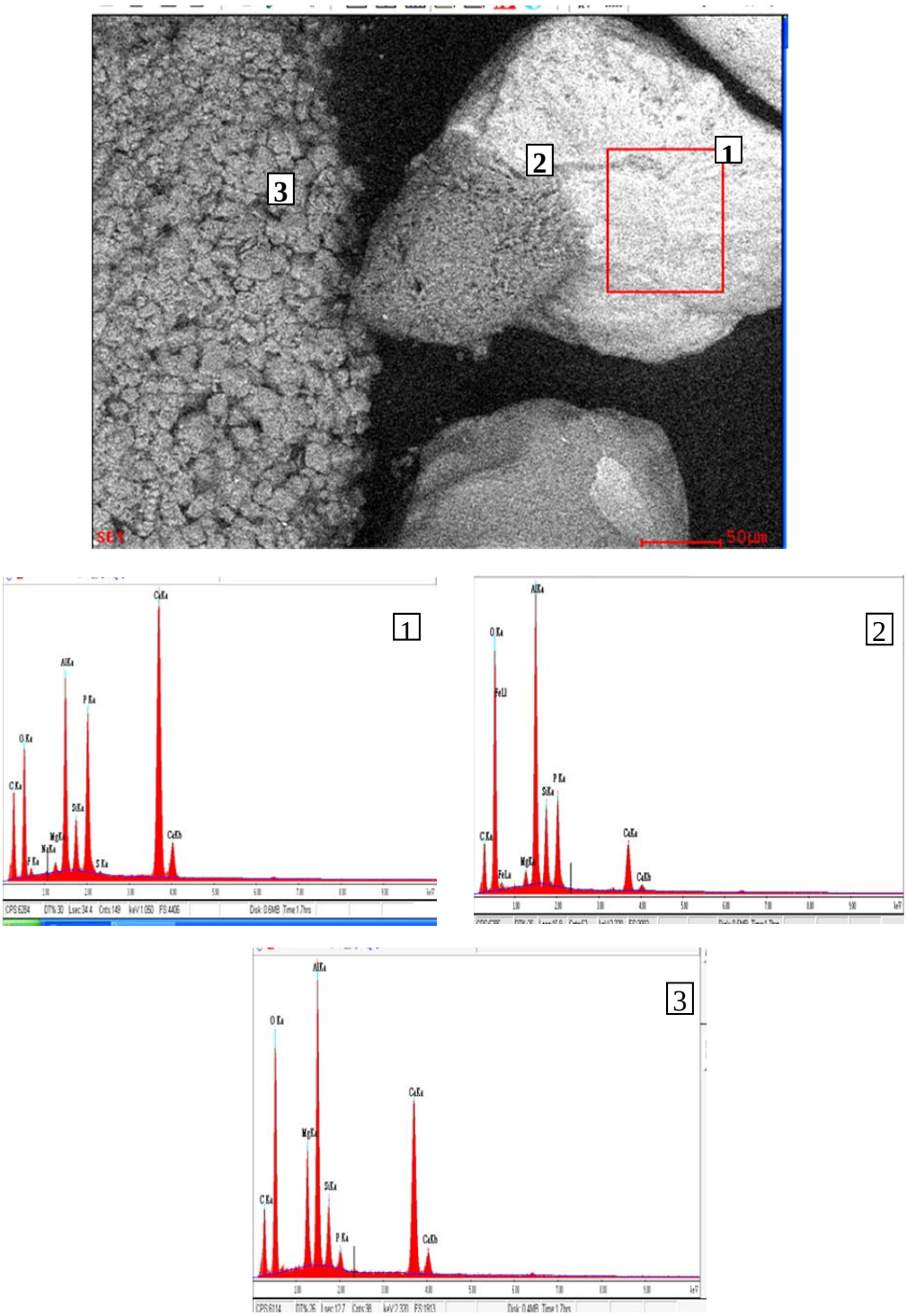

Figure 75. SEM Micrograph of CF Combined Concentrate with Phosphate Particle (1) with Some Clays, Kaolinite Particle of Vermicular Structure (2), and Montmorillonite Comprised of Nanoparticles (3).

CF Combined Concentrate

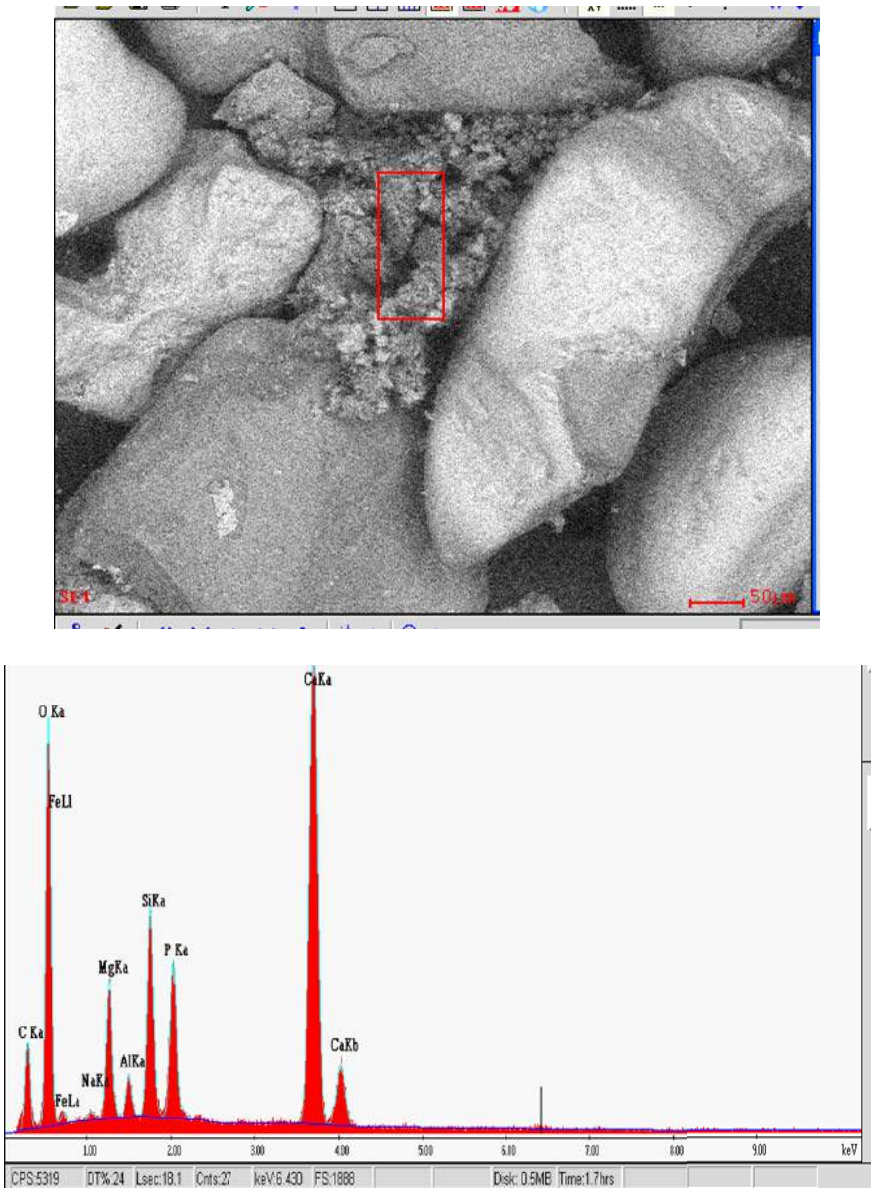

Figure 76. SEM Micrograph of CF Combined Concentrate Showing Intermixed Dolomite-Phosphate-Quartz Particle, and Its EDS Spectrum. Note that elongated phosphate particles are common.

CF Combined Concentrate

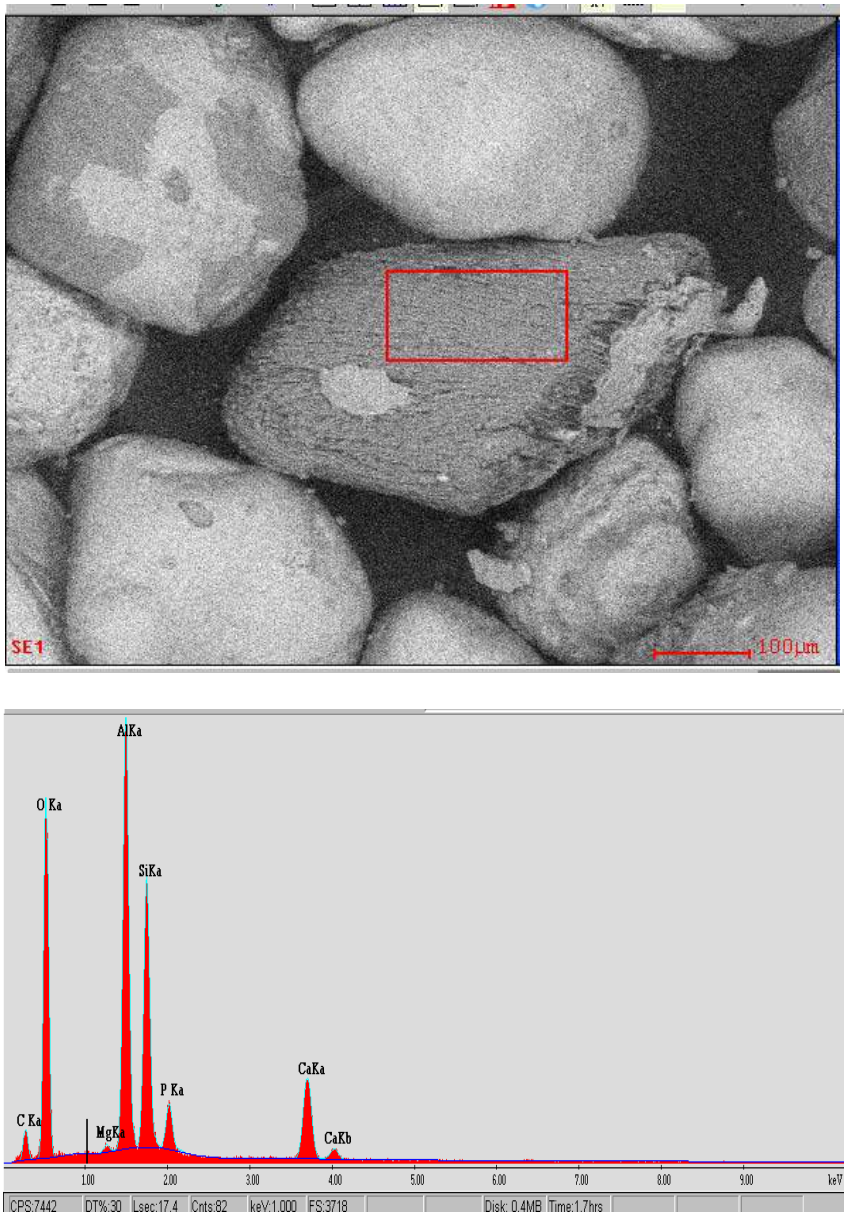

Figure 77. SEM Micrograph of the Concentrate of CF Combined Showing Kaolinite Mineral Particle in the Form of Cylinder of Rope-like Structure Around Phosphate Particle, and Its EDS Spectrum.

CF West Pit

SEM analysis (Figures 78-82) of CF West Pit samples indicates that the feed has a narrow particle size distribution and to some extent good liberation. The feed is clean and free from clay particles or clay smeared on the phosphate or quartz particles. The rod-shaped particles are more common than rounded or spherical and irregular particles. Few dolomite particles are recorded in the feed. The concentrate is clean and has a close particle size range; the elongated phosphate particles are common in this product.

CF West Pit Feed

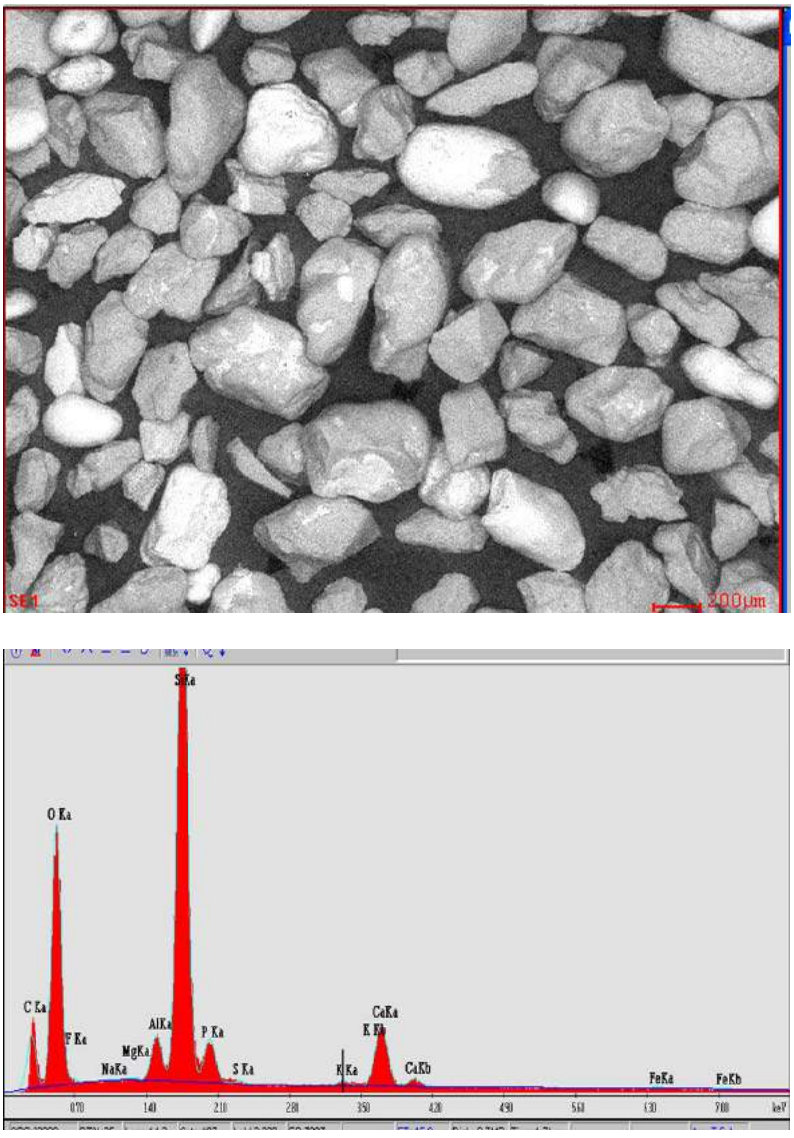

Figure 78. SEM Micrograph of CF West Pit Feed Showing a Narrow Particle Size Distribution and Quartz-Phosphate Interlocked Particles, and EDS Spectrum of Large Area.

CF West Pit Feed

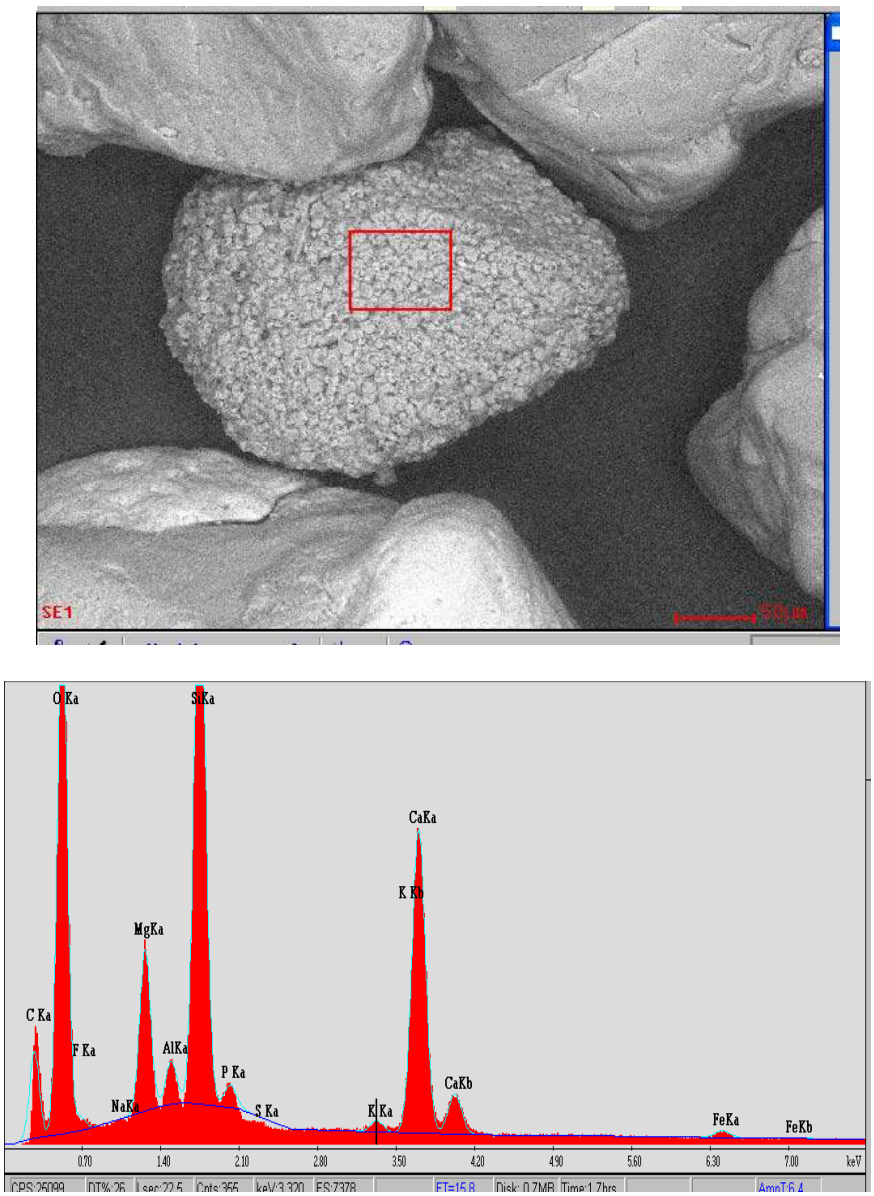

Figure 79. SEM Micrograph of CF West Feed Showing Dolomite Particle Composed of Colloidal Nanoparticles, and Its EDS Spectrum.

CF West Pit Concentrate

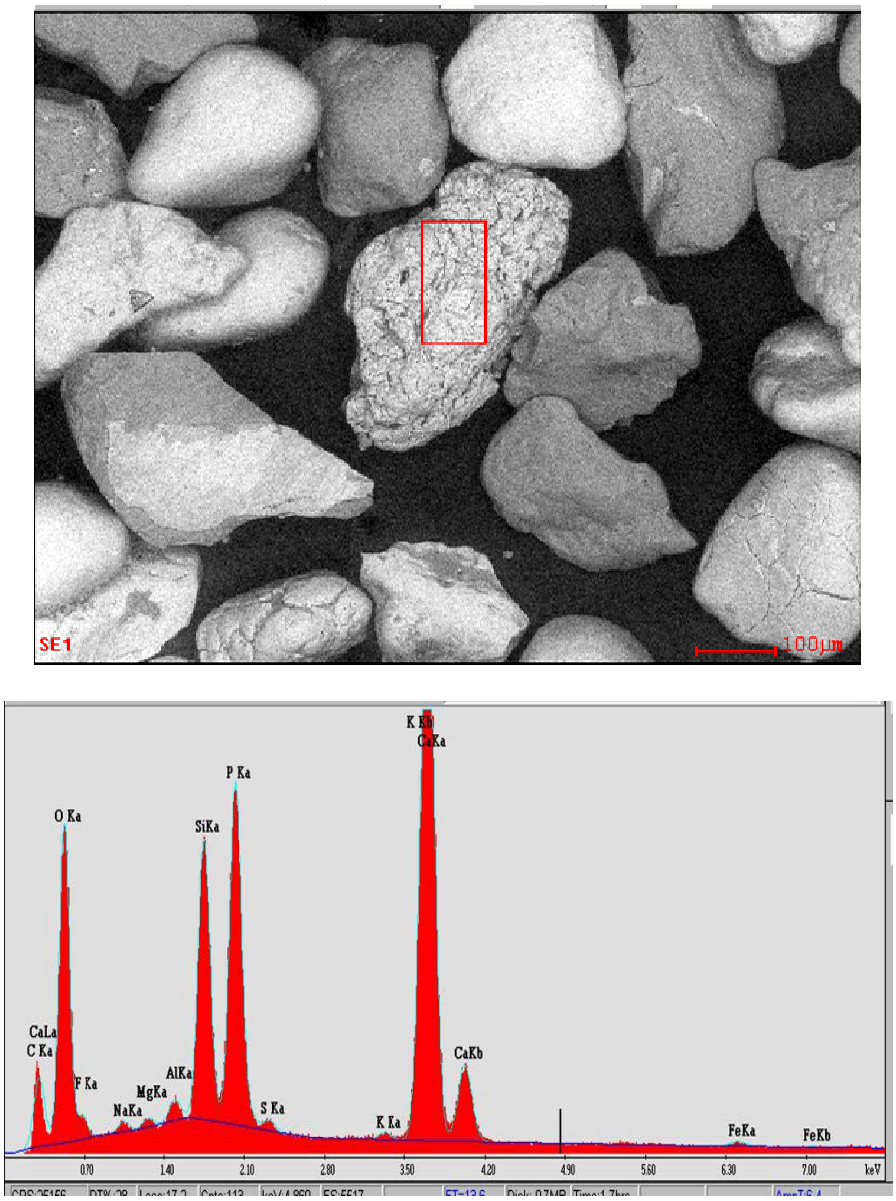

Figure 80. SEM Micrograph of CF West Pit Concentrate Showing Phosphate Particle Composed of Colloidal Nanoparticles and Its EDS Spectrum.

CF West Pit Concentrate

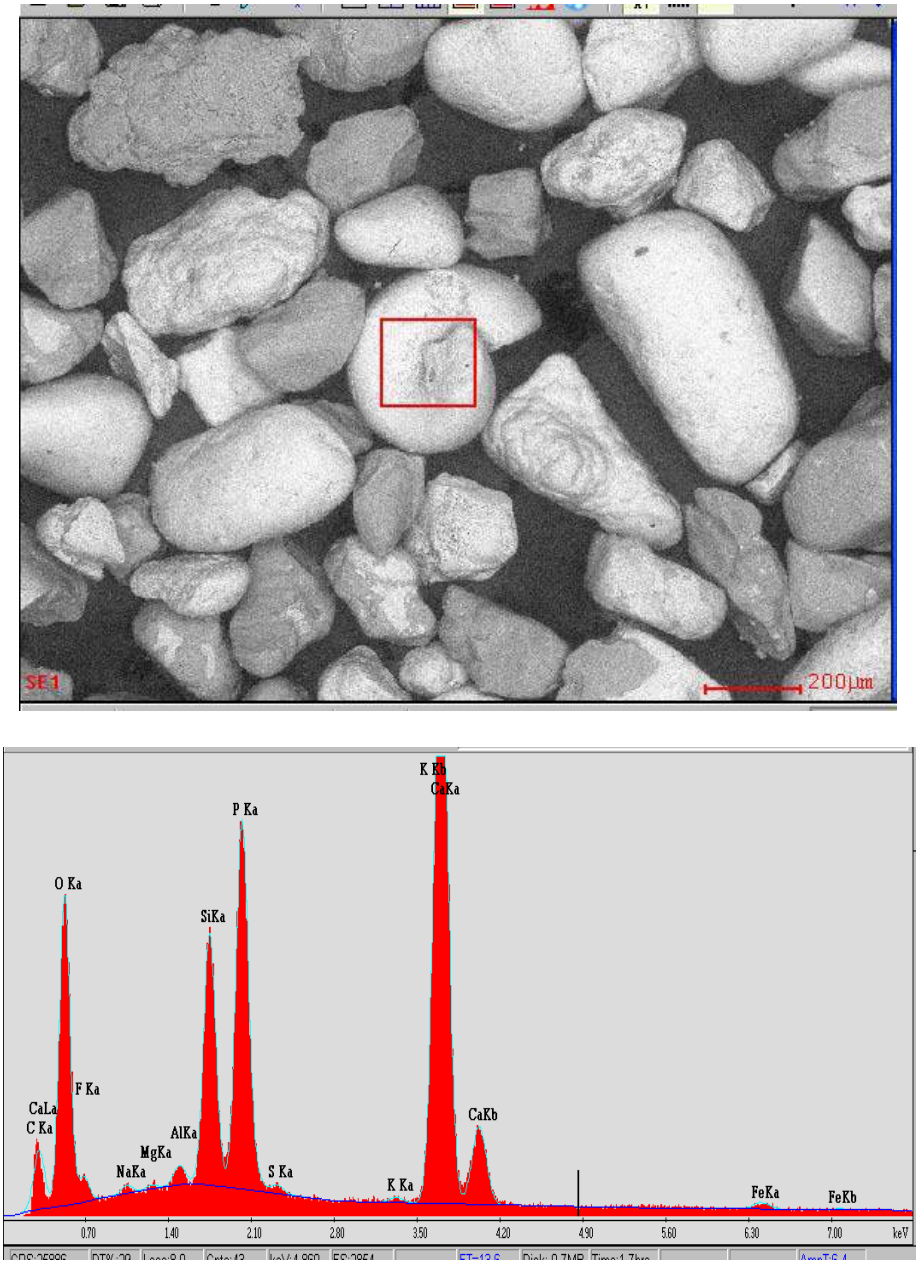

Figure 81. SEM Micrograph of CF West Pit Concentrate Showing Close Particle Size Range and Abundance of the Elongated Phosphate Particles, and EDS Spectrum of Phosphatized Shell Fragment.

CF West Pit Concentrate

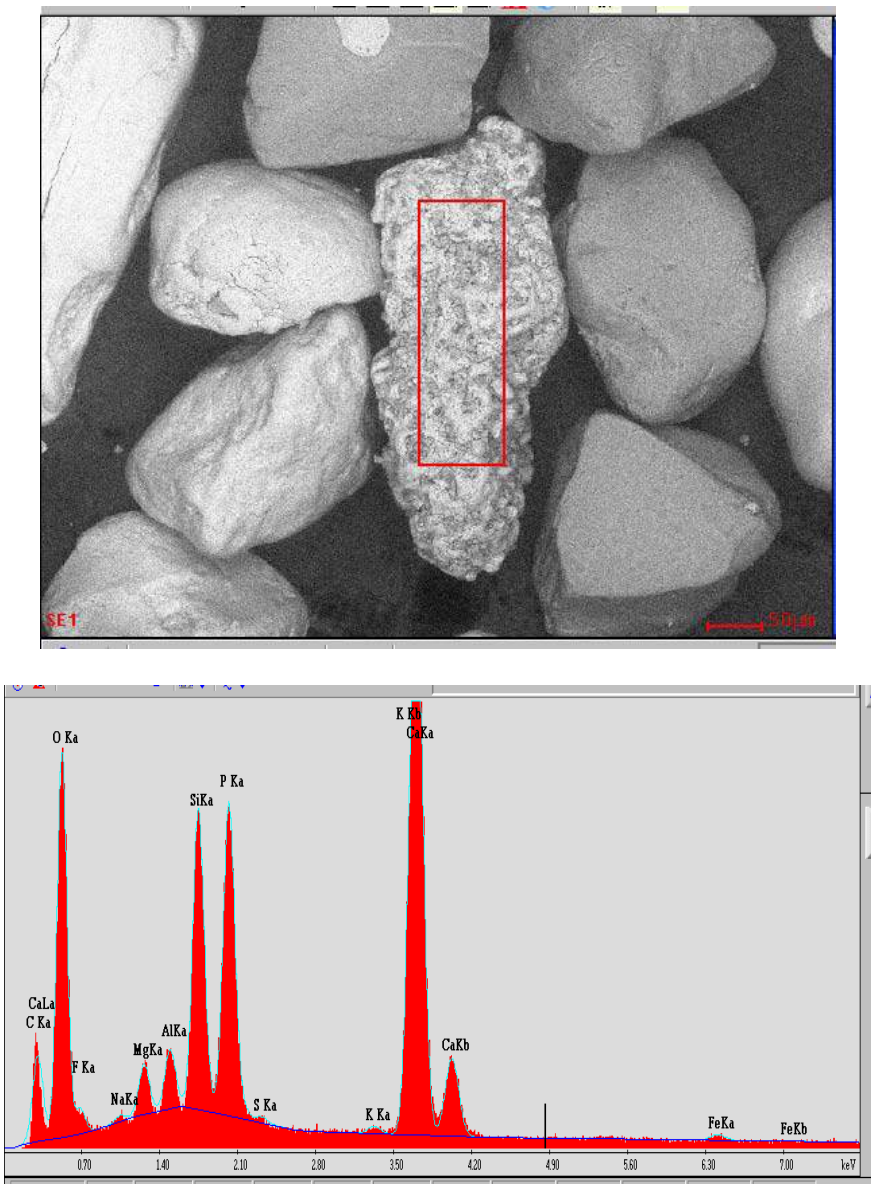

Figure 82. SEM Micrograph of CF West Pit Concentrate Showing Elongated, Irregular Phosphate Particle and Its EDS Spectrum.

Summary

SEM and EDS analysis revealed that the particle size distribution is narrow in the good feeds (CF West Pit and CF Combined), while in the bad feeds it is wide. There was a good phosphate percentage in the coarse to very coarse size fraction, significantly coarser than the associated quartz particles. The effect of particle size distribution is obvious on separation, where most of the coarse phosphate particles in the bad feeds are lost to the tailings, leaving the concentrates a uniform particle size.

In the 1862-S2 sample, gypsum is found in the feed in crystals of cylindrical shape surrounding phosphate particles and sometimes aggregated as coarse particles. Gypsum is a source of calcium which may interfere in the flotation process. The phosphate particles in the tailings are more porous than those in the concentrate, and the phosphate particles in the tailings are one of the following types: coarse, highly porous, kaolinite-coated, or unliberated.

In the feed for 464-S1, some phosphate particles show high porosity and kaolinite is present in the shape of worms, rods or ropes attached or stained on the surface of both phosphate and quartz particles. Sometimes the kaolinite forms a shell around the different particles. In the tailings, kaolinite is acting as a binding material for some phosphate and quartz particles, and the phosphate particles are very coarse, unliberated or attached to quartz particles by the kaolinite mineral. As in the other phosphate samples, the phosphate particles are elongated (rods or oval) and spherical or irregular. In this case, the elongated phosphate particles are more common in the concentrate than in the tailings.

CF Combined and CF West Pit feeds have no such features found in the bad feed material and separation efficiency is limited by liberation.

Surface Chemistry—X-Ray Photoelectron Spectroscopy (XPS) Analysis

EDS analysis of elemental composition was complemented by surface-sensitive XPS analysis of concentrate and tailing samples from 464-S1 and 1862-S2 in order to compare the phosphate particles in the concentrate with those in the tailing. XPS analysis depends on the interaction of the X-ray beam with the particle surface. During this interaction, photoelectrons are emitted from the particle and this energy is directly related to its elemental and chemical characteristics. Since these photoelectrons can escape only from the top few nanometers of the sample material, XPS is a powerful surface analysis technique. Unlike EDS, XPS gives only surface composition information, without a subsurface signal present. It is also very sensitive and allows for quantification of the elements. Modern XPS systems allow for imaging of the sample using an electron gun similar to that used in SEM imaging. This combination allows for collecting signals from selected single particles of a sample. It is important to note that the surface characteristics of the particle are a deciding factor during the flotation separation process.

Before the XPS analysis, initial dry coarse and fine phosphate particles were handpicked for this analysis of concentrates and tailings of two bad feeds, 464-S1 and 1862-S2. The Kratos Axis Ultra DLD XPS system was used. The sample was imaged using the electron gun, and XPS spectra 50 μm by 50 μm were taken. Spectra were quantified and surface elemental compositions of three individual selected particles of each sample were obtained. The mass concentration percentages of the elements phosphorus, calcium, fluorine, iron, magnesium, aluminum, silicon, and sulfur for each particle are given in Tables 17 and 18, while all results are given in the Appendix.

The XPS results of 464-S1 (Table 17, Figures 83-90) revealed that surface phosphorus, calcium and fluorine are higher in the concentrate than in the tailings. The mass concentration of surface phosphorus ranges from 12.70 to 13.12%, with an average of 12.89% in the concentrate, and ranges from 0.07 to 13.25%, with an average of 8.29% in the tailing. Calcium ranges from 12.77 to 17.01%, an average of 15.51% in the concentrate, and ranges from 1.54 to 20.23%, with an average of 11.38% in the tailing. Silica is higher in the tailing (average of 18.33%) than in the concentrate (average of 6.80%), while magnesium, iron, alumina and sulfur are higher in the concentrate.

These results can be explained by the fact that phosphorus and calcium are high in the concentrate while silica is high in the tailings, as expected due to the dominance of the phosphate particles in the concentrate and quartz particles in the tailings. Magnesium, iron, aluminum, and sulfur, which are related to dolomite, montmorillonite, kaolinite and gypsum minerals, are mostly attached to phosphate particles rather than quartz particles and are concentrated in the concentrate, as is given in the mineralogical results and confirmed by SEM images of these samples.

On the other hand, XPS results of 1862-S2 (Table 18, Figures 91-98) indicate that the surface phosphorus, calcium and fluorine are higher in the concentrate than in the tailing. The mass concentration of phosphorus ranges from 10.34 to 1.03%, an average of 7.71% in the concentrate, and ranges from 2.32 to 6.49%, an average of 5.04% in the tailing. Calcium ranges from 2.26 to 12.28%, an average of 6.17% in the concentrate, and ranges from 2.25 to 5.70%, an average of 4.03% in the tailing. Silica is higher in the concentrate (average of 19.06%) than in the tailing (average of 15.81%); this may be attributed to particle 3. Iron and sulfur are higher in the concentrate than the tailing, while for alumina and magnesium this was reversed.

Table 17. Surface Chemical Composition of Three Selected Particles in the Concentrate and Tailings of Hole 464 Split 1.

Element	Concentrate				Tailings			
	Particle 1	Particle 2	Particle 3	Average	Particle 1	Particle 2	Particle 3	Average
Mg	0.27	0.00	0.03	0.10	0.03	0.16	0.01	0.07
Fe	5.74	4.10	4.59	4.81	3.94	7.07	0.42	3.81
F	1.04	1.73	2.01	1.59	2.24	1.20	0.00	1.15
Ca	12.77	17.01	16.74	15.51	20.23	12.37	1.54	11.38
P	13.12	12.84	12.70	12.89	13.25	11.56	0.07	8.29
Si	8.03	6.21	6.17	6.80	3.29	5.32	46.38	18.33
Al	5.99	7.06	5.02	6.02	4.47	2.63	2.16	3.09
S	1.47	1.53	1.71	1.57	1.66	0.38	0.23	0.76

Table 18. Surface Chemical Composition of Three Selected Particles in the Concentrate and Tailings of Hole 1862 Split 2.

Element	Concentrate				Tailings			
	Particle 1	Particle 2	Particle 3	Average	Particle 1	Particle 2	Particle 3	Average
Mg	0.10	0.16	0.17	0.14	0.04	0.30	0.57	0.30
Fe	11.10	6.81	2.89	6.93	2.91	3.83	6.09	4.28
F	0.93	0.29	0.22	0.48	0.18	0.52	0.39	0.36
Ca	12.28	3.97	2.26	6.17	2.25	5.70	4.15	4.03
P	11.75	10.34	1.03	7.71	2.32	6.49	6.32	5.04
Si	6.89	15.42	34.88	19.06	19.09	8.70	19.63	15.81
Al	0.87	5.22	3.10	3.06	0.47	6.21	4.02	3.57
S	0.99	1.25	0.35	0.86	0.34	0.00	0.03	0.12

A comparison of the XPS results of the phosphate particles in flotation products of 464-S1 and 1862-S2 shows that calcium, phosphorus, fluorine, iron and sulfur exhibit the same behavior; silica exhibits similar behavior in the two samples if we ignore particle 3 of the concentrate of 1862-S2. On the other hand, magnesium and alumina exhibit the opposite behavior.

The mass concentration difference for phosphorus and calcium in the concentrate and tailing is about 4.2% in 464-S1 and about 2.2% in the case of 1862-S2, and that of fluorine was about 0.4% in 464-S1 and about 0.12% in the case of 1862-S2. This difference is a function of separation efficiency, and as this difference increases the separation efficiency increases. Therefore, the separation efficiency of 464-S1 is better than that of 1862-S2, according to the flotation and mineralogical results.

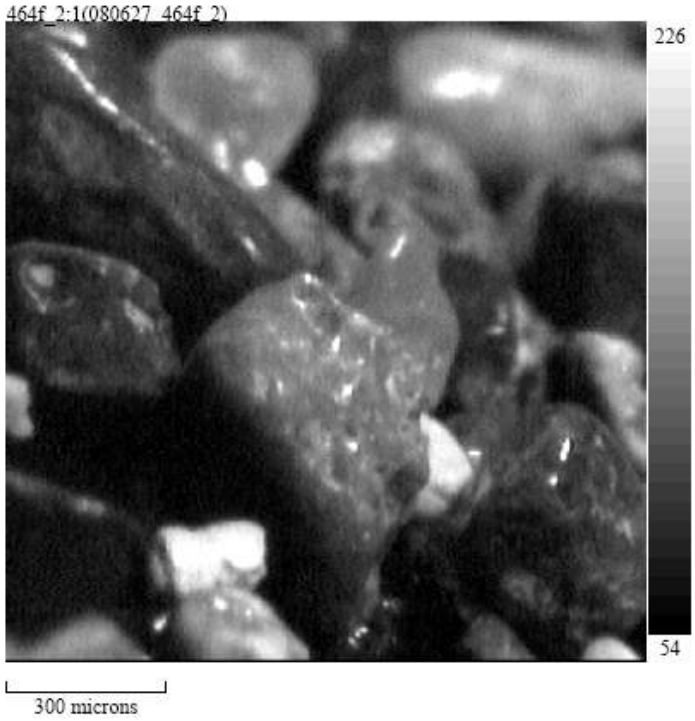

Figure 83. Electron Image of Hole 464 Split 1, Concentrate, Particle 2.

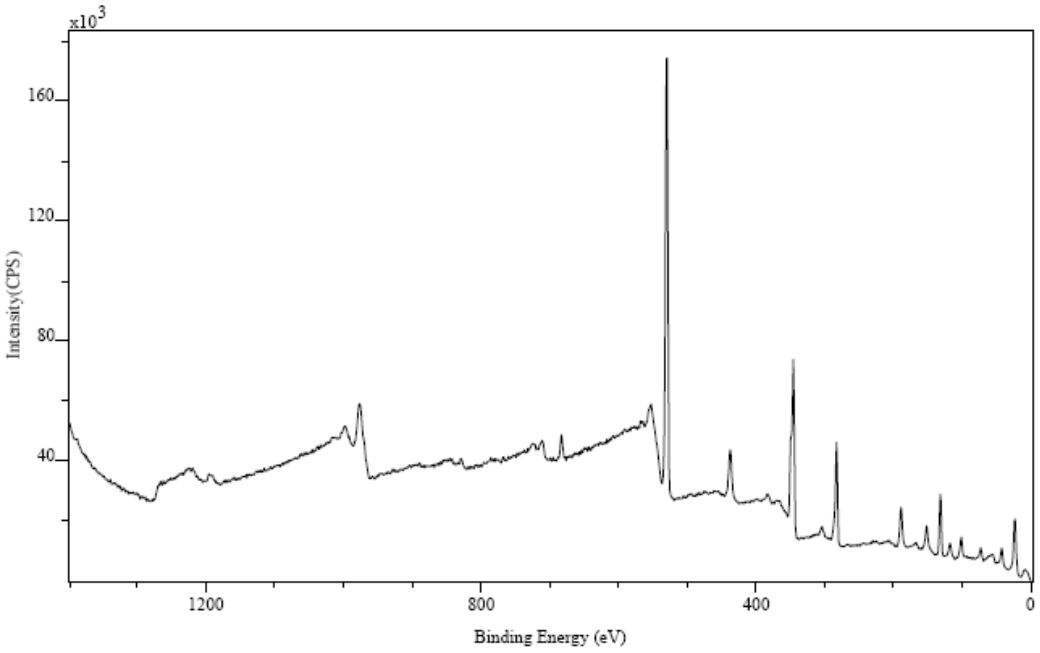

Figure 84. XPS Spectrum of Hole 464 Split 1, Concentrate, Particle 2.

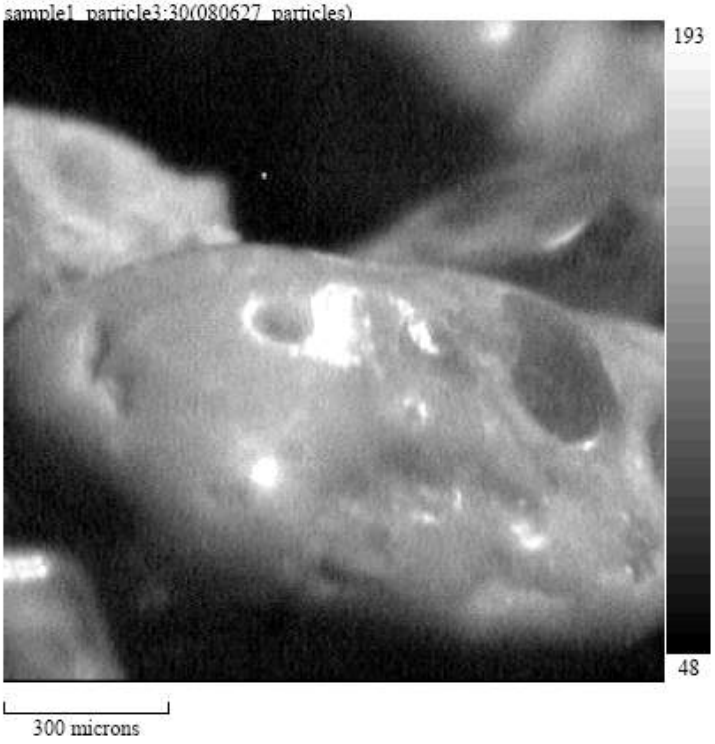

Figure 85. Electron Image of Hole 464 Split 1, Concentrate, Particle 3.

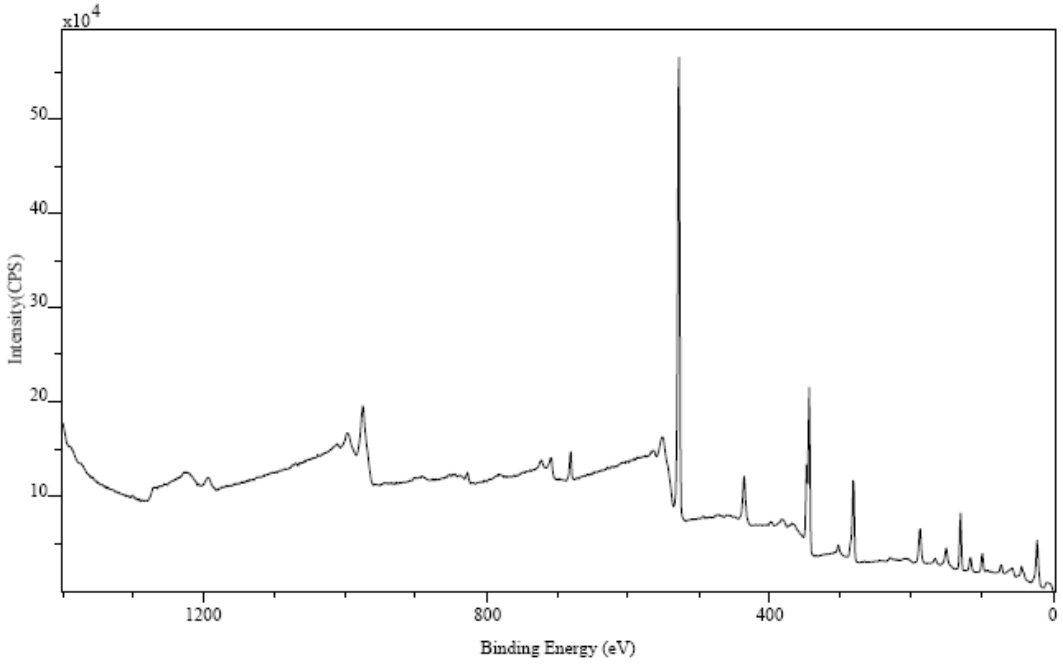

Figure 86. XPS Spectrum of Hole 464 Split 1, Concentrate, Particle 3.

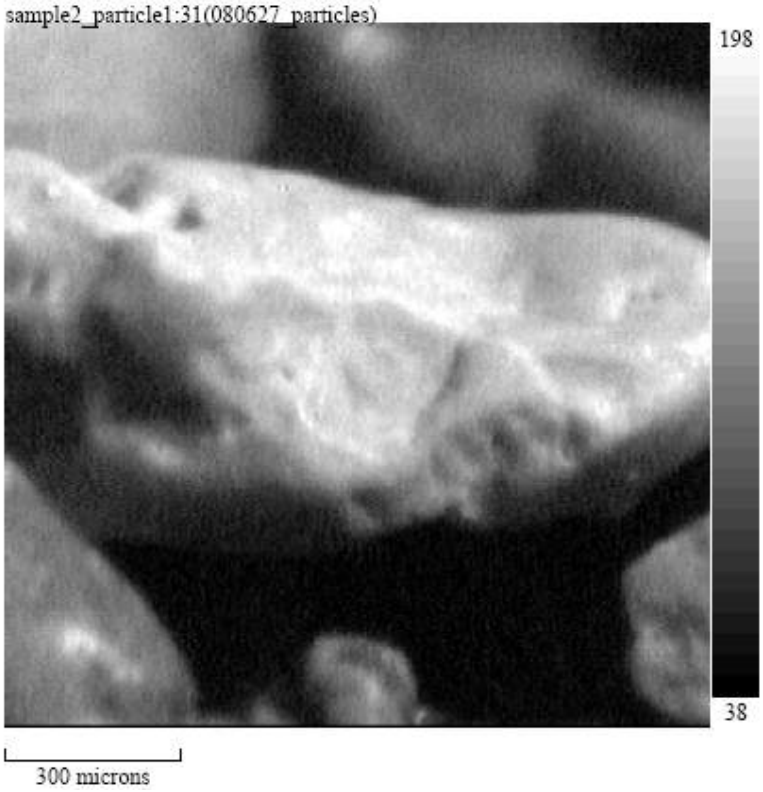

Figure 87. Electron Image of Hole 464 Split 1, Tailings, Particle 1.

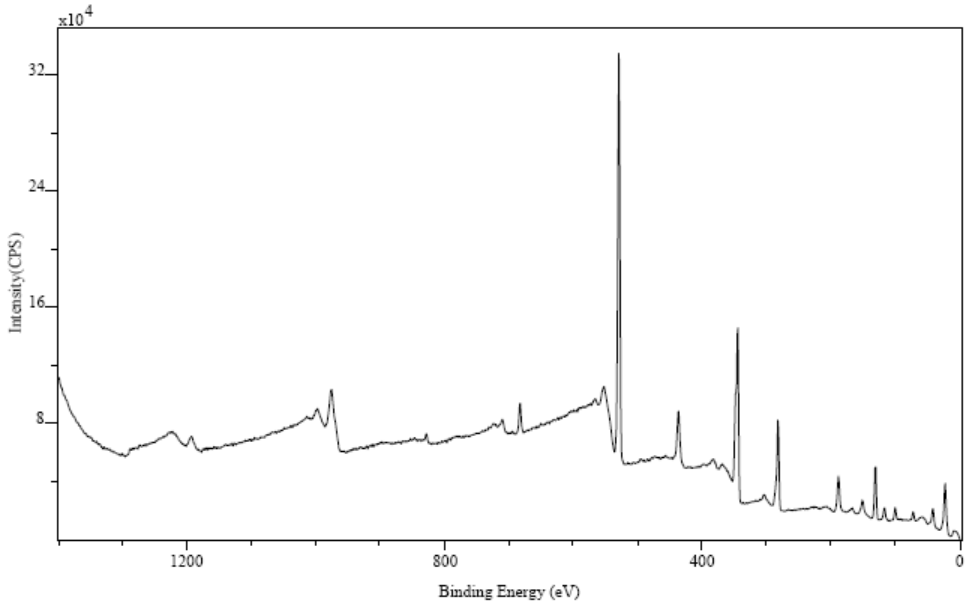

Figure 88. XPS Spectrum of Hole 464 Split 1, Tailings, Particle 1.

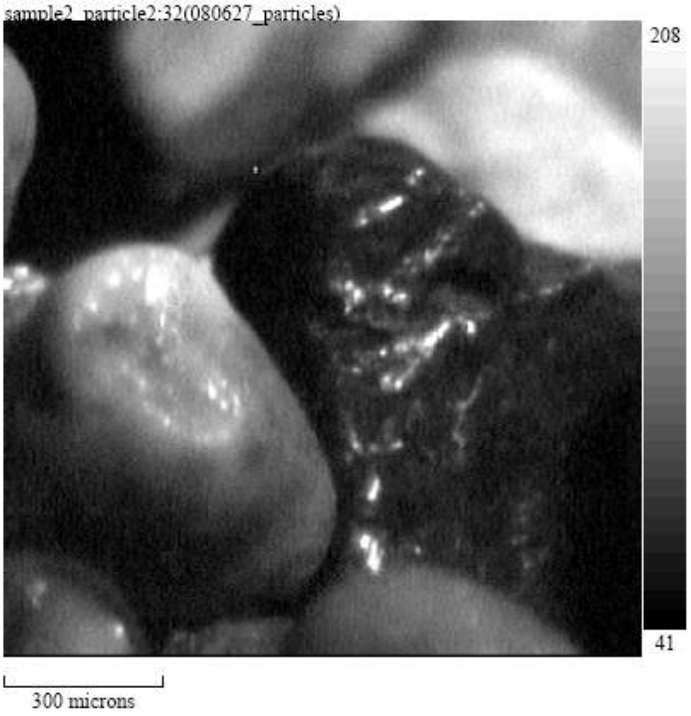

Figure 89. Electron Image of Hole 464 Split 1, Tailings, Particle 2.

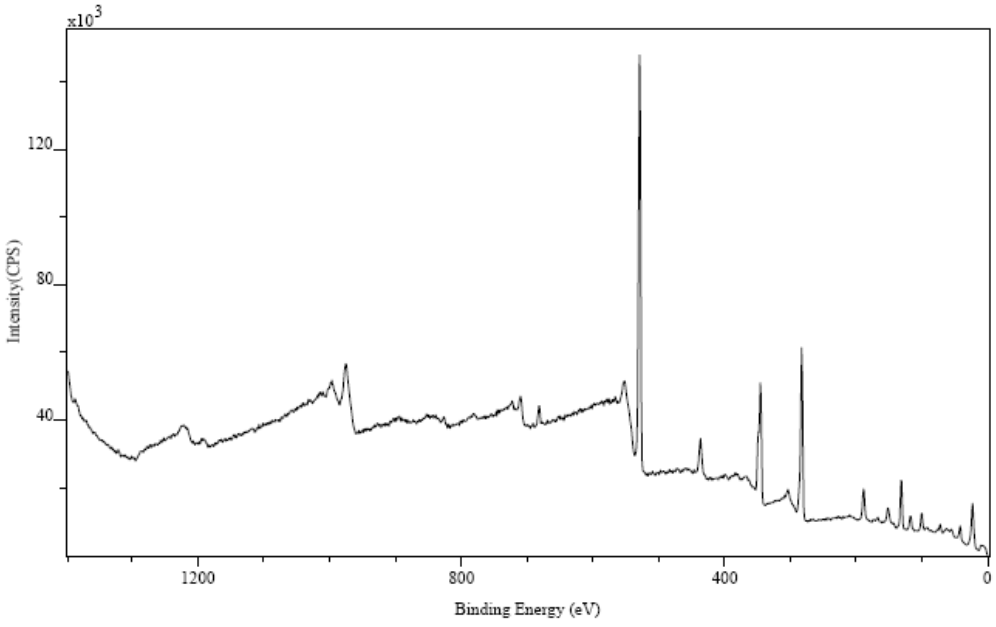

Figure 90. XPS Spectrum of Hole 464 Split 1, Tailings, Particle 2.

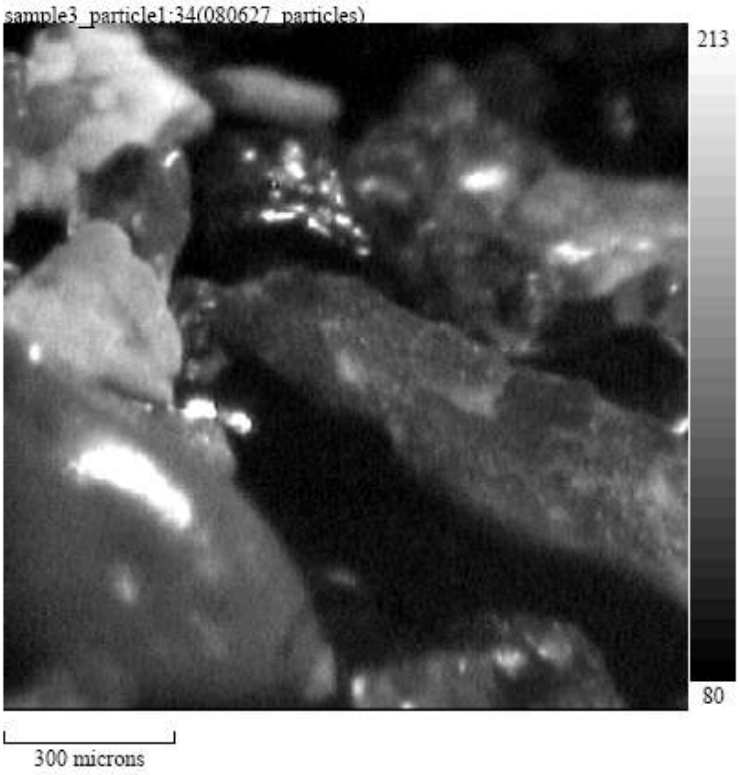

Figure 91. Electron Image of Hole 1862 Split 2, Concentrate, Particle 1.

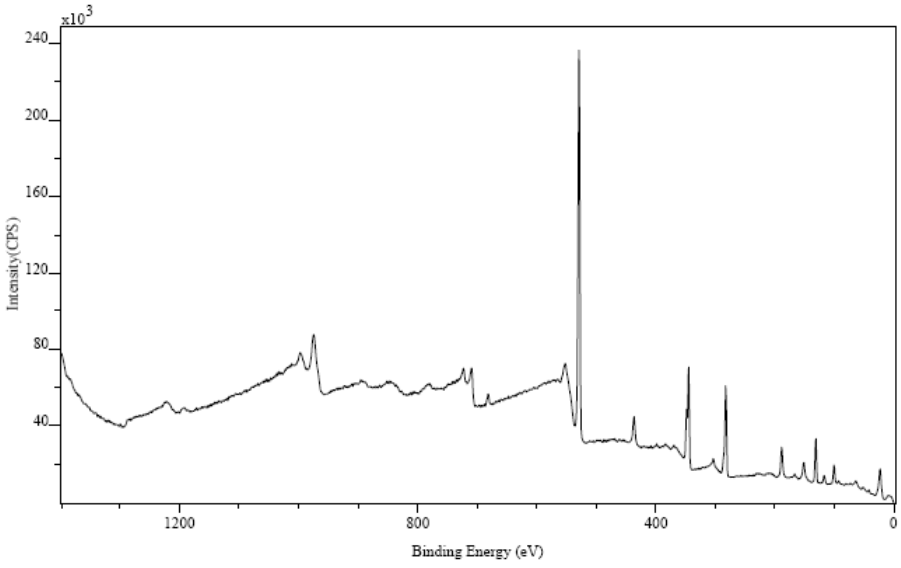

Figure 92. XPS Spectrum of Hole 1862 Split 2, Concentrate, Particle 1.

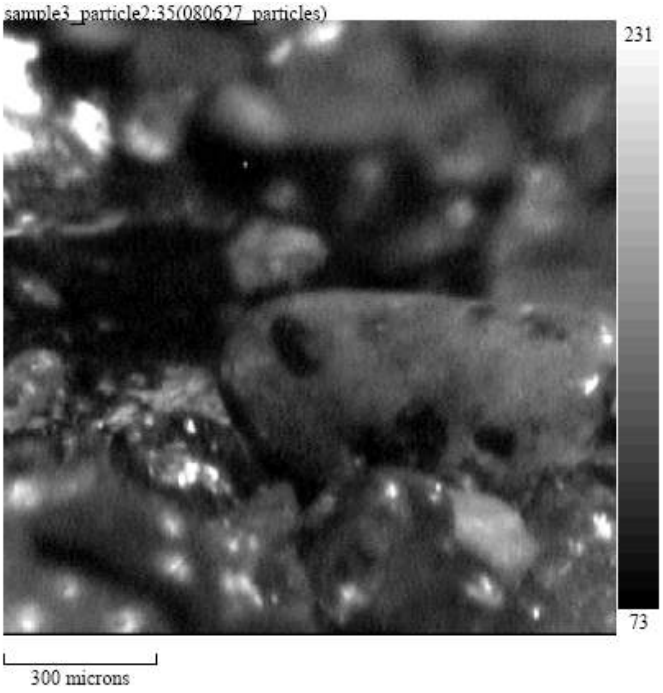

Figure 93. Electron Image of Hole 1862 Split 2, Concentrate, Particle 2.

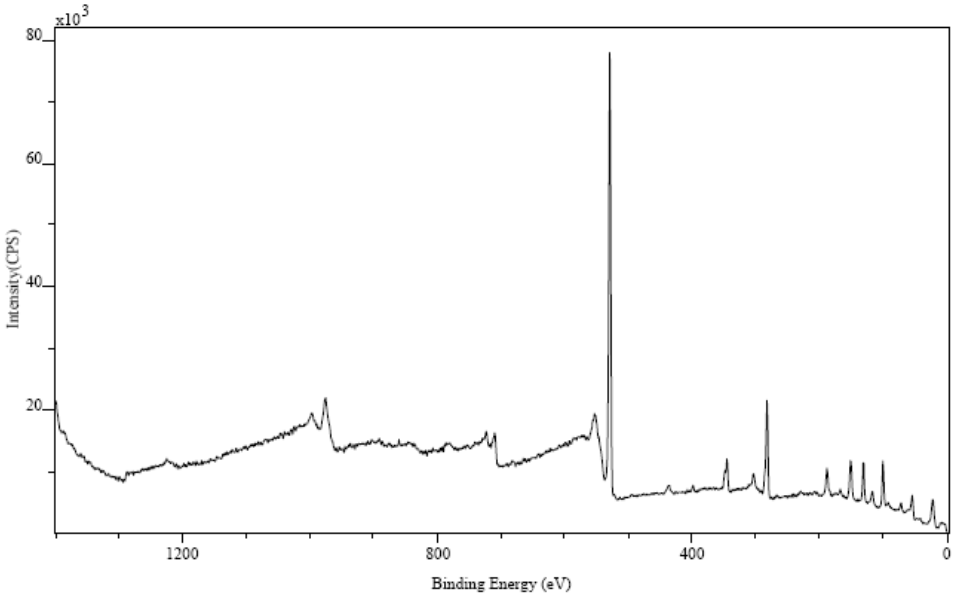

Figure 94. XPS Spectrum of Hole 1862 Split 2, Concentrate, Particle 2.

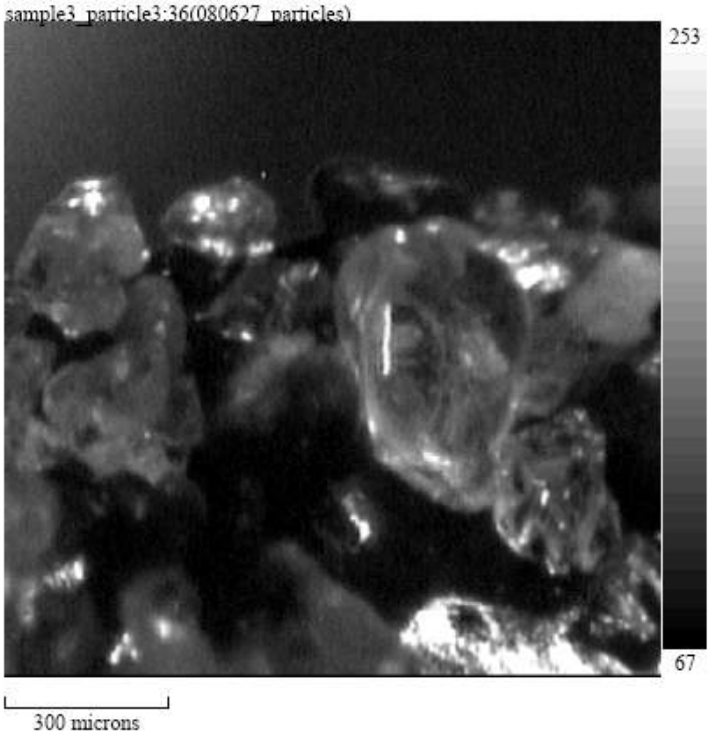

Figure 95. Electron Image of Hole 1862 Split 2, Concentrate, Particle 3.

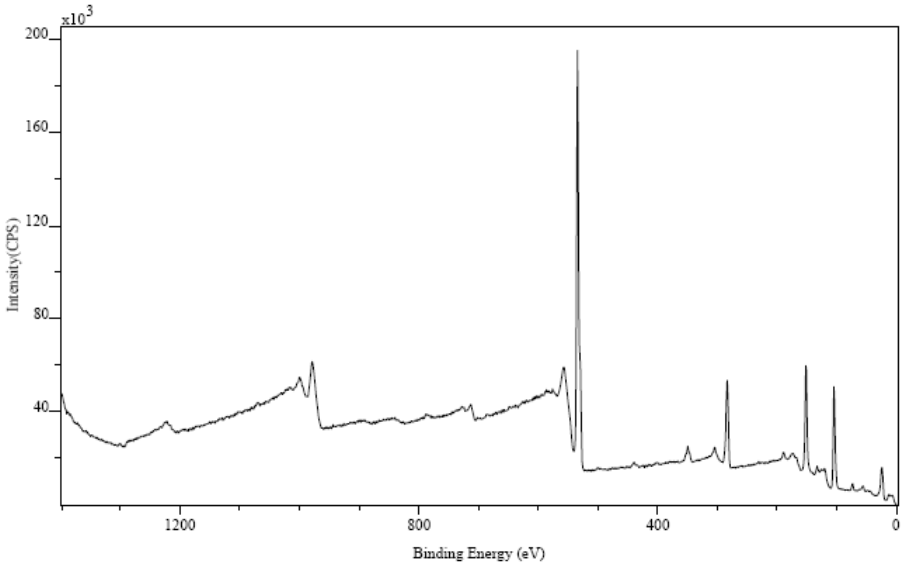

Figure 96. XPS Spectrum of Hole 1862 Split 2, Concentrate, Particle 3.

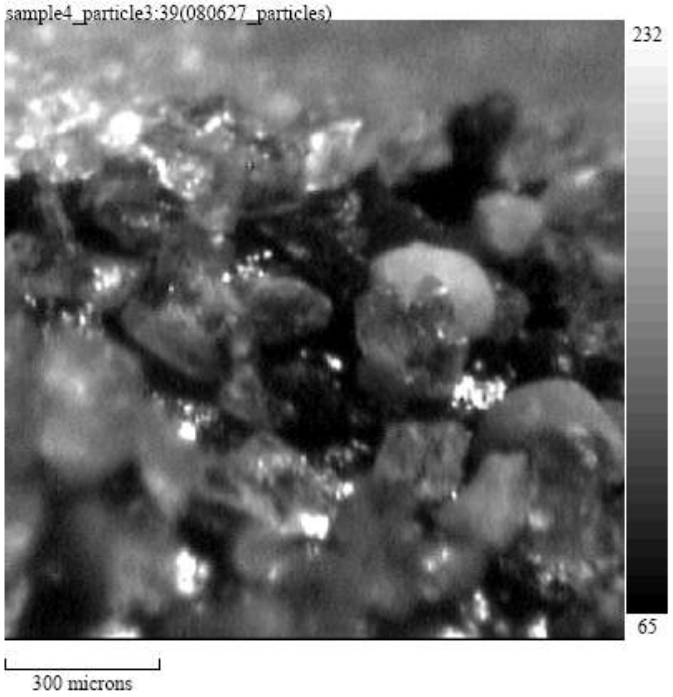

Figure 97. Electron Image of Hole 1862 Split 2, Tailings, Particle 3.

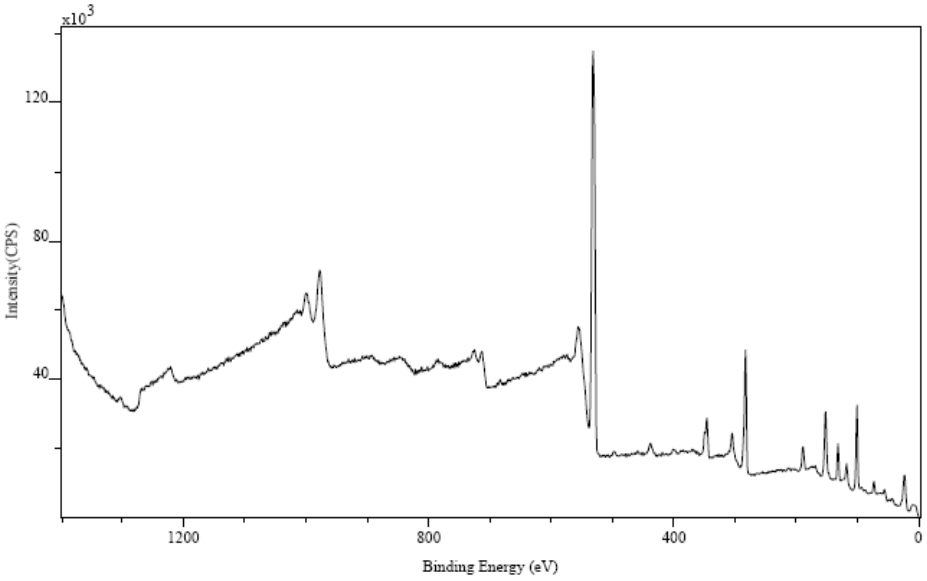

Figure 98. XPS Spectrum of Hole 1862 Split 2, Tailings, Particle 3.

Summary

The XPS results of phosphate particles in the flotation products of 464-S1 and 1862-S2 revealed that calcium, phosphorus, fluorine, iron and sulfur exhibit the same behavior and are rich on the surface of phosphate particles in the concentrates. Silica exhibits similar behavior and is abundant on the surface of phosphate particles in the tailings. On the other hand, magnesium and alumina exhibit opposite behavior, increasing in the concentrate of 1862-S2 and decreasing in the tailings of 464-S1.

The mass concentration difference for phosphorus, calcium, and fluorine in the concentrate and tailings is higher in the case of 464-S1 than in the case of 1862-S2. This difference is expected to explain separation efficiency, as if this difference increases the separation efficiency will increase. Therefore, the separation efficiency of 464-S1 is better than that of 1862-S2, according to the flotation and mineralogical results.

Micro CT Analysis, Liberation-Limited Grade Recovery Curves

Each sample was analyzed and the X-ray attenuation coefficient histogram (3D liberation spectrum) was obtained for feed and products from each sample. In order to establish the liberation spectra the volume fraction of phosphate and gangue material for each particle in each sample was determined, as reported in our first annual report.

In this way, particles were classified into twelve classes based on phosphate content. The classes are as follows; 0%, 5%, 15%, 25%, 35%, 45%, 55%, 65%, 75%, 85%, 95% and 100% phosphate. Thus for each stream (feed, concentrate and tailings) the 3D liberation spectrum of phosphate was prepared. Also, grade/recovery curves limited only by liberation characteristics were prepared from feed data only and compared with actual recovery calculated from the two-product formula. Points marked by a cross on a gray background square represent actual recovery calculated from the two-product formula. The feed grade is indicated by an arrow on the right side of the grade/recovery curves. For all samples, liberation spectra and liberation-limited grade/recovery curves are presented as follows:

Sample	Figures
Hole 1862 Split 2	99 and 100
Hole 3057 Split 2	101 and 102
CF Combined	103 and 104
CF West	105 and 106
CF East	107 and 108
FCO	109 and 110
FCO Bad	111 and 112
Hole 464 Split 1	113 and 114

Sample	Figures
Hole 464 Split 2	115 and 116
SFM	117 and 118

Hole 1862 Split 2

From CT analysis of the feed, concentrate and tailings streams for 1862-S2 sample (Figure 99), it is evident that the histograms (liberation spectra) do not differ much from one another. A poor phosphate separation was achieved. Much phosphate material is found in the tailings and the concentrate contains a lot of gangue material. Recovery of below 50% is reported for the 1862-S2 sample. Considerable improvement in recovery and grade should be possible up to around 98% recovery at 60% grade without an increase in liberation. To do this, the surface properties of the feed material as well as products should be investigated and a possible sliming effect has to be taken into account (see Figure 100).

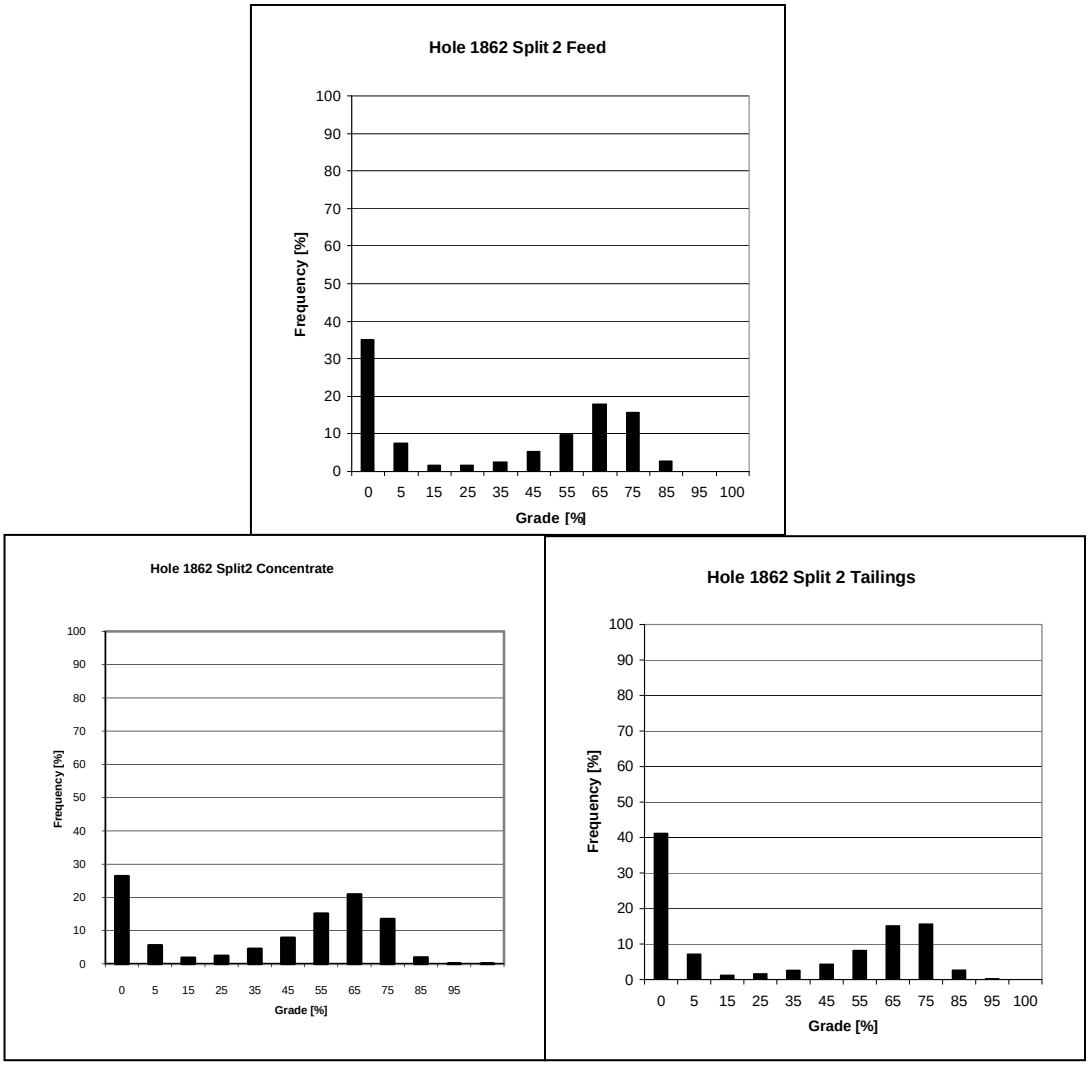

Figure 99. Liberation Spectra of Phosphate for Hole 1862 Split 2 Feed, Concentrate, and Tailings.

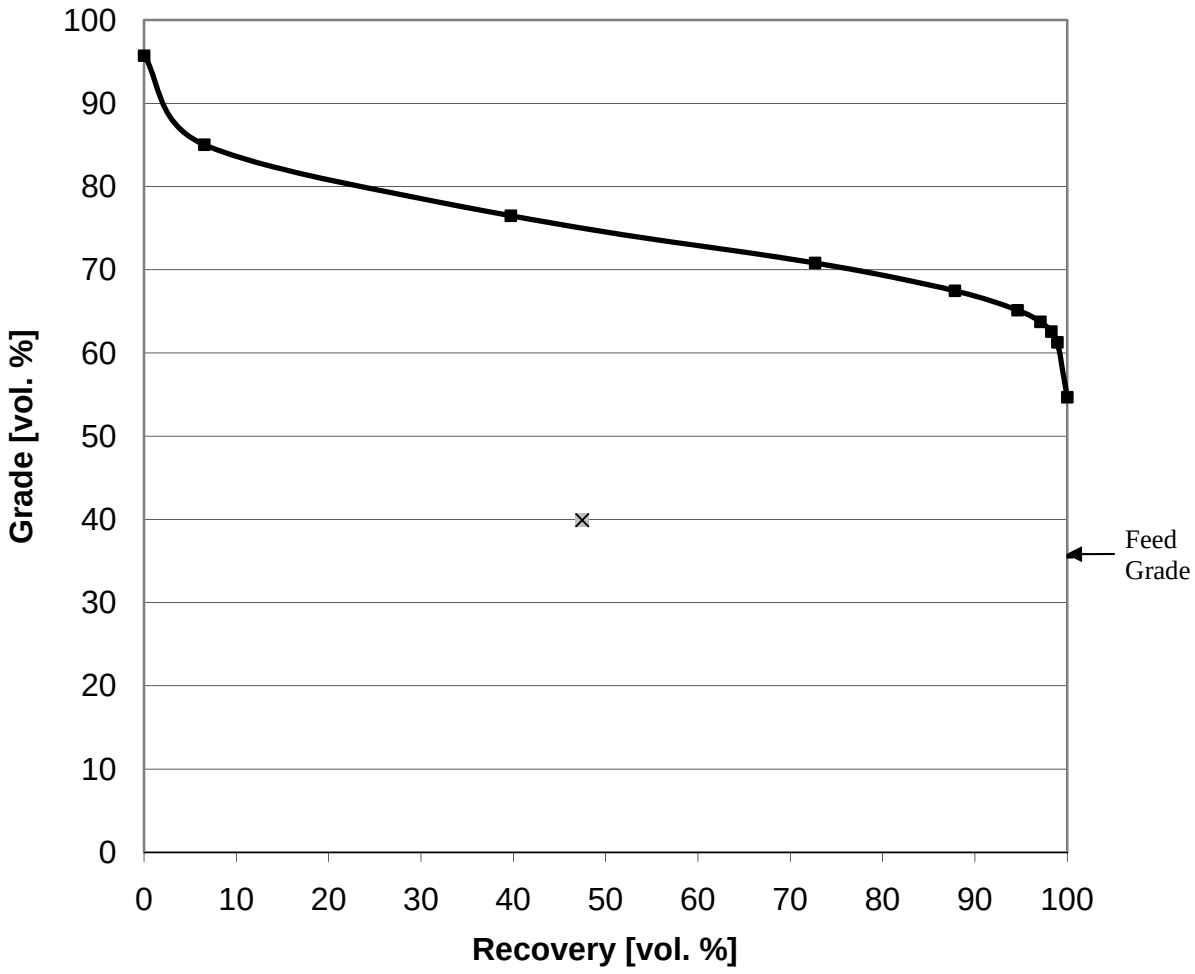

Figure 100. Liberation-Limited Grade/Recovery Curve for Hole 1862 Split 2 Feed. Actual recovery is marked with a cross on a gray background.

Hole 3057 Split 2

The feed material for 3057-S2 is characterized by relatively low grade (16% vol.), yet a fairly high-grade concentrate was achieved. However, similarly to 1862-S2, some increase in recovery (by about 20%) is possible. Liberation-limited recovery could be increased, from 75% to around 95%, without an increase in liberation, for 3057-S2 (see Figures 101 and 102).

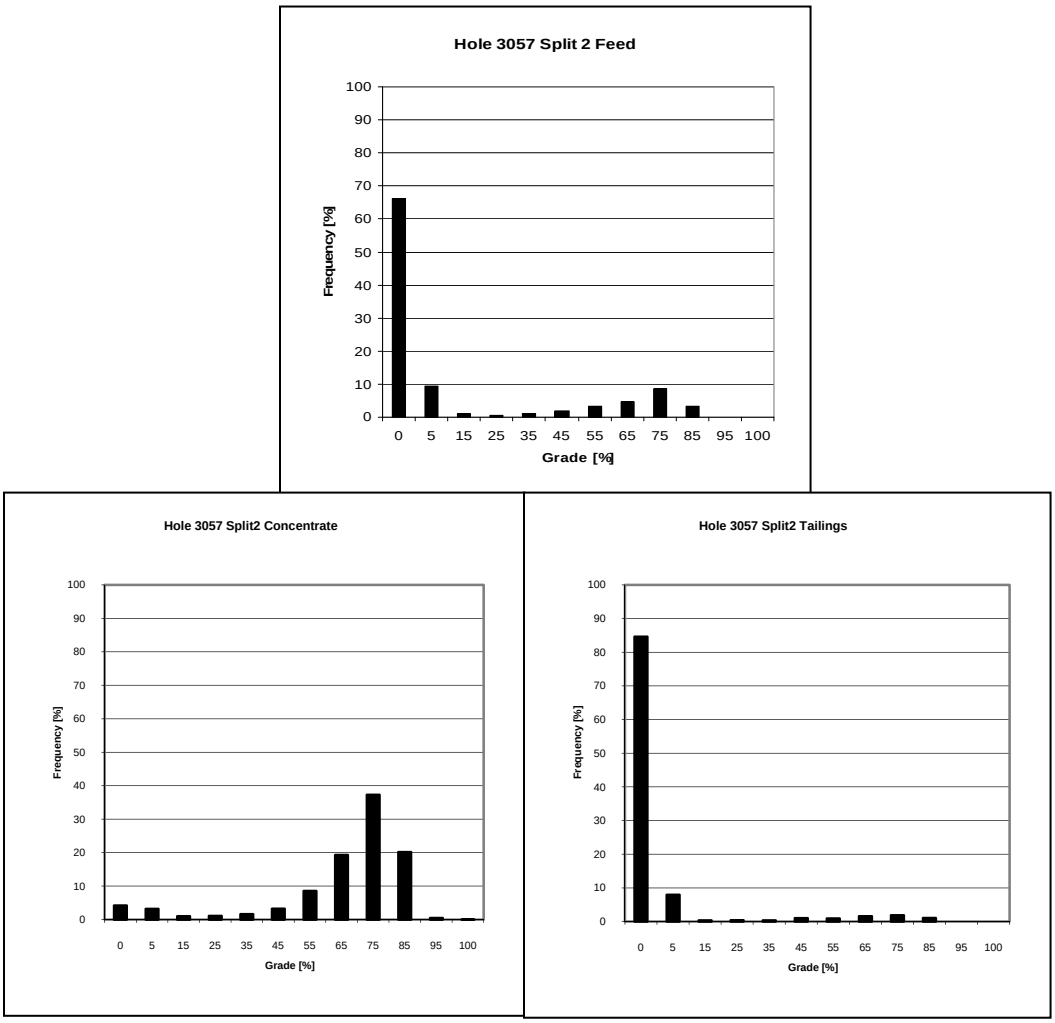

Figure 101. Liberation Spectra of Phosphate for Hole 3057 Split 2 Feed, Concentrate and Tailings.

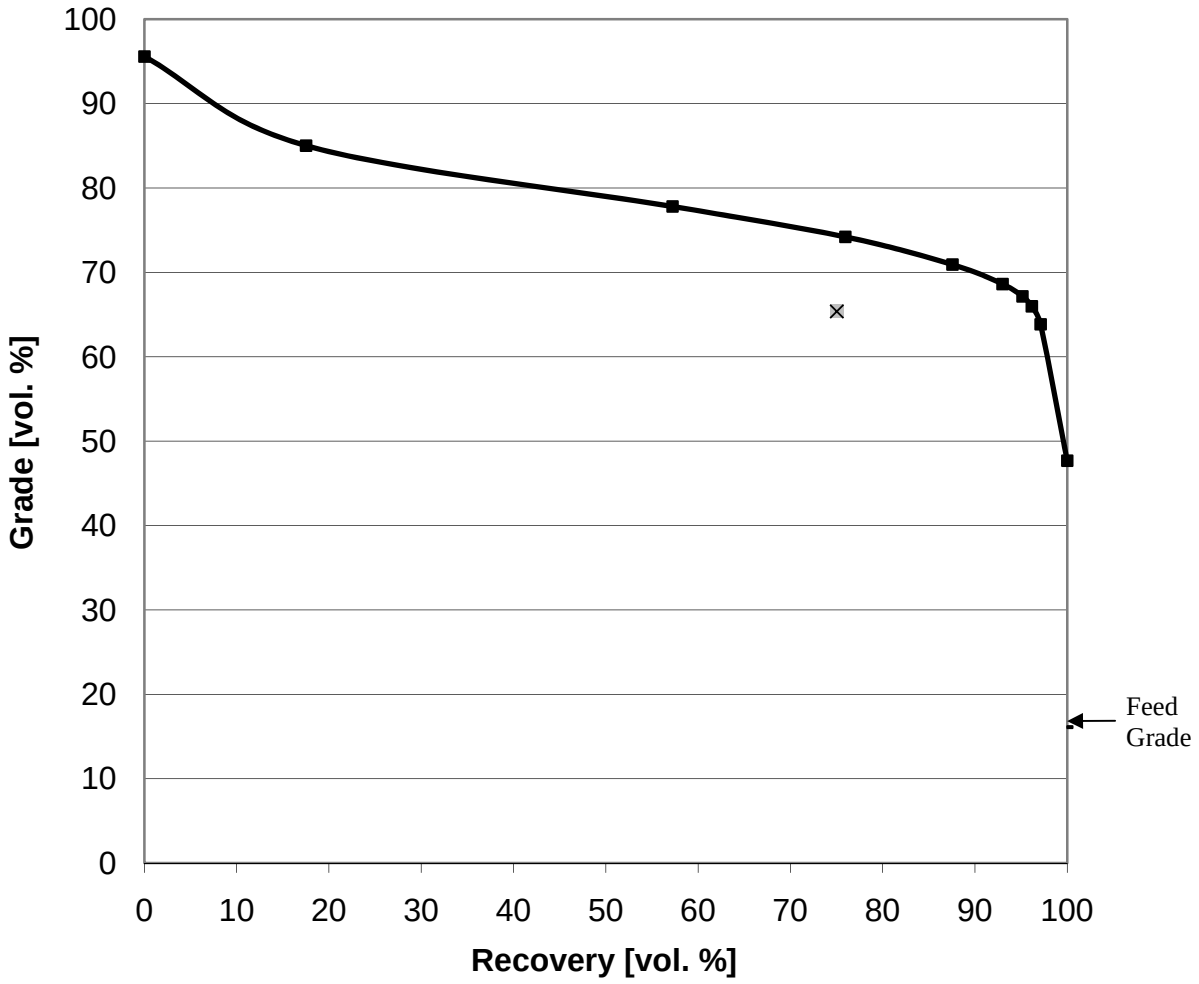

Figure 102. Liberation-Limited Grade/Recovery Curve for Hole 3057 Split 2 Feed. Actual recovery is marked with a cross on a gray background.

CF Combined

Very good separation is achieved for the CF Combined sample. More than 85% of the tailing is pure gangue material; the rest of the material may contain minor inclusions of phosphate grains, which constitute only 1.31% of the total volume for the CF Combined sample (see Figure 103). The concentrate, on the other hand, contains less than 10% of pure gangue material. Very little separation efficiency improvement can be achieved for the CF Combined sample without further size reduction (see Figure 104).

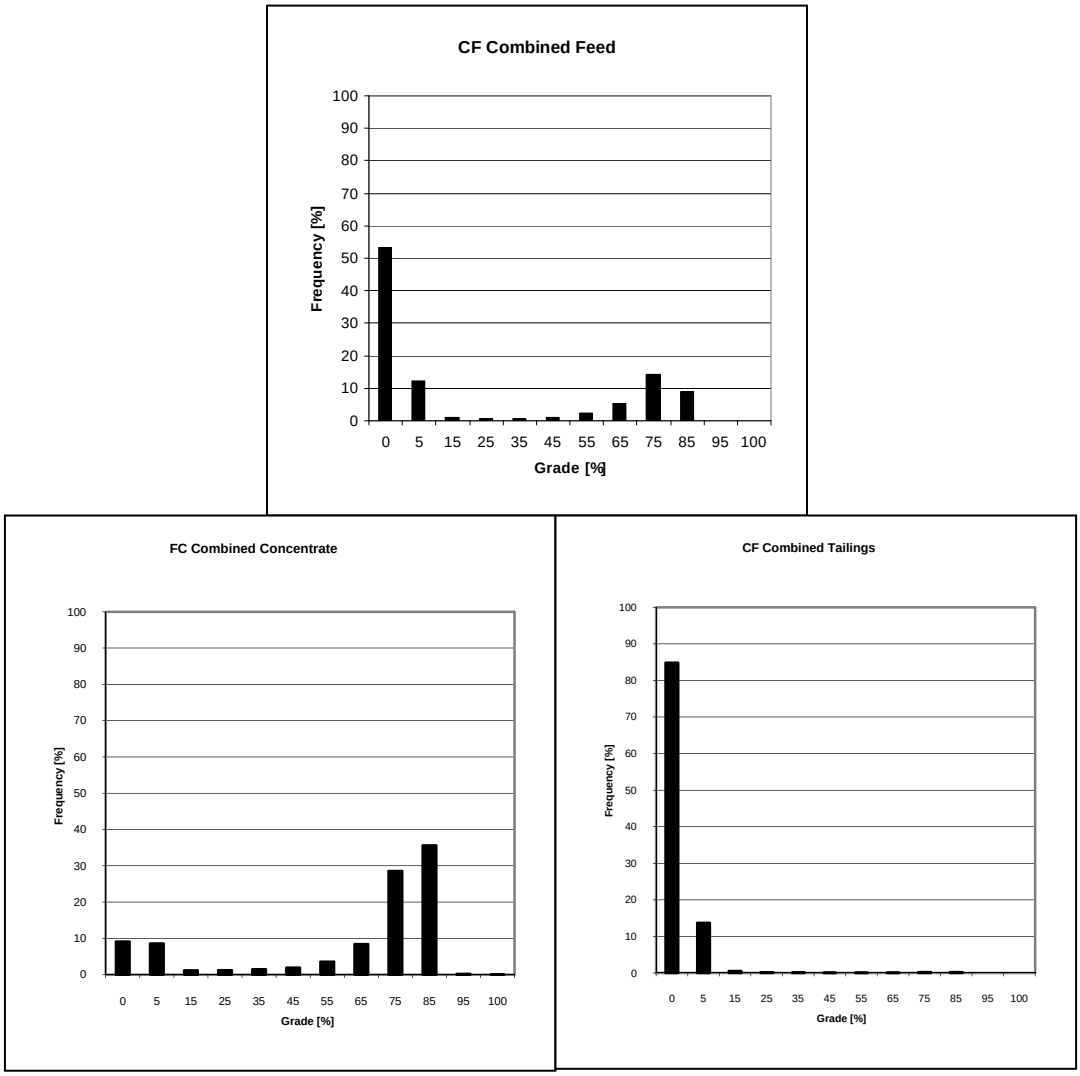

Figure 103. Liberation Spectra of Phosphate for the CF Combined Feed, Concentrate and Tailings.

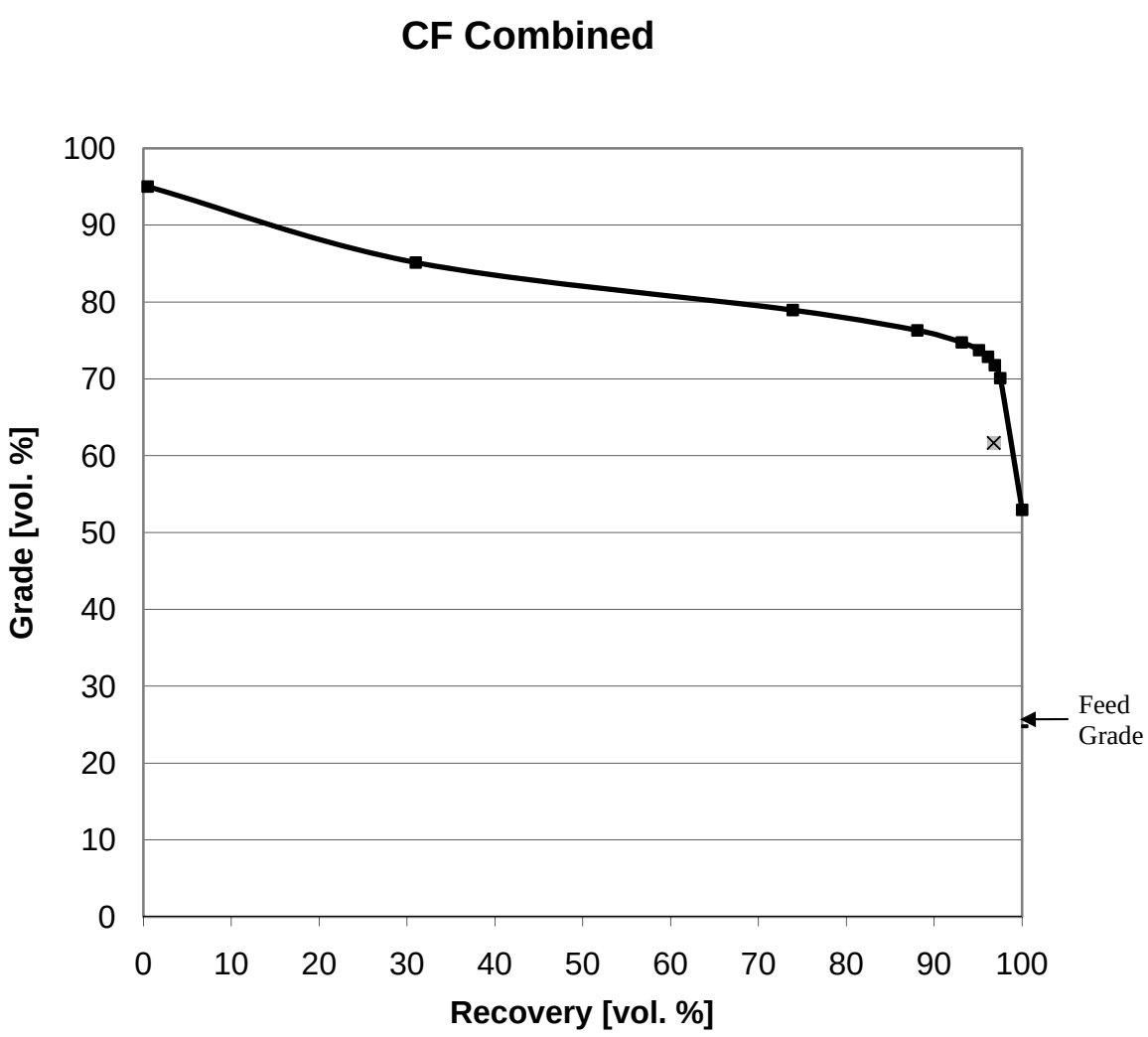

Figure 104. Liberation-Limited Grade/Recovery Curve for the CF Combined 2 Feed. Actual recovery is marked with a cross on a gray background.

CF West Pit

Similarly to CF Combined, very good separation is achieved for the CF West Pit samples. More than 85% of the tailings were pure gangue material; the rest of the material may contain minor inclusions of phosphate grains, which constitute only 1.65% of the total volume (see Figure 105). The concentrate, on the other hand, contains less than 15% of pure gangue material in the case of the CF West sample. Very little separation efficiency improvement can be achieved for the CF West sample without further size reduction (see Figure 106).

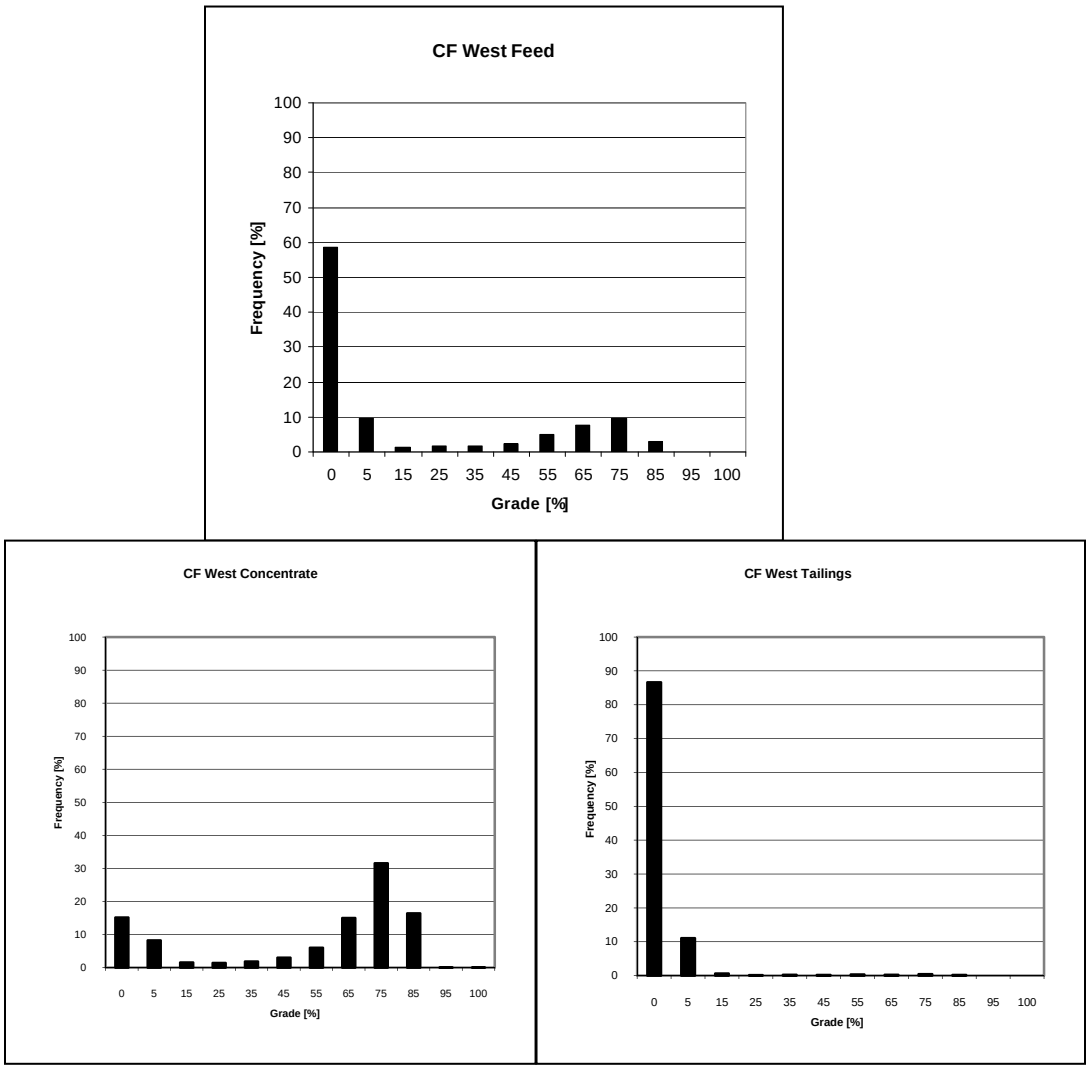

Figure 105. Liberation Spectra of Phosphate for the CF West Pit Feed, Concentrate and Tailings.

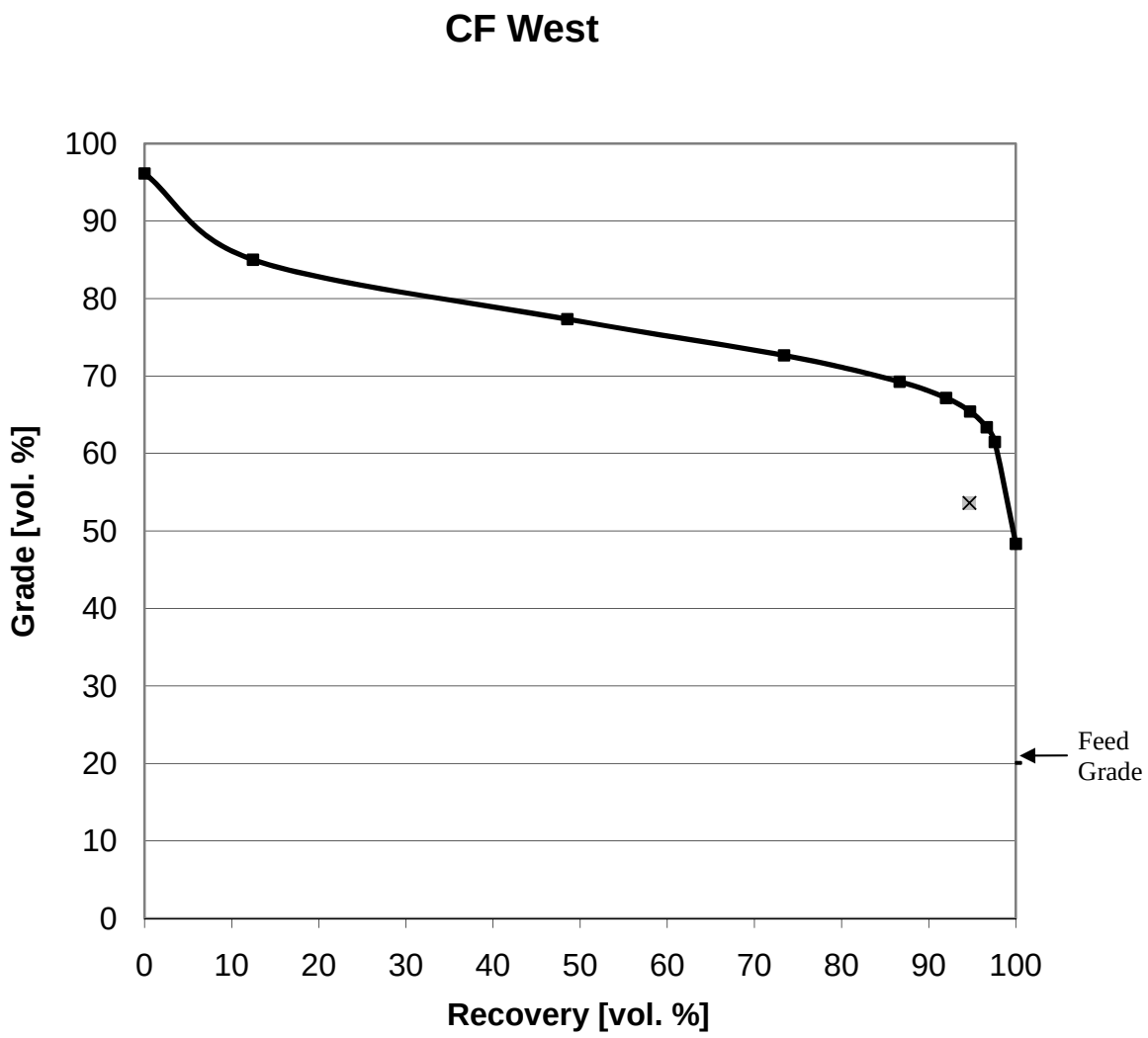

Figure 106. Liberation-Limited Grade/Recovery Curve for the CF West Pit Feed. Actual recovery is marked with a cross on a gray background.

CF East Pit

CF East Pit is another sample, similar to CF Combined and CF West, that is characterized by a very good separation. More than 85% of the tailing is pure gangue material; the rest of the material may contain minor inclusions of phosphate grains, which constitute around 1.75% of the total volume (see Figure 107). The concentrate contains less than 3.5% of pure gangue material and the separation efficiency, for such particle size, is nearly liberation-limited. No improvement can be achieved for the CF East sample without further size reduction (see Figure 108).

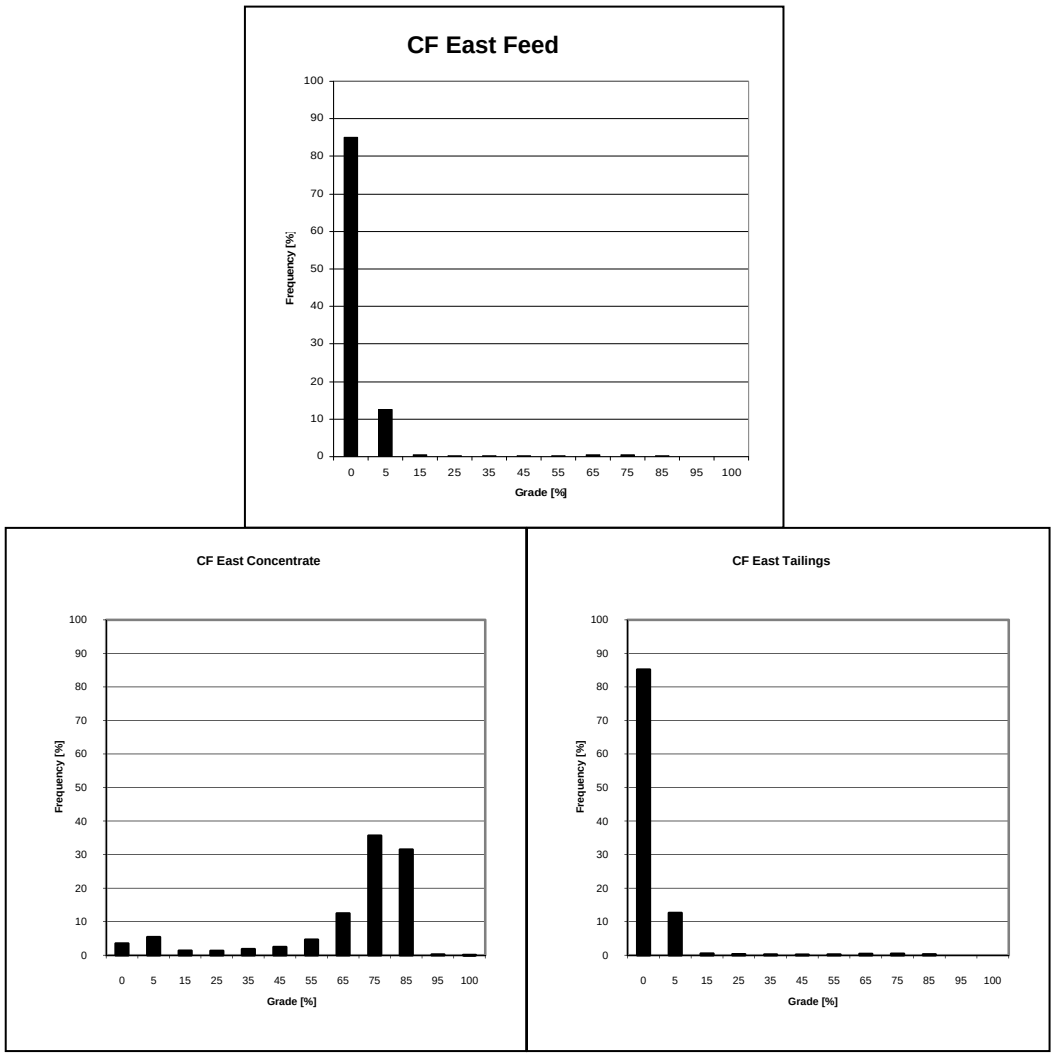

Figure 107. Liberation Spectra of Phosphate for the CF East Feed, Concentrate and Tailings.

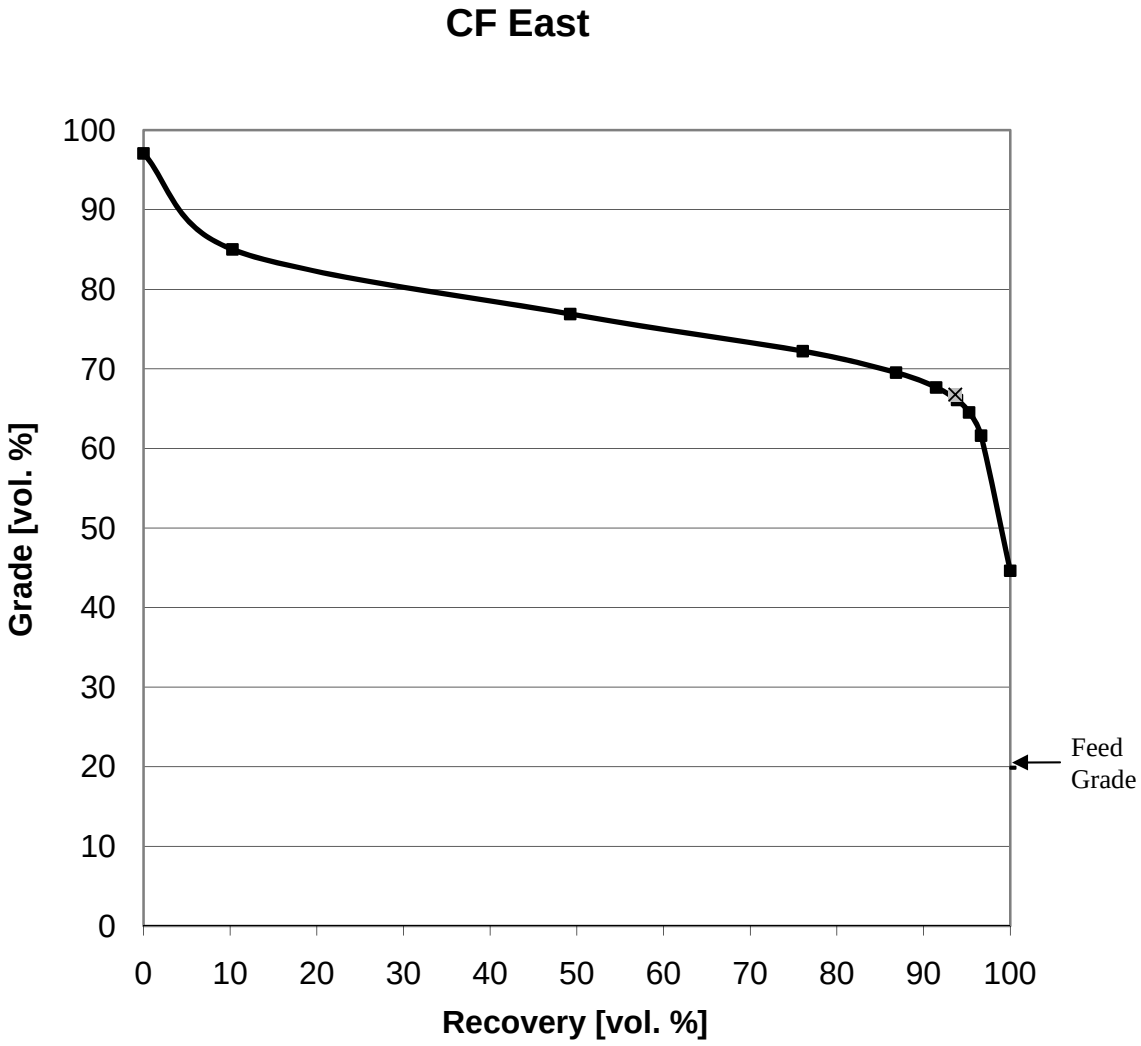

Figure 108. Liberation-Limited Grade/Recovery Curve for the CF East Feed. Actual recovery is marked with a cross on a gray background.

Four Corners (FCO)

This sample could be separated more efficiently. At actual concentrate grade of 50% phosphates by volume, only 65% of the total phosphates are recovered, whereas 97% recovery should be possible (see Figure 109). Approximately 10% of the phosphates is lost in the tailings and there is only around 67% of pure gangue material in the tailings. In this separation process the grade increases from 20% of phosphates in the feed to a little more than 50% of phosphates in the concentrate (see Figure 110).

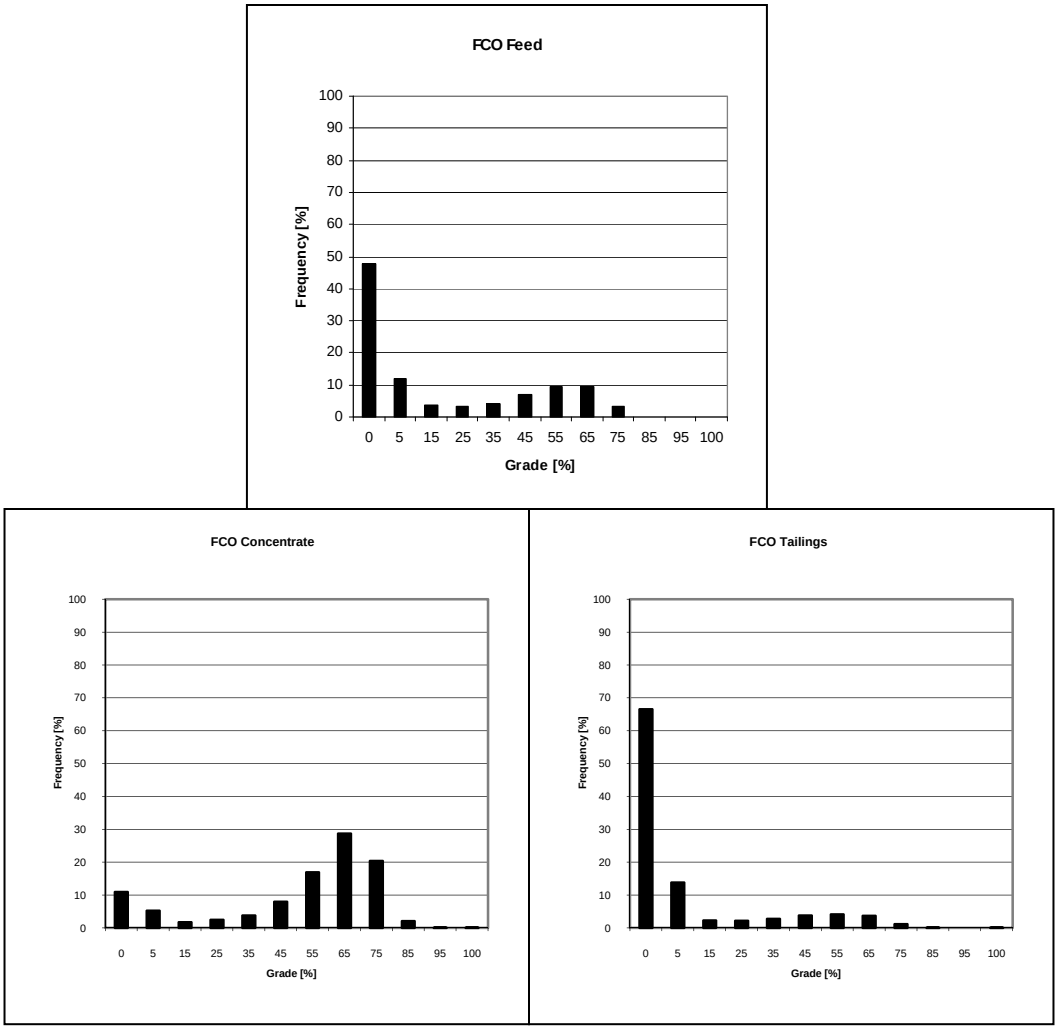

Figure 109. Liberation Spectra of Phosphate for the FCO Feed, Concentrate and Tailings.

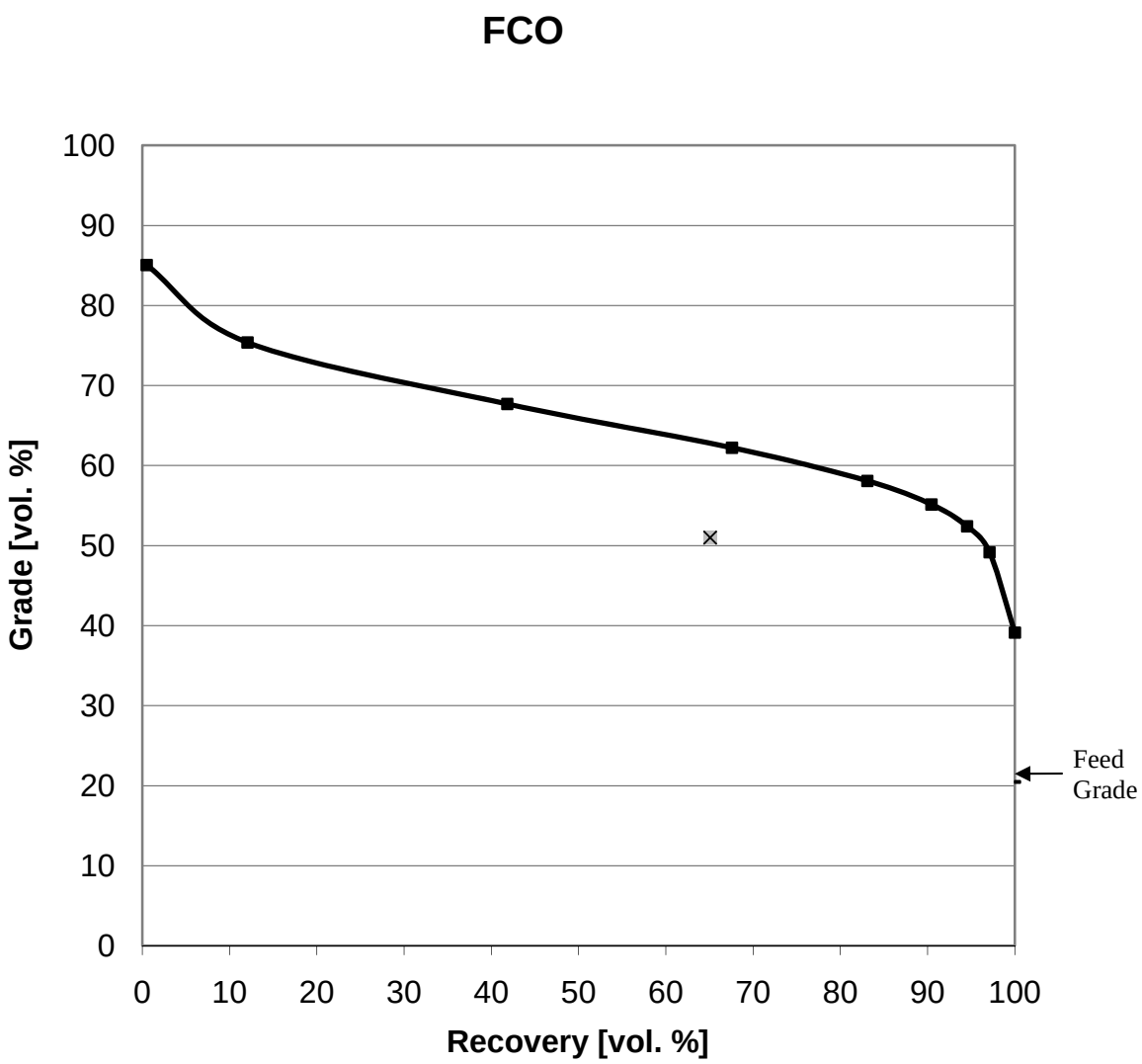

Figure 110. Liberation-Limited Grade/Recovery Curve for the FCO Feed. Actual recovery is marked with a cross on a gray background.

FCO Bad

This sample has two tailings streams. In Tailings #1 only 3% of the phosphates are lost and in the case of Tailings #2 it is almost 7% (see Figure 111). The recovery, therefore, is as high as 83% for Tailings #1 and only 57% for Tailings #2. The actual concentrate grade is only 37% and the feed grade is less than 13% of phosphates by volume. The ideal recovery at 37% grade is predicted to collect 98% of phosphate material (see Figure 112).

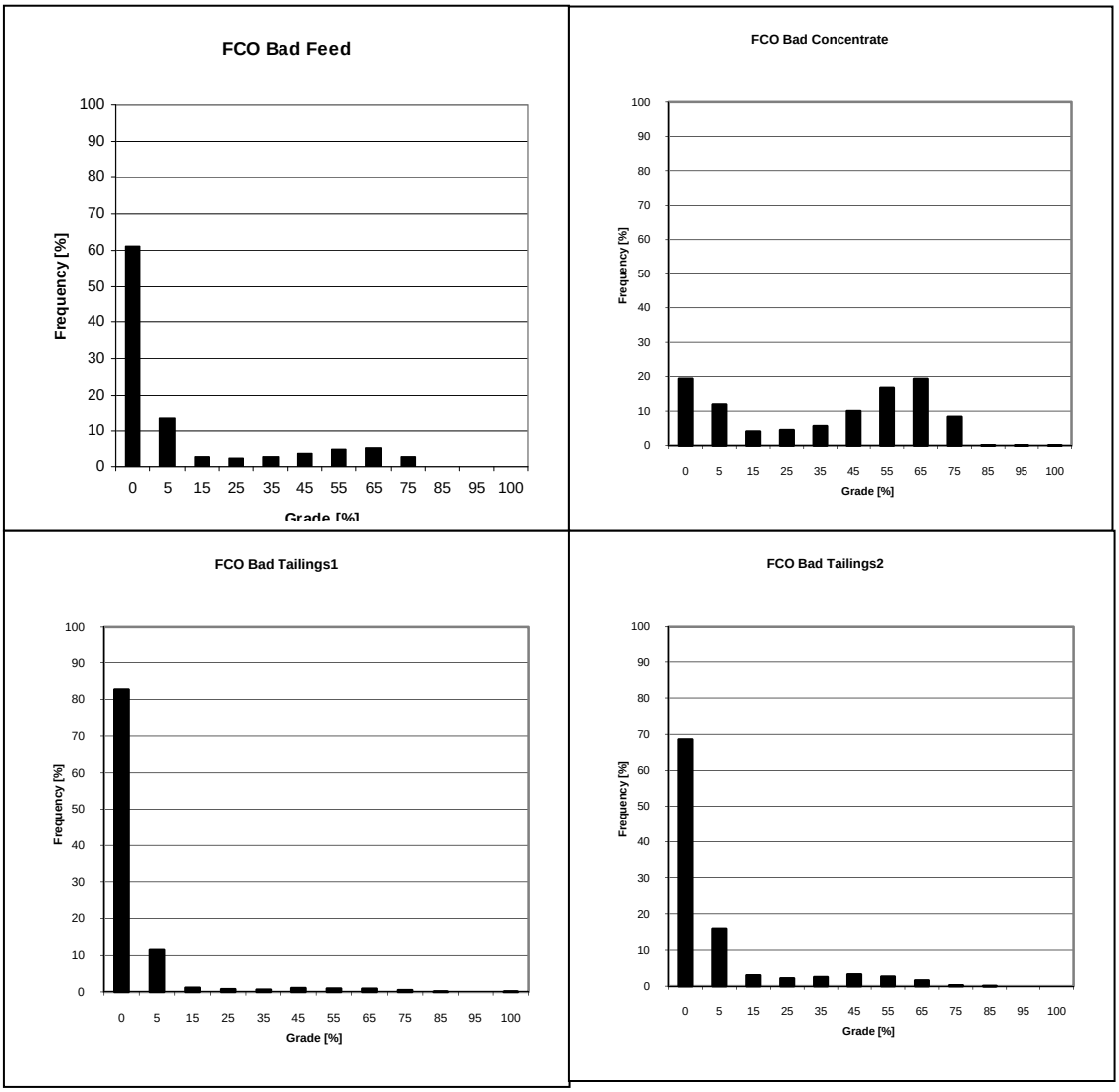

Figure 111. Liberation Spectra of Phosphate for the FCO Bad Feed, Concentrate and Tailings.

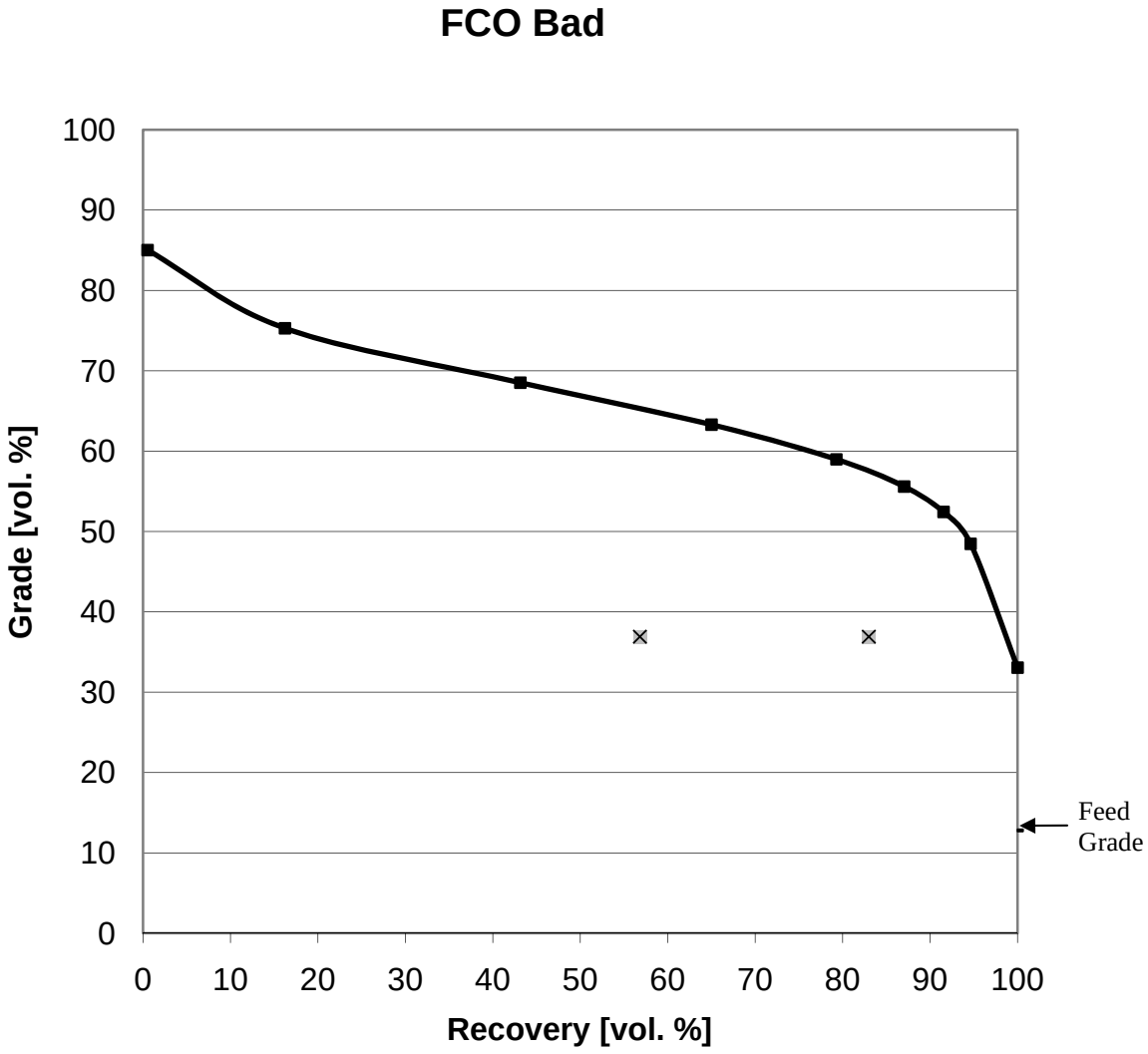

Figure 112. Liberation-Limited Grade/Recovery Curve for the FCO Bad Feed. Actual recovery is marked with a cross on a gray background.

Hole 464 Split 1

Hole 464 Split 1 samples are characterized by relatively low grade; feed material contains less than 17% percent phosphates and the concentrate achieves only 28.5%. There is much phosphate material found in the tailings; more than 10% by volume (see Figure 113). The recovery is around 60%. At such low concentrate grade (28.5%), all phosphate material should be recovered, according to Figure 114. Much improvement with respect to separation efficiency, without altering liberation, should be possible.

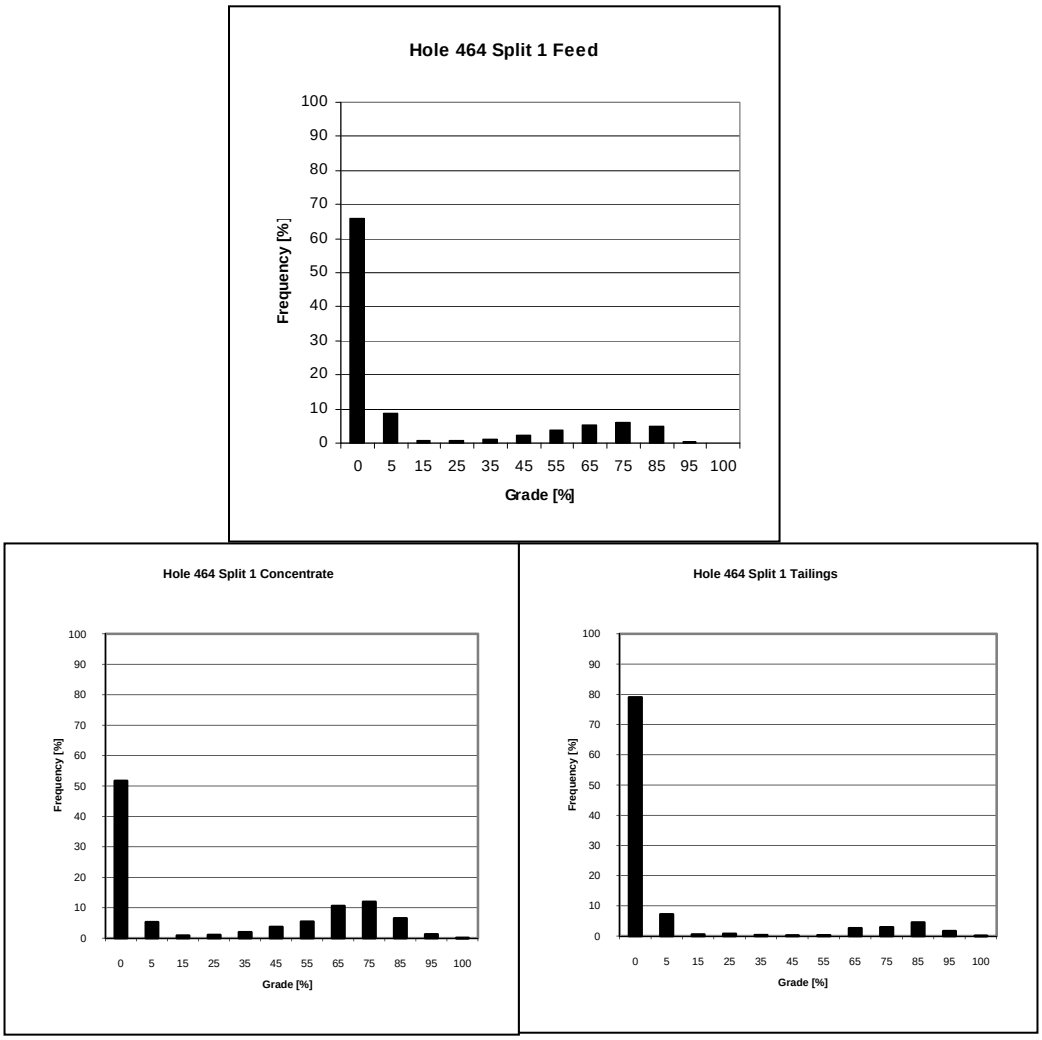

Figure 113. Liberation Spectra of Phosphate for the Hole 464 Split 1 Feed, Concentrate and Tailings.

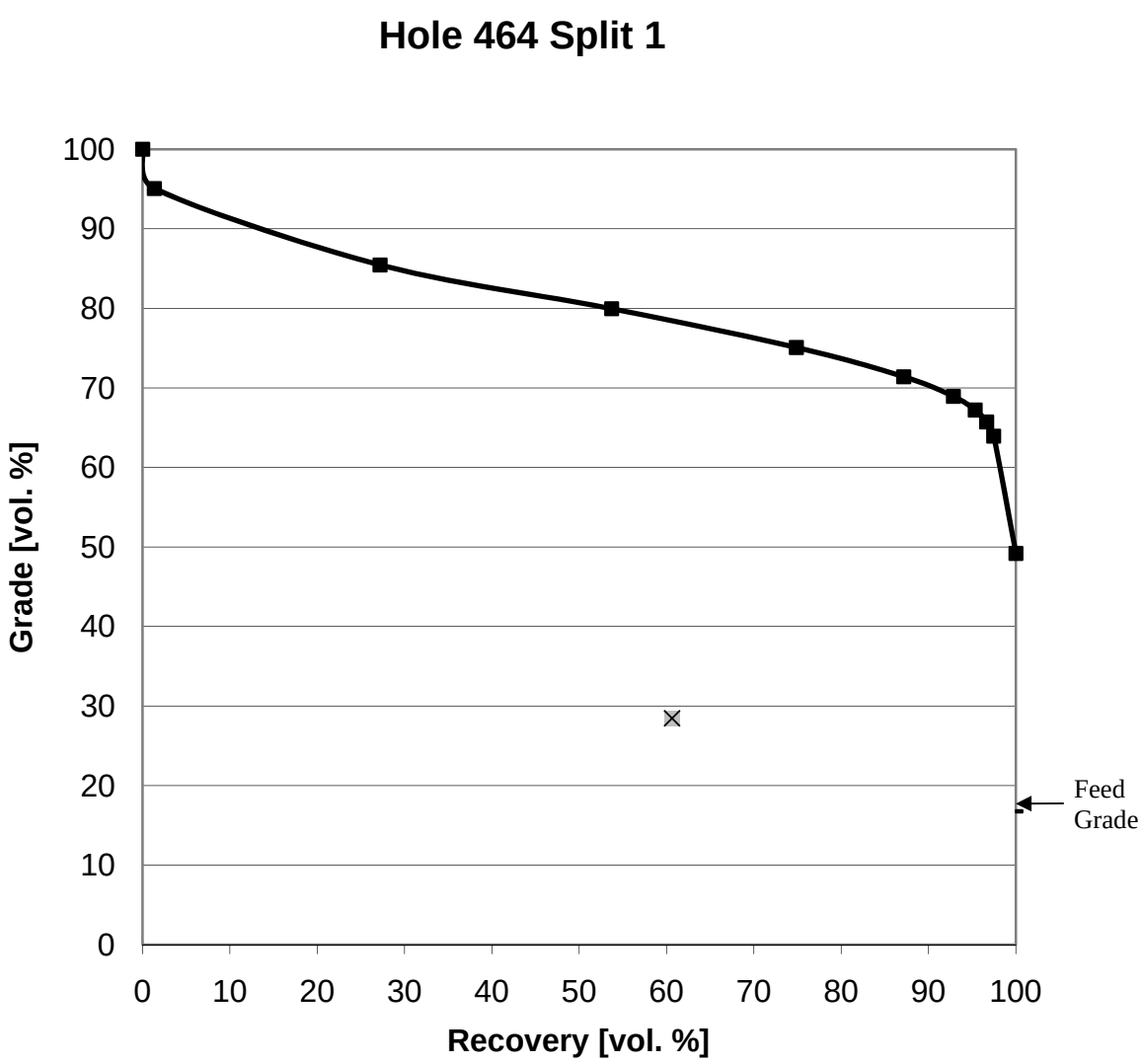

Figure 114. Liberation-Limited Grade/Recovery Curve for the Hole 464 Split 1 Feed. Actual recovery is marked with a cross on a gray background.

Hole 464 Split 2

The Hole 464 Split 2 sample achieves relatively high separation efficiency; the grade increases from 25% of phosphate material in the feed to 57% in the concentrate (Figure 115), giving an excellent recovery of over 98.5%. Very little phosphate material is found in the tailing stream; more than 92% of the tailings is pure gangue and the rest is gangue particles with less than 5% phosphate content. Separation efficiency cannot be increased without further liberation (Figure 116).

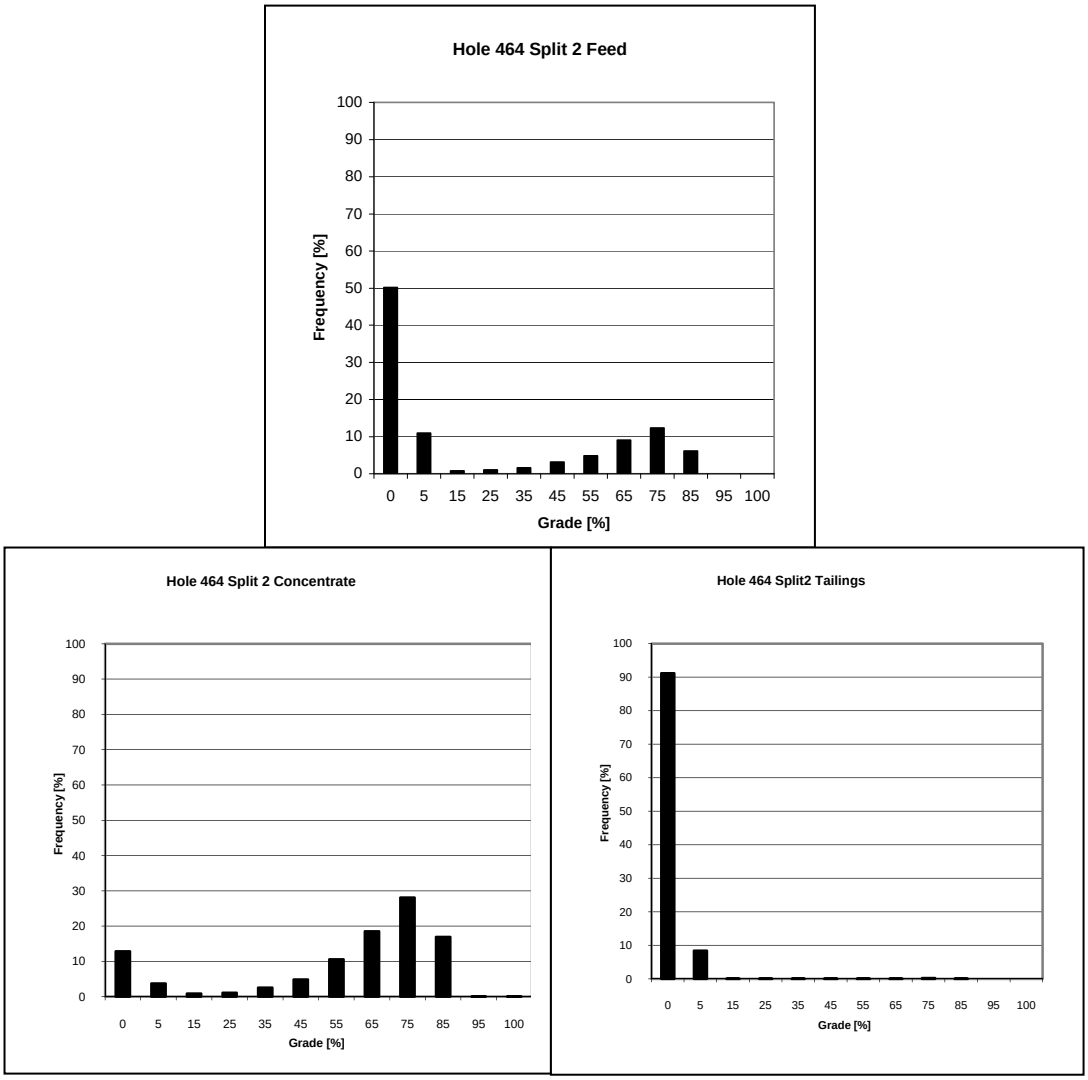

Figure 115. Liberation Spectra of Phosphate for the Hole 464 Split 2 Feed, Concentrate and Tailings.

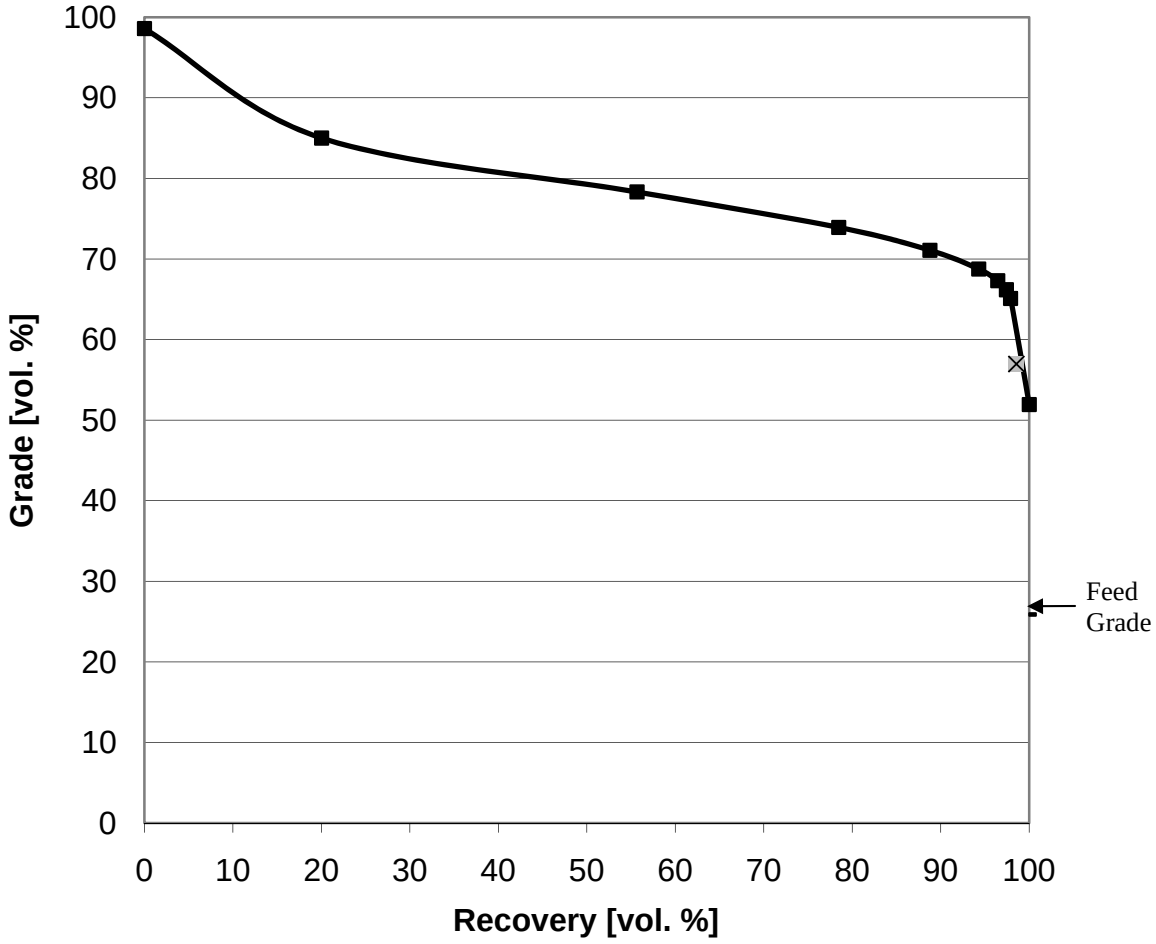

Figure 116. Liberation-Limited Grade/Recovery Curve for the Hole 464 Split 2 Feed. Actual recovery is marked with a cross on a gray background.

South Fort Meade (SFM)

SFM feed contains over 17% of phosphates and is concentrated to almost 40% of phosphate material by volume. Nearly 5% of phosphates are wasted into the tailings. SFM tailings contain 80% of pure gangue material and the concentrate contains as much as 29% of pure gangue (see Figure 117). The actual recovery for the SFM samples is only 82%, but the maximum recovery that could be achieved at this particle size and grade would be close to 100%, according to Micro CT analysis (see Figure 118).

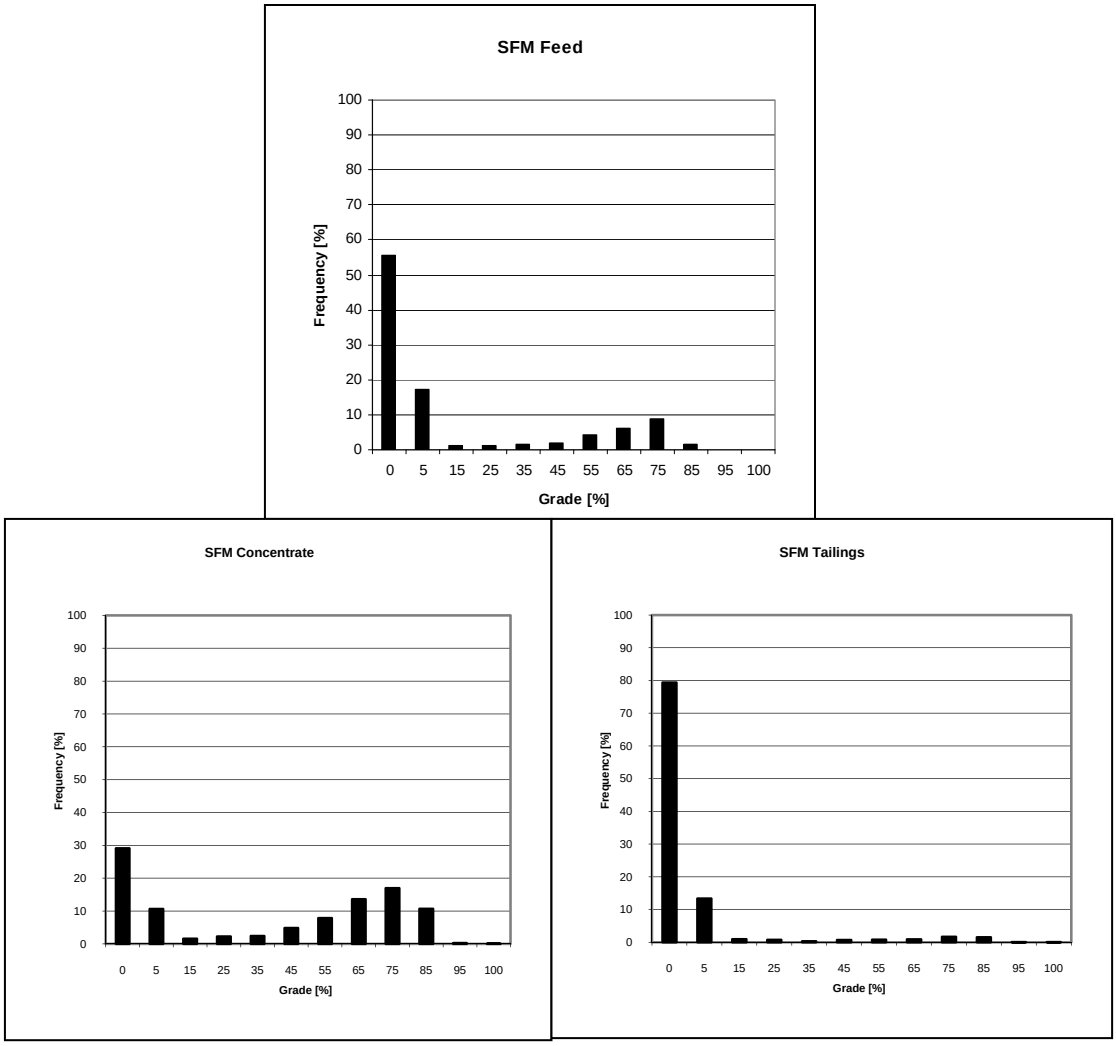

Figure 117. Liberation Spectra of Phosphate for the SFM Feed, Concentrate and Tailings.

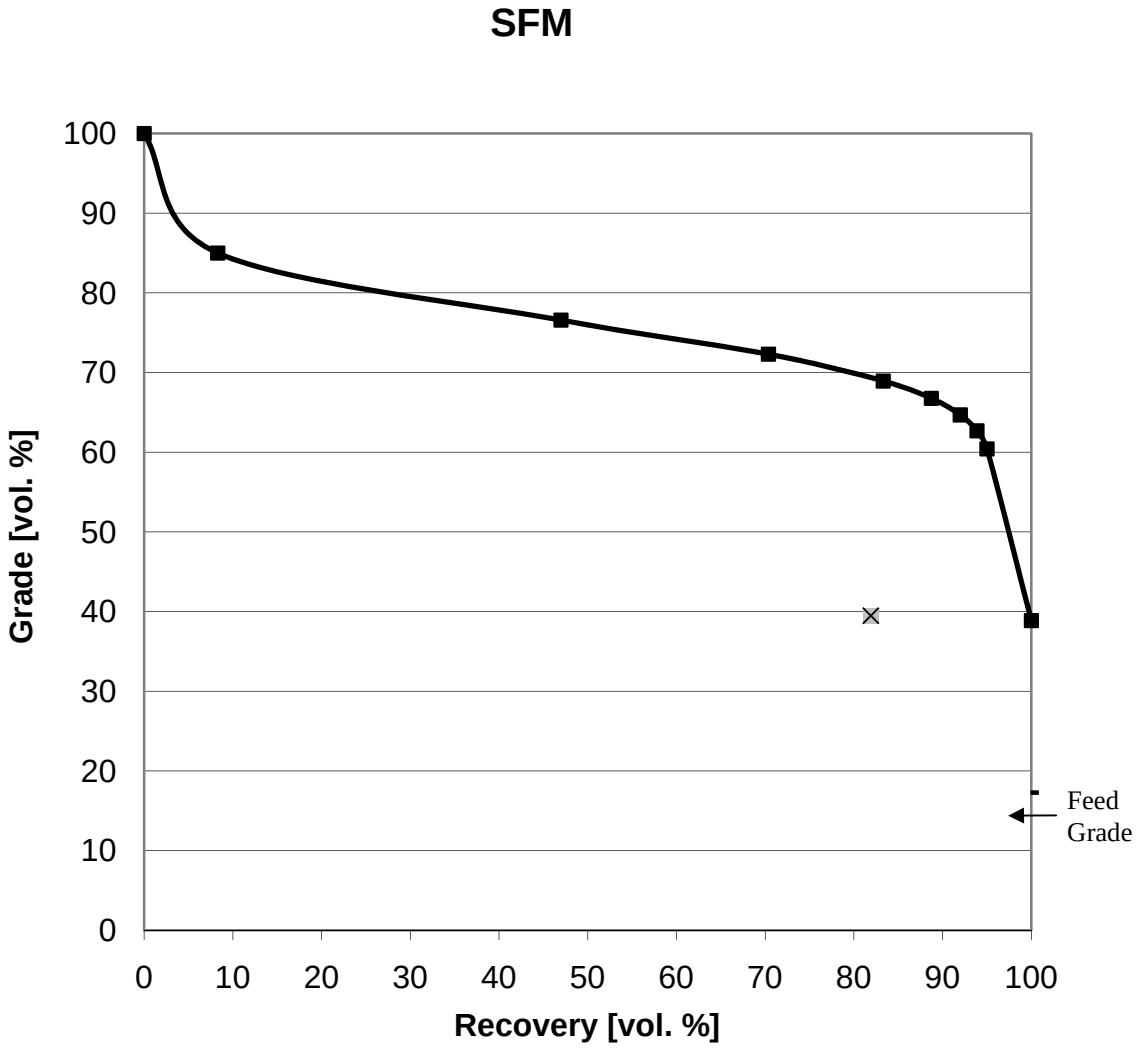

Figure 118. Liberation-Limited Grade/Recovery Curve for the SFM Feed. Actual recovery is marked with a cross on a gray background.

Summary

Liberation issues and grade/recovery curves were determined for the 2008 samples: 1862-S2, 3057-S2, CF Combined, CF West, CF East, FCO, FCO Bad, 464-S1, 3057-S2 and South Fort Meade**.** Detailed 3D Micro CT analyses of all 2008 samples were reported. Regarding these ten 2008 samples, CT analysis suggests that in the case of CF West, CF East, CF Combined and 3057-S2, the recovery is mostly limited by liberation. In the case of 3057-S2, SFM, FCO, and FCO Bad (Tailings 2), recovery is to some extent limited by factors other than liberation. Finally, in the case of 464-S1, 1862-S2 and FCO Bad (Tailings 1), the recovery is significantly limited by factors other than liberation (see Table 19).

Table 19. Recovery Limitations as Revealed by Micro CT Analysis of the 2008 Samples.

Sample	Micro CT			Flotation @ 1Lb/T, 180s	Limitation to Recovery
	No. of Particles Analyzed	Grade [%]	Recovery [%]	Recovery [%]	
Hole 1862 Split 2 Feed	27716	35.55	47.46	~66	Other Factors Major Effect
Hole 1862 Split 2 Concentrate	31394	39.91			
Hole 1862 Split 2 Tailings	22492	32.35			
Hole 3057 Split 2 Feed	15522	16.12	75.03	~67	Other Factors to Some Extent
Hole 3057 Split 2 Concentrate	32777	65.37			
Hole 3057 Split 2 Tailings	22935	4.94			
CF Combined Feed	16189	24.78	96.76	~97	Liberation
CF Combined Concentrate	14879	61.66			
CF Combined Tailings	14257	1.31			
CF West Feed	26789	20.07	94.69	~98	Liberation
CF West Concentrate	25147	53.62			
CF West Tailings	21819	1.65			
CF East Feed	26106	19.87	93.66	~97	Liberation
CF East Concentrate	23889	66.77			
CF East Tailings	21900	1.75			
FCO Feed	36030	20.45	65.08	~95	Other Factors to Some Extent
FCO Concentrate	36391	9.67			
FCO Tailings	38728	50.98			
FCO Bad Feed	29813	12.80	82.99	-	Other Factors Major Effect
FCO Bad Concentrate	33053	36.91			
FCO Bad Tailings 1	28572	3.06			
FCO Bad Tailings 2	27427	6.89	56.81		
Hole 464 Split 1 Feed	24000	16.76	60.62	~83	Other Factors Major Effect
Hole 464 Split 1 Concentrate	29373	28.45			
Hole 464 Split 1 Tailings	15708	10.26			
Hole 464 Split 2 Feed	25711	25.88	98.55	~79	Other Factors Major Effect
Hole 464 Split 2 Concentrate	29396	56.97			
Hole 464 Split 2 Tailings	17254	0.68			
SFM Feed	25127	17.28	81.91	~95	Other Factors to Some Extent
SFM Concentrate	23566	39.49			
SFM Tailings	12729	4.87			

CONCLUSIONS

MICRO CT ANALYSIS, LIBERATION-LIMITED GRADE RECOVERY CURVES

Based on Micro CT analysis of the 2007 and 2008 samples, the significance of liberation in flotation recovery was determined and is summarized in Tables 20a and 20b.

Table 20a. Recovery Limitations as Revealed by Micro CT Analysis of 2007 Samples.

Sample	Micro CT			Flotation @ 1Lb./T, 180s	Limitation to Recovery
	No. of Particles Analyzed	Grade [%]	Recovery [%]	Recovery [%]	
Four Corners Feed (Bad)	25122	15.97	38.42	~23	Other Factors Major Effect
Four Corners Concentrate (Bad)	32826	37.94			
Four Corners Tailings (Bad)	19610	11.73			
Four Corners Feed (Good)	20928	12.88	92.73	~92.5	Liberation
Four Corners Concentrate (Good)	33243	53.34			
Four Corners Tailings (Good)	20177	1.21			
CF Industries Feed (Bad)	5994	29.72	80.23	~89	Other Factors to Some Extent
CF Industries Concentrate (Bad)	3723	67.40			
CF Industries Tailings (Bad)	1757	9.10			
CF Industries Feed (Good)	7690	27.25	95.12	~97	Liberation
CF Industries Concentrate (Good)	9869	55.10			
CF Industries Tailings (Good)	15094	1.46			

Table 20b. Recovery Limitations as Revealed by Micro CT Analysis of 2008 Samples.

Sample	Micro CT			Flotation @ 1Lb./T, 180s	Limitation to Recovery
	No. of Particles Analyzed	Grade [%]	Recovery [%]	Recovery [%]	
Hole 1862 Split 2 Feed	27716	35.55	47.46	~66	Other Factors Major Effect
Hole 1862 Split 2 Concentrate	31394	39.91			
Hole 1862 Split 2 Tailings	22492	32.35			
Hole 3057 Split 2 Feed	15522	16.12	75.03	~67	Other Factors to Some Extent
Hole 3057 Split 2 Concentrate	32777	65.37			
Hole 3057 Split 2 Tailings	22935	4.94			
CF Combined Feed	16189	24.78	96.76	~97	Liberation
CF Combined Concentrate	14879	61.66			
CF Combined Tailings	14257	1.31			
CF West Feed	26789	20.07	94.69	~98	Liberation
CF West Concentrate	25147	53.62			
CF West Tailings	21819	1.65			
CF East Feed	26106	19.87	93.66	~97	Liberation
CF East Concentrate	23889	66.77			
CF East Tailings	21900	1.75			
FCO Feed	36030	20.45	65.08	~95	Other Factors to Some Extent
FCO Concentrate	36391	9.67			
FCO Tailings	38728	50.98			
FCO Bad Feed	29813	12.80	82.99	-	Other Factors Major Effect
FCO Bad Concentrate	33053	36.91			
FCO Bad Tailings 1	28572	3.06			
FCO Bad Tailings 2	27427	6.89	56.81		
Hole 464 Split 1 Feed	24000	16.76	60.62	~83	Other Factors Major Effect
Hole 464 Split 1 Concentrate	29373	28.45			
Hole 464 Split 1 Tailings	15708	10.26			
Hole 464 Split 2 Feed	25711	25.88	98.55	~79	Other Factors Major Effect
Hole 464 Split 2 Concentrate	29396	56.97			
Hole 464 Split 2 Tailings	17254	0.68			
SFM Feed	25127	17.28	81.91	~95	Other Factors to Some Extent
SFM Concentrate	23566	39.49			
SFM Tailings	12729	4.87			

MINERALOGICAL ANALYSIS AND SURFACE CHEMISTRY

Research work was concentrated on two good samples (CF West and CF Combined) and two bad samples (1862-S2, 464-S1). However, the mineralogical studies also included the 3057-S2 and CF East Pit samples. The samples considered are as follows:

Sample	Feed BPL %	Grade BPL%	Recovery %
	Bad Samples		
Hole 1862 Split 2	26.72	48.72	25.6
Hole 464 Split 1	27.65	36.79	76.5
Hole 464 Split 2	31.93	57.69	61.0
	Good Samples		
CF Combined	16.94	52.42	96.3
CF West Pit	9.88	43.62	96.6
CF East Pit	12.15	46.16	96.7

The present study indicates that the feed phosphate samples are composed essentially of quartz and apatite in variable percentages. In addition, subordinate amounts of clay minerals (kaolinite, illite, and montmorillonite), gypsum and carbonate minerals (mainly dolomite) were found except for the 464-S1 and 3057-S2 feed samples which are free of carbonate minerals. On flotation separation, almost all phosphate minerals are transferred into the concentrates for the good feeds and the phosphate mineral percentage in the good tails does not exceed 1.5%. In contrast, for the bad feeds there is no great difference between the grade of the concentrates and tailings, except 3057-S2 where the concentrate grade was found to be about 58% phosphate and the tailings grade about 7% phosphate.

The present study also reveals that the particle size distribution (PSD) has a narrow size range for the good feeds (CF West and CF Combined), while in the bad feeds PSDs have a wide size range and there is a good percent of phosphate in the coarse to very coarse size fraction, significantly coarser than the associated quartz particles. The effect of PSD on the efficiency of separation is obvious, where most of the coarse phosphate particles in the bad feeds are lost to the tailings, leaving the concentrates a uniform particle size.

In the 1862-S2 sample, gypsum was found in the feed in crystals of cylindrical shape surrounding phosphate particles and sometimes aggregated as coarse particles. Gypsum is a source of calcium which may interfere in the flotation process. The phosphate particles in the tailings are more porous than those in the concentrate, and are one of the following types: coarse, highly porous, kaolinite-coated, or unliberated.

In the feed for 464-S1, some phosphate particles show high porosity and kaolinite is present in the shape of worms, rods or ropes attached or stained on the surface of both phosphate and quartz particles. Sometimes the kaolinite forms a shell around the different particles. In the tailings, kaolinite is acting as a binding material for some

phosphate and quartz particles, and the phosphate particles are very coarse, unliberated or attached to quartz particles by the kaolinite mineral. As in the other phosphate samples, the phosphate particles are elongated (rods or oval) and spherical or irregular. In this case, the elongated phosphate particles are more common in the concentrate than in the tailings. CF Combined and CF West Pit good feeds have no such features found in the bad feed material but there is a limited liberation.

The XPS results of phosphate particles in the flotation products of bad samples 464-S1 and 1862-S2 revealed that calcium, phosphorus, fluorine, iron and sulfur exhibit the same behavior and are rich on the surface of phosphate particles in the concentrates. Silica exhibits similar behavior and is abundant on the surface of phosphate particles in the tailings. On the other hand, magnesium and alumina exhibit the opposite behavior and increase in the concentrate of 1862-S2 and decrease in the tailings of 464-S1.

The mass concentration difference for phosphorus, calcium, and fluorine in the concentrate and tailings was higher in the case of 464-S1 than in the case of 1862-S2. This difference is expected to explain separation efficiency, as if this difference increases the separation efficiency will increase. Therefore, the separation efficiency of 464-S1 is better than that of 1862-S2, according to the flotation and mineralogical results.

Finally, the factors affecting separation efficiency of the bad feeds (1862-S2 and 464-S1) include the following:

- Particle size distribution
- Presence of a remarkable amount of associated clay, gypsum and dolomite minerals
- High porosity of phosphate particles in some feeds
- Liberation

Particle shape has some effect on separation as the elongated particles have a greater ability to float than the spherical particles.

REFERENCES

Al-Wakeel MI. 1997. Geology and beneficiation of some Egyptian talc-carbonate rocks [PhD dissertation]. Cairo (Egypt): Ain Shams University.

Barbery G. 1991. Mineral liberation measurement, simulation and practical use in mineral processing. Quebec (Canada): Editions GB.

Fandrich R, Gu Y, Burrows D, Moeller K. 2007. Modern SEM-based mineral liberation analysis. International Journal of Mineral Processing 84(1-4): 310-20.

Gaudin AM. 1939. Principles of mineral dressing. New York: McGraw-Hill. p 70-91.

Gu Y, Napier-Munn T. 1997. JK/Philips mineral liberation analyzer--an introduction. In: International Conference Minerals Processing '97, 16th Annual Minerals Processing Symposium; 1997 Aug 6-8; Cape Town, South Africa. p 2.

King RP, Schneider CL. 1993. An effective SEM-based image analysis for quantitative Mineralogy. KONA Powder and Particle Journal 11: 165-77.

King RP. 1994. Linear stochastic models for mineral liberation. Powder Technol. 81(3): 217-34.

Latti D, Adair BJI. 2001. An assessment of stereological adjustment procedures. Minerals Engineering 14(12): 1579-87.

Lin CL, Miller JD. 1996. Cone beam X-ray microtomography for three-dimensional liberation analysis in the 21st century. International Journal of Mineral Processing 47(1-2): 61-73.

Lin CL, Miller JD. 2001. A new cone beam X-ray microtomography facility for 3D analysis of multiphase materials. In: Proceedings of the 2nd World Congress on Industrial Process Tomography; 2001 Aug 29-31; Hannover, Germany. [Leeds]: Virtual Centre for Industrial Process Tomography. p 98-109.

Lin CL, Miller JD, Herbst JA, Sepulveda JE, Prisbrey KA. 1985. Prediction of volumetric abundance from two dimensional mineral images. In: Park WC, Hausen DM, Hagni RD, eds. Applied mineralogy: proceedings of the Second International Congress on Applied Mineralogy in the Minerals Industry; 1984 Feb 22-25; Los Angeles, CA. Warrendale (PA): The Metallurgical Society of AIME. p 157-170.

Miller JD, Lin, CL. 1988. Treatment of polished section data for detailed liberation analysis. International Journal of Mineral Processing 22(1-4): 41-58.

Miller JD, Lin CL. 2004. Three-dimensional analysis of particulates in mineral processing systems by cone-beam X-ray microtomography. Minerals and Metallurgical Processing 21(3): 113-24.

Miller PR, Reid AF, Zuiderwyk MA. 1982. QEM*SEM image analysis in the determination of modal assays, mineral associations and mineral liberation. In: XIV International Mineral Processing Congress: worldwide industrial application of mineral processing technology; 1982 Oct 17-23; Toronto, Canada. Montreal: CIM.

Schneider CL, Lin CL, King RP, Miller JD. 1991. Improved transformation technique for the prediction of liberation by random fracture model. Powder Technology 67(1): 103-11.

Videla AR, Lin CL, Miller JD. 2007. 3D characterization of individual multiphase particles in packed particle beds by X-ray microtomography (XMT). International Journal of Mineral Processing 84(1-4): 321-6.

Appendix A

MINERALOGY OF FEED SLIMES FROM 2007 SAMPLES

The fine particles of the Four Corners and CF Industries bad feed samples were separated by attritioning and decantation of the supernatant with the suspended particles. The Four Corners feed produced a considerable amount of fines (clay minerals), while the CF Industries feed produced a very small or negligible amount of fines. Unlike the Four Corners fines, the CF Industries fines consisted completely of silica. A suspension of the Four Corners fines was transferred with a 20 ml pipette to glass slides to make oriented samples of the clay particles. The oriented samples were left overnight to dry, then one sample was heated in the oven at 600^{o}C for one hour. Both untreated and heated samples were analyzed with XRD. The diffractometer was a Rigaku Model D2000. The samples were scanned at 2Θ range 2-40^{o} and a scan speed of 1/min.

The results are given in Figure A-1 and indicate that Four Corners fines are composed of different types of clay minerals such as illite, kaolinite and mixed-layer montmorillonite-illite minerals in addition to quartz, gypsum and apatite. Quartz, apatite and illite are not affected by heating, while kaolinite disappears on heating due to the collapse of its structure. The mixed layer montmorillonite-illite d-spacing was reduced from 12.45Å to 11.52Å, and gypsum disappeared because of its decomposition on heating.

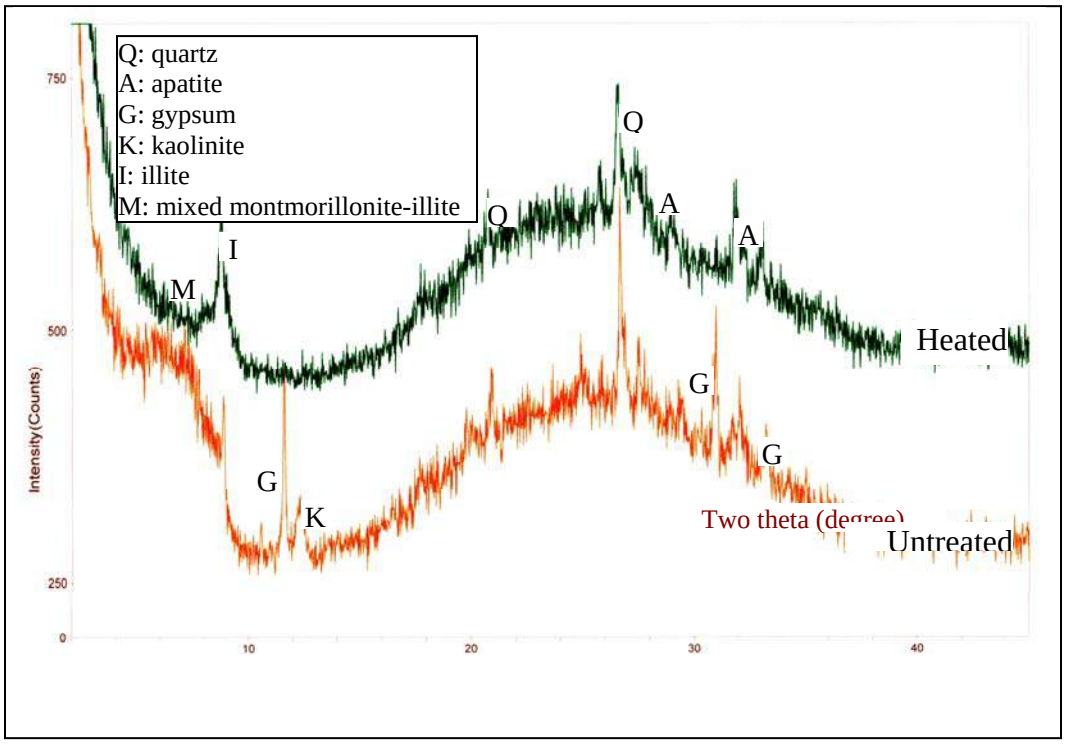

Figure A-1. X-Ray Diffraction Patterns of the Four Corners Bad Feed Fines.

Appendix B

MICROPROBE ANALYSIS OF CF INDUSTRIES BAD FEED

Microchemical analysis of some phosphate particles from CF Industries bad feed (Figure B-1) was carried out by a Microprobe Analyzer. The results show that the calcium and phosphorus are decreased towards the surface of some phosphate particles, this reduction being replaced by silica.

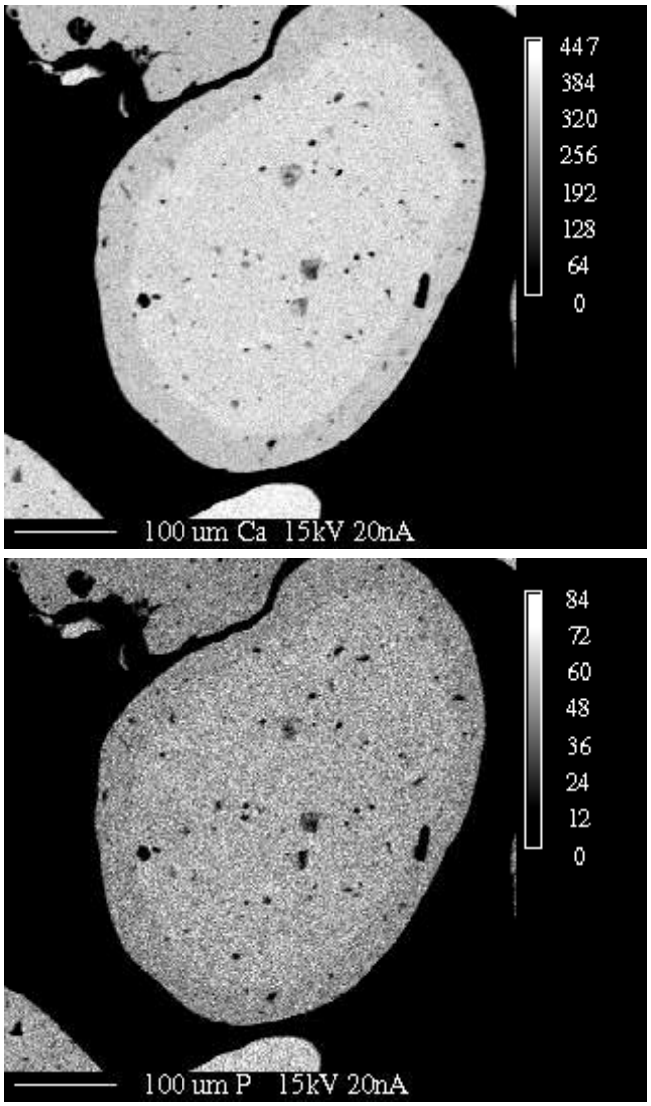

Figure B-1. Microprobe Micrograph Showing Chemical Maps by Microprobe of Phosphorous and Calcium of a Phosphate Particle in CF Industries Bad Feed.

Appendix C

XPS SURFACE CHEMICAL COMPOSITION FOR SELECTED 2008 SAMPLES

Table C-1. Surface Chemical Composition of Particle 1 in the Hole 464 Split 1 Concentrate.

Element	Atomic Conc. (%)	Mass Conc. (%)
Mg	0.22	0.27
Fe	2.04	5.74
F	1.08	1.04
O	42.38	34.23
Ca	6.31	12.77
C	28.61	17.35
P	8.39	13.12
Si	5.67	8.03
Al	4.40	5.99
S	0.91	1.47

Table C-2. Surface Chemical Composition of Particle 2 in the Hole 464 Split 1 Concentrate.

Element	Atomic Conc. (%)	Mass Conc. (%)
Mg	0.00	0.00
Fe	1.48	4.10
F	1.84	1.73
O	42.20	33.50
Ca	8.55	17.01
C	26.88	16.02
P	8.35	12.84
Si	4.46	6.21
Al	5.27	7.06
S	0.96	1.53

Table C-3. Surface Chemical Composition of Particle 3 in the Hole 464 Split 1 Concentrate.

Element	Atomic Conc. (%)	Mass Conc. (%)
Mg	0.02	0.03
Fe	1.65	4.59
F	2.12	2.01
O	44.15	35.27
Ca	8.37	16.74
C	26.28	15.76
P	8.21	12.70
Si	4.40	6.17
Al	3.73	5.02
S	1.07	1.71

Table C-4. Surface Chemical Composition of Particle 1 in the Hole 464 Split 1 Tailings.

Element	Atomic Conc. (%)	Mass Conc. (%)
Mg	0.03	0.03
Fe	1.41	3.94
F	2.36	2.24
O	41.69	33.36
Ca	10.09	20.23
C	29.19	17.54
P	8.55	13.25
Si	2.34	3.29
Al	3.31	4.47
S	1.03	1.66

Table C-5. Surface Chemical Composition of Particle 2 in the Hole 464 Split 1 Tailings.

Element	Atomic Conc. (%)	Mass Conc. (%)
Mg	0.12	0.16
Fe	2.31	7.07
F	1.16	1.20
O	35.18	30.81
Ca	5.64	12.37
C	43.31	28.48
P	6.82	11.56
Si	3.46	5.32
Al	1.78	2.63
S	0.22	0.38

Table C-6. Surface Chemical Composition of Particle 3 in the Hole 464 Split 1 Tailings.

Element	Atomic Conc. (%)	Mass Conc. (%)
Mg	0.01	0.01
Fe	0.15	0.42
F	0.00	0.00
O	44.01	36.14
Ca	0.75	1.54
C	21.17	13.05
P	0.04	0.07
Si	32.17	46.38
Al	1.56	2.16
S	0.14	0.23

Table C-7. Surface Chemical Composition of Particle 1 in the Hole 1862 Split 2 Concentrate.

Element	Atomic Conc. (%)	Mass Conc. (%)
Mg	0.08	0.10
Fe	3.91	11.10
F	0.96	0.93
O	44.63	36.27
Ca	6.03	12.28
C	30.85	18.82
P	7.47	11.75
Si	4.83	6.89
Al	0.63	0.87
S	0.61	0.99

Table C-8. Surface Chemical Composition of Particle 2 in the Hole 1862 Split 2 Concentrate.

Element	Atomic Conc. (%)	Mass Conc. (%)
Mg	0.12	0.16
Fe	2.31	6.81
F	0.29	0.29
O	44.73	37.80
Ca	1.87	3.97
C	29.57	18.76
P	6.32	10.34
Si	10.39	15.42
Al	3.66	5.22
S	0.74	1.25

Table C-9. Surface Chemical Composition of Particle 3 in the Hole 1862 Split 2 Concentrate.

Element	Atomic Conc. (%)	Mass Conc. (%)
Mg	0.13	0.17
Fe	0.97	2.89
F	0.22	0.22
O	42.78	36.66
Ca	1.05	2.26
C	28.69	18.45
P	0.62	1.03
Si	23.19	34.88
Al	2.14	3.10
S	0.21	0.35

Table C-10. Surface Chemical Composition of Particle 1 in the Hole 1862 Split 2 Tailings.

Element	Atomic Conc. (%)	Mass Conc. (%)
Mg	0.02	0.04
Fe	0.83	2.91
F	0.15	0.18
O	31.22	31.36
Ca	0.90	2.25
C	54.41	41.03
P	1.20	2.32
Si	10.83	19.09
Al	0.28	0.47
S	0.17	0.34

Table C-11. Surface Chemical Composition of Particle 2 in the Hole 1862 Split 2 Tailings.

Element	Atomic Conc. (%)	Mass Conc. (%)
Mg	0.22	0.30
Fe	1.19	3.83
F	0.48	0.52
O	48.88	44.96
Ca	2.47	5.70
C	33.71	23.28
P	3.64	6.49
Si	5.39	8.70
Al	4.01	6.21
S	0.00	0.00

Table C-12. Surface Chemical Composition of Particle 3 in the Hole 1862 Split 2 Tailings.

Element	Atomic Conc. (%)	Mass Conc. (%)
Mg	0.43	0.57
Fe	2.03	6.09
F	0.39	0.39
O	46.27	39.82
Ca	1.93	4.15
C	29.39	18.99
P	3.79	6.32
Si	12.99	19.63
Al	2.77	4.02
S	0.02	0.03


GREAT SEAL OF THE STATE OF FLORIDA
IN GOD WE TRUST